PM2.5 SOURCE IMPACT ANALYSIS ON A CATTLE FEEDYARD USING AN ALTERNATIVE SECONDARY PM2.5 EMISSION FACTOR AND DISPERSION MODELLING

A Thesis

by

EL JIRIE NAVARRA BATICADOS

Submitted to the Office of Graduate Studies and Professional Studies of
Texas A&M University
in partial fulfillment of the requirements for the degree of

MASTER OF SCIENCE

Chair of Committee,	Sergio C. Capareda
Committee Members,	Gerald L. Riskowski
	Qi Ying
Head of Department,	Stephen W. Searcy

May 2018

Major Subject: Biological and Agricultural Engineering

ABSTRACT

This research was primarily focused on how much particulate matter (PM2.5) can be obtained from reactions of ammonia with sulfur dioxide inside two controlled reaction environments – flow reactor and wind tunnel. The PM2.5 generated were dominated by ammonium sulfite and ammonium sulfates based on Fourier Transform Infared (FTIR) and energy dispersive (EDS) x-ray analyses, particularly at conditions of high excess ammonia and higher O_2 inside a continuous flow reactor. The particles formed appear to be white in color ranging from powdery to crystal-like. A wind tunnel was used to simulate the interaction of fugitive fine dusts with precursors gases. Wall loss effects and heterogeneous nucleation were both observed to be the dominating factors during particle formation. The idealized 2^o $PM_{2.5}$ formed per ammonia used was calculated to be within the range of 5.64 – 10.70 mg of PM2.5 per 1000 mg of NH_3 used from the flow reactor study and 0.13 mg of PM2.5 per 1000 mg of NH_3 from the wind tunnel study. The PM ratio between the 2^o $PM_{2.5}$ and the 1^o $PM_{2.5}$ based on the wind tunnel tests was estimated to be 2.81%. A source impact analysis was conducted on a selected concentrated animal feeding operations (CAFOs) in Texas. The PM ratio generated from this research should provide an implicit conservative approach in estimating the effects of secondary PM2.5 to the total PM2.5 levels in a CAFO based on the dispersion modelling. This conservative approach assumes that both maximum impacts of secondary and primary PM2.5 occur at the same place and same time. In reality, formation of the sulfate particles should be a fairly slow process, and maximum impact maybe further downwind from the maximum primary PM2.5 impact. The knowledge gained about the formation rates, yield and

characteristics of secondary PM2.5 from this research should provide sufficient vital information for future field studies in order to generate an acceptable secondary PM2.5 emission factor for CAFOs based on different geographic factors and more realistic ambient atmospheric variables.

ACKNOWLEDGEMENTS

My sincerest gratitude to Dr. Sergio Capareda for the chance to attend graduate school in Texas A&M University. His invaluable guidance, encouragement and funding allowed me to finish this work. I would also thank my committee members, Dr. Qi Ying and Dr. Gary Riskowski for their listening ears and helpful suggestions. My gratitude is also extended to Col. Russell McGee for the wonderful TA experience from the air pollution engineering class.

This research would be impossible without the generous help and warm company of the awesome people of BETA Laboratory. All these people and many more, in one way or another, were critical to completing this research. To all of my friends here in TAMU, cheers!

Most importantly, my utmost gratitude to my parents and all my loved ones in the Philippines for their infinite understanding and tolerance of me throughout this journey.

CONTRIBUTORS AND FUNDING SOURCES

This work was supervised by a thesis committee consisting of Dr. Sergio Capareda and Dr. Gary Riskowski of the Department of Biological and Agricultural Engineering and Dr. Qi Ying of the Department of Civil Engineering. The electron imaging and energy dispersive x-ray analysis were conducted by Dr. Michael Pendleton of the Microscopy and Imaging Center of Texas A&M University. All other work conducted for the thesis was completed by the student independently.

This work was made possible in part by the Texas A&M AgriLife Research Air Quality Research Seed Grant Program. Its contents are solely the responsibility of the author and do not necessarily represent the official views of the Texas A&M Agrilife Research.

TABLE OF CONTENTS

Page

LIST OF FIGURES

LIST OF TABLES

CHAPTER I

INTRODUCTION

I.1. Research Overview

Texas is one of the nation's largest cattle feeding states. Shifting into concentrated cattle feeding operations (CAFO) in the past few decades has arguably increased production and improved local economic conditions (Hribar, 2010). The growth of the CAFOs resulted into the conversion of formerly rural lands and sparingly populated agricultural lands into suburbanized areas. The increase in the scale of operation and geographic concentration of animal feeding facilities has raised environmental and health issues about the effects of its air emissions. It was until recently that the livestock sector became one of the targets for environmental compliance under several air regulatory legislations.

The Texas cattle industry is faced with challenges in complying with the Environmental Protection Agency's (EPA) National Ambient Air Quality Standards (NAAQS) for particulate matter (PM), expressed in terms of PM10 and PM2.5. The current NAAQS for all particulate matter less than 10 microns (μm) in diameter (PM10) is 150.0 micrograms per cubic meter ($\mu g/m^3$), with 24-hour averaging time and not to be exceeded more than once per year and averaged over three years. Meanwhile, for particles less than 2.5 μm in diameter (PM2.5), the annual threshold is 35.0 $\mu g/m^3$ with 24-hour averaging time, taking the 98^{th} percentile and averaged for 3-years. The PM2.5 is further assessed based on its primary and secondary form. For primary PM2.5, the

design value is 12.0 μg/m^3 while 15.0 μg/m^3 for the secondary PM2.5. Both threshold concentrations should have annual averaging time, with annual means averaged over 3 years (EPA, NAAQS Table, 2016). Facilities requiring a permit would traditionally limit their PM10 emissions in order to stay below the NAAQS off-property threshold. However, legislative changes has shifted the permitting focus towards limiting PM2.5 off-property concentrations. These major changes on air quality permitting process are expected to have significant impact to all agricultural operations in Texas.

The State Air Pollution Regulatory Agencies (SAPRA) and the agriculture industry are both faced with increasing pressure to reduce PM2.5 emissions in response to stricter federal rules and state regulations. In 2014, the EPA released the "Guidance for PM2.5 Permit Modelling" which details appropriate technical approaches to demonstrate compliance with the PM2.5 regulations. In the case wherein precursor gases exceeds the Significant Emission Rates (SER) for a given area, the new guideline demands that the contribution of secondary PM2.5 needs to be evaluated. The complexity of secondary PM2.5 formation has been one of the bottlenecks for the development of any universal model for assessing PM2.5 impacts of individual stationary sources (Chen & Tsai, 2017; Cohan & Napelenok, 2011; EPA, 2014). The most widely adopted model by the EPA to evaluate secondary PM2.5 emissions is the Community Multi-scale Air Quality (CMAQ) modeling system. It involves a complex software that is typically challenging to execute without a comprehensive data coming from actual atmospheric measurements.

The conduct of a source impact analysis to estimate the total PM2.5 emissions requires scientifically sound yet practically appropriate approach to account both primary and secondary formations. The primary PM2.5 are often assumed to be consist of fine fugitive dusts and soil particles generated by animal movement and vehicular traffic on unpaved grounds. On the other hand, secondary PM2.5 is formed primarily from a series of multi-step complex reactions in the atmosphere. In CAFOs, ammonia is the main precursor gas that could primarily form secondary PM2.5 upon reaction with low volatile species containing sulfates, nitrates and other acid-based substances (Sakirkin, et al., 2012).

A full quantitative photochemical grid modeling such as the use of CMAQ is only one of the approved options to estimate secondary PM2.5 concentrations. Most recently, another option specified in the PM2.5 permitting guidelines is to develop a hybrid qualitative/quantitative technique for secondary PM2.5 accounting. This option acknowledges the possibility of quantifying secondary PM2.5 impacts by converting emissions of precursors into equivalent amounts of direct PM2.5 emissions (EPA, Guidance for PM2.5 Permit Modelling , 2014). At present, there is still no available secondary PM2.5 emission factor (EF) established for agricultural operations.

This research is an initial investigation on the formation of secondary PM2.5 from ammonia in CAFOs with other precursor gas. A flow reactor study (Chapter II) and a wind tunnel study (Chapter III) were separately conducted to simulate idealized and semi-ambient reaction environment, respectively. Both studies resulted into an estimate of the amount of PM2.5 generated per unit of ammonia. A source impact analysis was

then conducted on a selected cattle feed facility in Tulia, Texas, by accounting both the primary and secondary PM2.5 contributions.

I.2. Overall Research Objectives

The over-all goal of this research was to conduct an initial investigation on the formation of secondary PM2.5 from ammonia in CAFOs with other precursor gas. The resulting unit formation of PM2.5 might be eventually used as basis for the development of a secondary EF for CAFOs and for PM2.5 source impact analysis.

Specifically, this study has the following over-all objectives:

1. To develop a science-based alternative method for determining an equivalent direct PM2.5 emission factor from an estimated ammonia emission from cattle feed yards.
2. To characterize the secondary PM2.5 produced based on chemical composition, elemental analysis, surface morphology, and particle size distribution.
3. To evaluate the contribution of the secondary PM2.5 EF on the PM2.5 source impact analysis for NAAQS compliance on a selected TX cattle feed facility.

I.3. Significance and Potential Impact

The main premise of SAPRA permitting process is to protect public health and welfare by making sure that PM downwind concentrations are within the NAAQS threshold. However, the SAPRAs are continuously pressured to meet mandated time-lines set by the CAA. In most cases, due to lack of acceptable protocol and non-existing emissions data, they have no choice but to estimate emission factors used for regulatory

purposes. With the new requirements for secondary PM2.5 regulations, agricultural stakeholders will again be faced with a dilemma on how to showcase compliance without an existing secondary PM2.5 emission factor.

A non-existent or incorrect emission factor will result into a flawed permitting process. An overestimated emission factor might result into requiring target agricultural operations to install expensive air pollution controls that might not be actually needed and result into many small agribusiness to shut down. Furthermore, emission factors are normally basis for emission inventories (Parnell & Parnell-Molloy, 2002). The State Implementation Plan (SIP) utilizes the emission inventory in order to develop strategies to bring non-attainment area into attainment. If the emission factor generated is incorrect, there is a possibility that the strategy developed in the SIP may not work.

The secondary PM2.5 generated from this study can provide SAPRAs with a preliminary basis to help address the challenges of accounting secondary PM2.5 contributions, particularly for cattle feed yards or any facility emitting ammonia. The knowledge gained about the formation rates, yield and characteristics of secondary PM2.5 from this research should provide sufficient vital information for future field studies in order to stream line the secondary PM2.5 EFs based on different geographic factors and more realistic ambient atmospheric variables.

CHAPTER II

PM2.5 FORMATION FROM AMMONIA & SULFUR DIOXIDE REACTIONS USING AN AEROSOL FLOW REACTOR

II.1. Introduction

There is no available secondary $PM_{2.5}$ emission factor (EF) established for agricultural operations. Despite of the absence of the latter, EPA has aggressively mandated the inclusion of secondary $PM_{2.5}$ on agricultural air pollution regulations and impact analysis for permitting purposes.

However, EPA also acknowledges the complexity of developing a particular model to assess secondary $PM_{2.5}$ impacts. The EPA provides adequate flexibility to the SAPRAs and permit applicants to showcase any methods or alternative models on a case-by-case basis, subject to EPA's regional office approval (EPA, 2014).

The new guideline for PM2.5 permitting details three types of secondary PM2.5 assessments. The first type is a qualitative assessment. An acceptable qualitative assessment requires,

> "a well-developed modelling protocol that includes a detailed conceptual description of the current air pollution concentrations in the area and of the nature of the emissions sources surrounding the new or modifying emissions source" (*Guidelines for PM2.5 Permitting*, US EPA, 2014)

Qualitative assessment demands very detailed description of PM2.5 concentrations which are almost impossible to generate. Some of these details include but not limited to establishment of several PM2.5 monitoring networks, full PM

chemical speciation, spatial and temporal pattern analysis on ambient pollutant levels for a number of years, seasonality and characterization of meteorological conditions on such great details (EPA, 2014).

The second type is the full quantitative assessment which is basically the use of CMAQ modelling system. This method surely demands multi-level data inputs in order to structure the appropriate photochemical grid application. The EPA actually does not prescribe in detail how to use the photochemical grid models for demonstrating NAAQS compliance since the required data inputs involve case-specific factors that would necessitate a long-term continuous consultative process with the appropriate permitting authority (EPA, 2014).

A good compromise is the hybrid assessment. It acknowledges the possibility of quantifying secondary PM2.5 impacts by converting emissions of precursors into equivalent amounts of direct PM2.5 emissions.

By using an idealized aerosol flow reactor, the formation of secondary aerosols from ammonia and sulfur dioxide was empirically studied. The resulting direct secondary PM2.5 from ammonia could potentially provide a preliminary basis for the development of a more refined value for secondary PM2.5 EF based on future field studies. The development of a secondary PM2.5 EF is essential for the conduct of an appropriate and fair PM2.5 impact analysis, particularly for commercial cattle feed operations.

II.1.1. Ammonia Emissions from CAFOs

Livestock production is the largest emitter of ammonia (NH_3) in the atmosphere amongst agricultural activities (Arago & Heber, 2006). Farm animals normally consume huge amount of nitrogen-rich substances as part of their feeding operations. Ammonia emissions normally come from the animal housing, manure storage, feedlots, and manure land applications. Figure 1 shows the relative contribution made by various U.S. sectors in terms of NH_3 emissions. Roughly about 85% of NH_3 emissions come from livestock operations with more than half coming from feed yards.

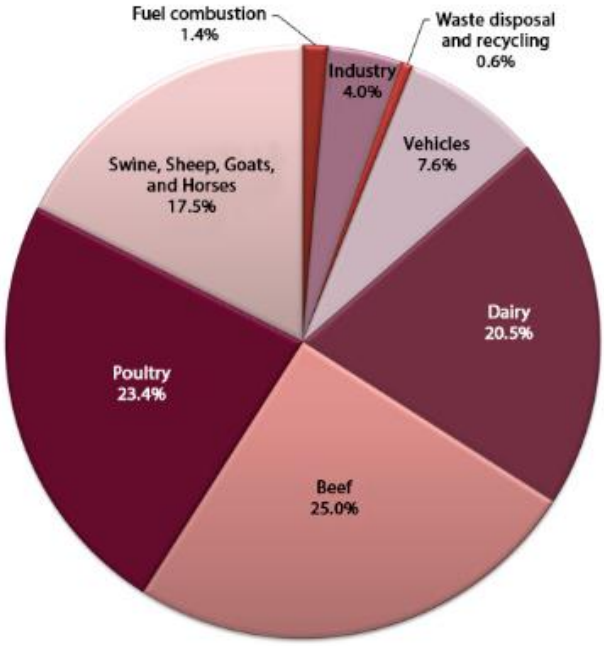

Figure 1. Estimated contributions of various US ammonia sources based on the National Emissions Inventory (EPA, National Emissions Inventory, 2008)

In the United States, ammonia is classified to be a hazardous substance due to its potential threat to health and environment (Preece, Cole, Todd, & Auvermann, 2012). Previously, farms were exempted from reporting hazardous substance released to the air. However, the U.S. Court of Appeals overruled this exemption and required farms to report NH_3 emissions in excess of 100 pounds (45 kilograms) per day as early as January of 2018 (EPA, 2018). These regulations were under two environmental laws, the Emergency Planning and Community Right-to-Know Act (EPCRA) and Comprehensive Environmental Response, Compensation and Liability Act (CERCLA). Non-compliance with NH_3 emission reporting could result to criminal charges, fines of $37,500 per day and up to five years of imprisonment.

Ammonia is perceived to be one of the major precursors of fine particulate matter from agricultural operations. Federal and state regulations could indirectly address NH_3 emissions in relation to $PM_{2.5}$ concentrations under the NAAQS. It may be necessary to directly reduce NH_3 emissions to obtain a reduction in $PM_{2.5}$ concentrations, especially for non-attainment areas. States like Idaho and California have already started to impose PM2.5 regulations directed towards ammonia emissions. Dairy farms with the potential of emitting more than 100 tons per year of ammonia were required to comply under the Permit by Rule program (Preece, Cole, Todd, & Auvermann, 2012).

In Central Texas open lot dairies, ammonia emission rates of 24.7 ± 25.4 kg/day for winter and 63.1 ± 31.1 kg/day for summer were reported using

chemiluminescence-based analyzers. In summer, about 65% of overall NH_3 emissions come from the dairy lagoons. Compost and free-stalls contribute to 77% NH_3 emissions during winter (Mutlu, et al., 2004). In 2009-2012, a team of researchers from Texas A&M University and Kansas State University simultaneously launched air sampling on cattle feed yards in the Southern Plains. Ammonia emission factors in dairy farms were within the range of 0.82 to 250 g ammonia per cow per day, with an annual average of 52 g per cow per day. Higher emission factors were reported for beef feedlots where the average is 199 g ammonia per animal per day. The daily ammonia N loss was between 25 to 50% of the N excreted in manure (Hristov, et al., 2010). Another independent study was conducted in the Texas Panhandle for two commercial cattle feedlots. Data were collected from 2007 to 2009 with average seasonal emission factors reported to be 71 g NH3-d per hear per day during the winter and 158 g NH3-N per head per day during the summer (Todd, et al., 2010). For a Texas feed yard with 24,000 cattle feeding capacity, a per head pen surface emission was reported to be 85.3 g NH3 per animal per day (Rhoades, et al., 2010).

II.1.2. Formation of Ammonia in Feedyards

When NH_3 combines with other airborne chemicals and particles, PM or solid aerosol formation is encouraged. At the lower atmosphere, NH_3 reactions with sulfur oxides (SOx) and nitrogen oxides (NOx) in the air are much favored to form ammonium aerosol particulates. These ammonium fine aerosols account for 40% to 50% of secondary $PM_{2.5}$ (Anderson, Strader, & Davidson, 2003). Upon conversion to

ammonium aerosols, they can stay suspended in the air for up to 15 days and can travel larger distances downwind of CAFO facilities (Aneja, Chauhan, & Walker, 2009).

In a feedyard, ammonia is often assumed to move from the source area to the atmosphere. Ammonia deposition might occur when the atmospheric NH_3 concentration is higher than the concentration at the surface. However, this is rarely observed at the feedyard surface (Rhoades, et al., 2010). Much of the excreted N from the animals are often in the form of urea. In order to transform urea into ammonium (NH_4) and NH_3, it has to undergo either urea hydrolysis or manure decomposition (Waldrip, Rotz, Hafner, Todd, & Cole, 2014).

Most of NH_3 in CAFOs is volatilized from urine areas via urea hydrolysis. Up to 80% of the urea (CH_4N_2O) in urine can be hydrolyzed into ammonium within 2 hours of urination. Ammonium can then be easily converted into NH_3, a form which is ready for volatilization (Vallis, Harper, Catchpoole, & Weier, 1982). The generally accepted pathway for urea conversion to NH_3 is shown in equation II.1a to II.1c (Hausinger, 2004)

$$CH_4N_2O + H^+ + 2H_2O \rightarrow HCO_3^- + 2NH_4^+ \quad \textit{normally within pH of 6.5 to 8.0} \qquad \text{(II.1a)}$$

$$HCO_3^- + H^+ \rightarrow CO_2 + H_2O \qquad \text{(II.1b)}$$

$$2NH_4+ \leftarrow\rightarrow 2NH_3^- + 2H^+ \qquad \text{(II.1c)}$$

The equilibrium reaction 1c favors the forward conversion of ammonium (NH_4) to NH_3 as pH increases. At pH of greater than 8, a molecule of urea can be rapidly hydrolyzed into two molecules of NH_3 which is readily released into the atmosphere.

Another source other than the urine areas are the manure spots. Bacterial degradation converts the N present in the manure into NH_3. The urease produced by microorganisms in the feces transforms the readily available urea once manure is exposed to air on the barn floor or feed lots. Cattle manure pH is typically around 8 which encourage fairly rapid ammonia loss into the atmosphere (Ishler, 2015).

II.1.3. Ammonia as Secondary PM2.5 precursor

In July of 2016, the EPA Final Rule for areas designated as non-attainment for $PM_{2.5}$ identifies sulfur dioxide, NOx, volatile inorganic compounds and NH_3 as $PM_{2.5}$ precursors. It is presumed that these precursors should be addressed in attainment planning, particularly if their levels contribute significantly to $PM_{2.5}$ formation (EPA, 2016).

The portion of PM2.5 components coming from secondary formations (sulfates, nitrates, ammonium and organic carbon) was previously reported by EPA to vary within a wide range from 30% to 90%. Table 1 presents the relative breakdown of these major components and their precursors (Hodan & Barnard, Evaluating the Contribution of PM2.5 Precursor Gases and Re-entrained Road Emissions to Mobile Source PM2.5 Particulate Matter Emissions, 2004). The main sources of primary PM2.5 are black carbon (or soot) and fugitive dusts or soil particles. Majority of the secondary PM2.5 are formed through the chemical reactions of ammonia with either SO_2 or NOx (in the presence of water) which usually produces ammonium sulfates or nitrates, respectively.

Table 1. Minimum, maximum and average contributions of major species to ambient PM2.5 concentration levels.

PM2.5 Component*	Minimum	Maximum	Average
Soil (1^o)	2%	25%	7%
Black Carbon (1^o)	11%	41%	27%
Sulfate (2^o)	7%	47%	24%
Nitrates (2^o)	4%	37%	13%
Ammonium (2^o)	3%	20%	13%
Organic Carbon (2^o)	2%	22%	10%

*1^o = primary; 2^o= secondary

The ammonium aerosols from the hydrous reaction between SO_2 and NOx are considered highly variable and depends on spatial and meteorological factors such as temperature and humidity. NOx reactions was not considered on this study because of unstable physical state of resulting PM (shift between gas and condensed phase). For hydrous reaction involving ammonia and SO_2, the typical chemical reaction pathway involves the oxidation of SO_2 to SO_3 via reactions with hydroxides (OH^-), the latter produced by interaction between water vapor and gaseous oxygen. The reaction of SO_3 with water then produces sulfuric acid (H_2SO_4). However, SO_2 can also be directly oxidized upon reaction with O_2 (Hirota, Makela, & Tokunaga, 1996).

The resulting sulfuric acid can form sulfate aerosols with ammonia or ammonium, based on the two over-all reactions shown in eq'n II.2 (Hirota, Makela, & Tokunaga, 1996).

$$2NH_4^+ + SO_4^{2-} + ½\ O_2 + H_2O \rightarrow (NH_4)_2SO_4 \qquad \text{(II.2.a)}$$

$$2NH_{3(g)} + SO_{2(g)} + ½\ O_{2(g)} + H_2O_{(g)} \rightarrow (NH_4)_2SO_{4\,(s)} \qquad \text{(II.2.b)}$$

The abundance of ammonia in cattle feed operations can potentially encourage the formation of secondary particulates upon reacting with precursor gases such as SO_2. Aside from ammonia, hydrogen sulfides (H_2S) are also present in the cattle feed yards at a considerable level of concentration (Preece, Casey, & Auvermann, 2012). These gases are naturally occurring and accompanied by a foul smell like rotten eggs. The H_2S is commonly produced from feedyard surfaces, particularly in areas such as feeding pens and manure piles. A considerable amount of H_2S in the atmosphere can also contribute to the SO_2 levels upon reaction with gaseous oxygen according to the equation II.3. shown below,

$$2H_2S_{(g)} + 3O_{2\,(g)} \rightarrow 2H_2O_{(l)} + 2SO_{2(g)} \qquad \text{(II.3)}$$

II.1.4. Scope and Limitations of the Study

For this study, the primary goal was only to generate a preliminary estimate of a direct secondary $PM_{2.5}$ from ammonia, mg $PM_{2.5}$ per mg of NH_3.

The resulting PM was characterized based only on general appearance and particle morphology, elemental composition, final products formed, and particle size distribution (PSD). There was no attempt to distinguish the identified compounds based on their compositional distribution in the PM sample. Only the presence of the possible compounds was considered from the results of the characterization analysis. Fundamentals of aerosol nucleation and particle growth were used to elucidate the PM formation process. However, in-depth analyses of particle formation were considered beyond the scope of this study.

The conditions of this experiment do not aim to simulate the atmospheric conditions. It is a well-known fact that the atmosphere is a stochastic medium and almost all variables governing the simultaneous physical and chemical processes are impossible to control. There is no way to single out a single mechanism to fully explain particle formation from precursor gases. The gas-to-particle (GTC) conversion for secondary particles is a complex process, and despite increasing sophistication of analysis techniques and detection instruments, these technologies are still not enough to answer all questions concerning the mechanism for secondary particle formations (Lushnikov, Zaganov, & Lyubovtseva, 2010).

The use of aerosol flow reactors was meant to provide better control of experimental variables, thereby generating an idealized condition to fully account the PM formation only from the intended reacting gases, NH_3 and SO_2, in the presence or absence of air. The controlled variables in this study primarily include reactant ratio, reaction time and gas mixing flow rates.

However, the use of laboratory-scale flow reactors could provide some significant limitations. The concentrations of precursor species involved in the flow system are normally higher than those found in the lower atmosphere, which could potentially contribute to inconsistencies between laboratory and field results (Ezzell, et al., 2010). The possible interaction of the gaseous species with the internal wall surface might also be an issue. Although heterogeneous reactions is a natural occurrence on boundary layer surfaces in the ambient environment, there is insufficient knowledge about these wall interactions.

II.1.5. Objectives

This study was conducted to characterize and empirically estimate the actual secondary PM formed resulting from the interactions of ammonia and sulfur dioxide, with and without the presence of O_2 (air).

Specifically, it was aimed to:

1. Empirically observe the behavior of gas mixing and particle formation from the reactions involving ammonia and sulfur dioxide in an aerosol flow reactor.
2. Characterize the particles formed from the ammonia-sulfur dioxide gas systems based on morphology, chemical composition, and size distribution.
3. Empirically estimate the direct secondary $PM_{2.5}$ formed from a unit amount of ammonia used.

II.2. Methodology

II.2.1. Experimental Flow Set-up

For the purpose of this investigation, simplified concentric tubular flow reactors were designed and fabricated. A rigid Polytetrafluoroethylene (PTFE) material was used to ensure excellent chemical resistance to corrosive gases, particularly anhydrous ammonia. It can withstand temperature range of -350 ^{o}F to 500 ^{o}F and in compliance with the ASTM D1710. The reactor consisted of a 2-in. diameter by 1-ft. long tube with four inlet swagelok fittings on the upstream portion, each with perforated feed teflon tubings that extend up to the closed tube end (see Figure 2). It was designed to accommodate up to four gas mixtures that can disperse radially along the centerline. Each reactor was carefully cleaned of any visible debris and dried inside a convection oven at 35^{o} C prior to installation.

There were four reactors prepared and each was assigned for an experimental treatment. All reactors were completely sealed to minimize any influences from the external environment. All three replicates were done for every treatment using the same reactor. The only method of cleaning was N_2 sweeping at an elevated flow rate to remove possible residual PM inside the system. However, this method was later considered ineffective as PM residues on the internal wall surface were recovered after using each reactor.

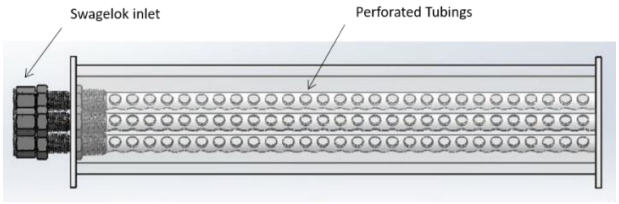

(a)

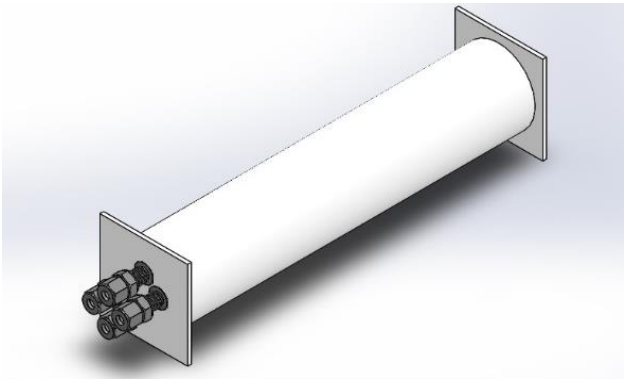

(b)

Figure 2. Fabricated Reactor Vessel (a) Internal view showing perforated feed tubings; (b) external view of the reactor

A schematic of the experimental gas mixing system is shown in Figure 3. The reacting gases consist of a certified pre-mixture of SO_2 (1.70% v/v) with N_2 balance, N_2 with 2% v/v water content and pure, anhydrous NH_3. Zero air with combined CO and CO_2 impurities not to exceed 1 ppm was also introduced into the system (Airgas, Inc). The inlet flows for each gas to the reactor were fine adjusted using the needle valves installed to each gas lines prior to the Aalborg flow controllers. Each controller has one channel read-out, with an accuracy of ± 1.0 %. All flow rates were recorded every minute. Check valves were installed to ensure no backflow of gases from the reactor will occur during the experimental runs. The reactor was connected to a modified total suspended particle (TSP) sampler loaded with a PTFE 47 mm quartz microfiber filter with an effective pore size of 2 µm. A vacuum was induced downstream of the gas

mixing system to direct the total flow towards the filter and overcome the pressure drop across the filter.

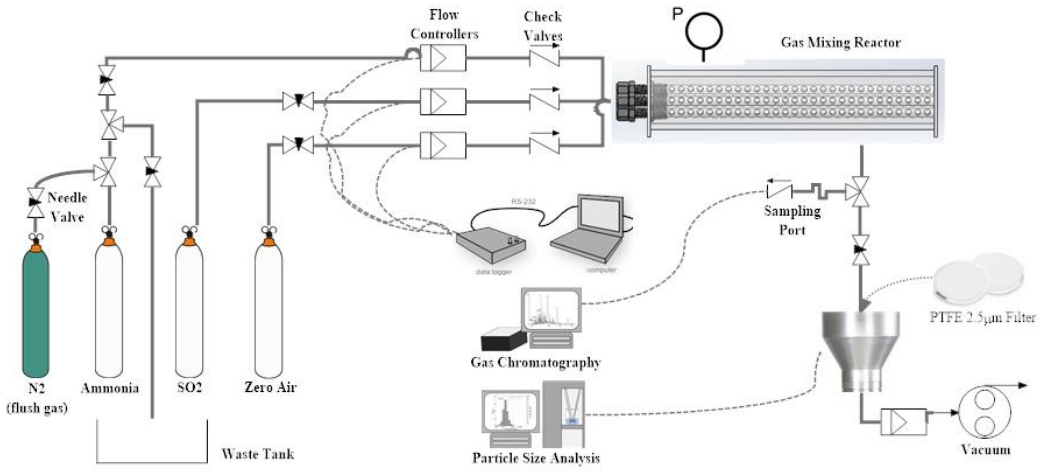

Figure 3. Experimental Schematic for the Gas Mixing System.

The gas flow line for the pure NH_3 has a bypass valve for initial purging every start-up and sweeping (cleaning) prior to shut down. Purging and sweeping using N_2 was done to remove traces of possible residual NH_3 and moisture in the gas line.

II.2.2. Operating Protocol

The procedure developed for the experiment consist of four main steps as shown in Figure 4. The first is the *start-up phase* which involves cleaning the gas lines and reactor with a non-reacting gas, in this case N_2 gas. The needle valve leading into the reactor was kept closed to initiate purging of NH_3 gas towards a waste reservoir. This process is necessary to minimize any trace moisture or ammonia from previous runs. The only source of water vapor during the reaction was assumed to come from the N_2

gas tank. After purging for 3 minutes, the valve leading towards the waste tank was closed and N_2 gas was introduced into the system for another 5 minutes at a flowrate of 2 L/min. The total start-up phase lasted for about 8 minutes.

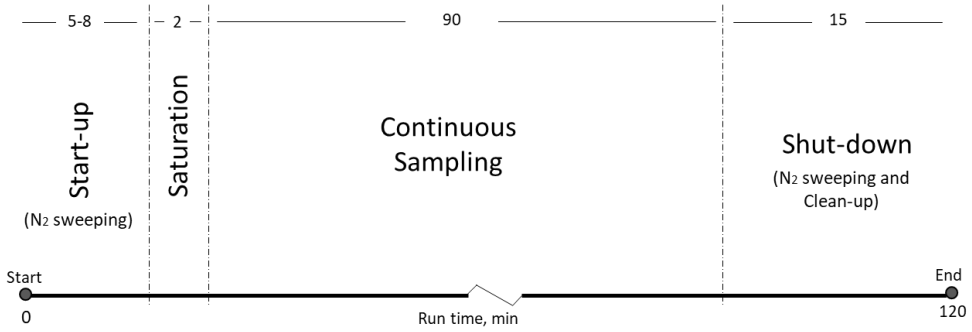

Figure 4. Four-stages of the Experimental Operating Protocol

The second stage is the *saturation phase.* The reacting gases were introduced into the system until the whole reactor was completely filled. The time required to saturate the reactor was based on the equation II.4.,

$$t_{sat} = \frac{\dot{v}}{V} \qquad \text{(II.4)}$$

Where,

$\dot{v}$ = total gas flowrate, L/min

V = volume of the reactor, L (~0.20 L)

The total gas flow within the system was kept under 1 L/min. It takes about 10 – 15 s to achieve saturation which corresponds to a pressure reading of about 0.10 psig. All downstream valves remained closed for another 2 minutes before starting the actual sampling period. The third stage is the *continuous sampling* using a modified TSP filter collector connected downstream of the reactor. The vacuum pump was set at

approximately 0.8 to 1 L/min to start the sampling phase. Once the needle valve was opened towards the filter, the pressure at the reactor started to drop and stabilize around 0 psig. The whole process continued until either the reactor pressure reading started to increase or the vacuum flow rate started to decrease significantly which signals the accumulation of the PM on the surface of the filter. This usually takes place for about 60 minutes after the onset of sampling phase. Sampling is continued for another 30 minutes and all valves were then closed. The vacuum was turned off and all gas lines were shutdowned. The total sampling time lasted for about 90 minutes.

The final stage was the *shutdown phase.* After closing the vacuum and all reacting gas lines, the filter was carefully removed from the sample collector and immediately transferred into a filter cassette. The filter cassette should undergo a static eliminator prior usage. This step is important to minimize the attachment of the PM, which are primarily fine and charged particles, unto the cover of the container. Any attached PM can be considered as losses prior to weighing of the final filter.

After the filter was removed, the collector was closed and the N_2 gas was reintroduced into the system at 2 L/min for about 15 minutes. All downstream gas lines were cleaned with acetone solution and dried inside a convection oven in preparation for the next replicate.

II.2.3. Sample Characterization

The preparation of filters (Whatman) used, PM recovery and post-weighing were all based on the Standard Operating Procedure for PM Gravimetric Analysis (EPA, 2008). All filter cassettes (Pall Laboratory) were sterilized by gamma irradiation and are

tight sealed to lock in humidity. Each cassette was passed through an anti-static system (Mettler Toledo) prior usage.

Filters were pre-weighed and conditioned inside a desiccator under room temperature. After each run, the filters together with the recovered PM passed through an anti-static system in order to neutralize disruptive electrostatic charged particles that may distort precise weighing. The pre- and post-weighing of the PM samples continue until the change in the mass read-outs was within ± 5%. An ultra-microbalance (Sartorius) with 0.1 µg readability was used. The difference between the initial and final weights corresponds to the weight of the PM particles, reported in milligrams (mg).

The PM particles were subjected into physical and chemical characterization. The summary of the analyses is presented on Table 2.

Table 2. Summary of analytical techniques used for PM characterization.

Target Characteristics	Instrument/Technique
Carbon, hydrogen, oxygen, nitrogen, sulfur (elemental composition, C-H-O-N-S)	vario El Cube Elemental Analyzer
Chemical Composition	Fourier Transform Infrared Spectroscopy (FTIR)
Surface Elements	Energy-dispersive X-ray spectroscopy (EDS)
Physical Appearance (shape and morphology)	Scanning Electron Microscopy (SEM)
Particle Size Distribution	Beckman Coulter Counter

Elemental analysis was carried out using a vario El Cube Elemental Analyzer (Elementar). About 2 mg of the PM sample was used for the elemental analysis. The results were reported as percent by weight of each element corresponding to C, H, O, N

and S with a precision of ±0.30% and a limit of detection of < 0.10%. Since the reacting gases were assumed to contain negligible amount of C, any C present in the PM sample should indicate probable presence of any carbon-based contaminants such as dusts inside the gas flow system.

To further validate the identity of the PM sample, a Fourier-Transform Infrared spectrophotometer (IRAffinity-1S Shimadzu). The use of FTIR has been recognized globally in identifying and characterizing different materials and products. Only qualitative FTIR analysis was carried out for this experiment.

The analysis procedure follows that of the ASTM E168 for standard practices for general techniques of infrared qualitative analysis (ASTMInternational, 2017). FTIR identifies functional groups and characterizes covalent bonds of the unknown sample by producing an infrared absorption spectrum. The resulting spectra produce a sample profile that serves as a "molecular fingerprint" that can be scanned and compared with the profiles of universally accepted standard compounds.

The FTIR measures the infrared region which is within the 0.7 μm to 1000 μm of the electromagnetic radiation (ER) spectrum. The basic idea at work is that the different bonds that exist between element or functional groups absorb light at different frequencies when subjected to infrared radiation (IR). The most attractive wavelength of the infrared region for chemical analysis is between 2.5 μm and 25 μm (4000/cm to 400/cm). This portion of the spectra ideally includes the frequencies representing the fundamental vibrations of virtually all of the functional groups of both organic and inorganic molecules (Doyle, 1992). The analysis was carried out on that infrared region.

At specific wavelength ranges, spectral bands are generated for a certain number of functional groups which then serve as the fingerprint for the unknown compound. Figure 5 illustrates the wave numbers and functional group correspondence which are typically used as guide for compound identification. For N-H compounds such as NH_3 and NH_4, it is expected to produce a spectral band at wavelength number between 1500/cm to 1200/cm and another at the range of 4000/cm to 3000/cm.

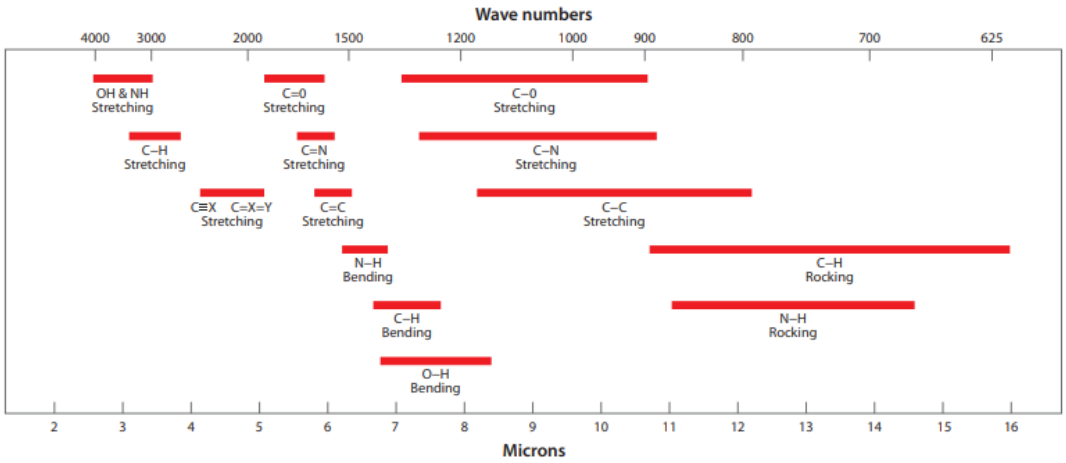

Figure 5. Example IR absorption of functional groups for identifying unknown products (Sigma-Aldrich, 2012)

The over-all particle morphology and surface elemental characterization was also determined using a Tescan Vega Scanning Electron Microscope (SEM) of the Microscopy and Imaging Center of Texas A&M University. It is equipped with an Oxford EDS detector that allows elemental analysis, particularly on the surface of the particle. Unlike the FTIR that depends on the vibrational absorbance of functional groups, the EDS relies on the uniqueness of the atomic structure that produces a unique set of spectral peaks (bands) upon interaction with X-ray light.

The particle size distribution (PSD) was generated for every reactant ratio. The PM sample was mechanically agitated for 5 min and subjected to coulter counter analysis. The sample is suspended on a low concentration electrolyte (3% Lithium chloride-methanol) solution. Two electrodes can be found, one inside the aperture tube and another outside of the tube, to generate an electric field. Particles pass through the aperture that serves as the "sensing zone" while being mechanically agitated. When particles enter the aperture, it creates an impedance that is measured as a voltage pulse or a current pulse. The basic theory at work is that the pulse height is proportional to the volume, and with a given density, as well as mass of the sensed particle (Beckman Coulter, 2016). About 100,000 particles were counted in about 300 bins with different size thresholds to generate a smooth particle size distribution.

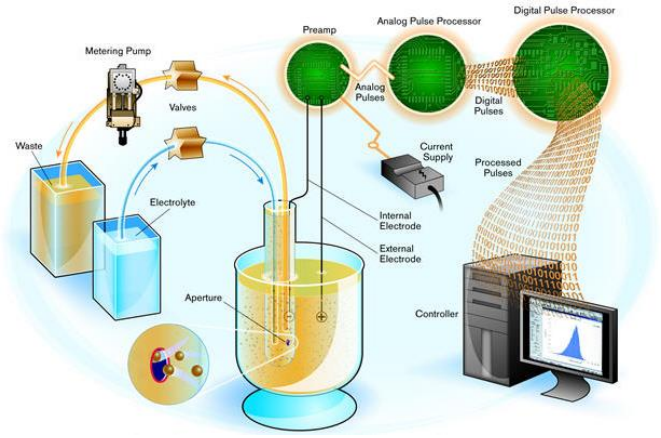

Figure 6. The coulter counter principle adapted from (Beckman Coulter, 2016).

II.2.4. Data Analysis

The experiments were conducted at approximate ammonia to sulfur dioxide reactant ratios of 5:1, 10:1 and 30:1 for the treatments without air; and two more

treatments where SO_2 is further diluted producing a 60:1 ratio in the presence of 10% and 20% O_2 (Table 3). All treatment levels were replicated three times.

Table 3. Summary of treatments at different reactant ratio and concentration levels.

	Treatments (Reactant Ratio)				
	without Air			with Air	
	5:1	10:1	30:1	60:1:10%	60:1:20%
NH3 concentration, ppm	10 000	10 870	10 000	9 850	10 800
SO2 concentration, ppm	1 850	1 100	340	165	180
O2 concentration, %	-	-	-	10	20

The elemental analysis results were used to estimate the N/S atomic ratio of the product PM. On the basis of the total sulfur content in the solid products, SO_2 conversions at different reactant ratios were determined by equation II.5 (Guo, Liu, Huang, Liu, & Guo, 2005).

$$X\%\ (SO_2) = \frac{m_s/M_s}{\dot{V}\, C_{SO_2}\, t} \text{ x } 22400 \text{ x } 100\% \qquad \text{(II.5)}$$

Where,

$X\%\ (SO_2)$ = SO_2 conversion efficiency

m_s = mass of sulfur in the solid PM, mg

M_s = atomic mass of S, 32 g/mol

$\dot{v}$ = total volumetric flow rate, ml/min

t = sampling time, min

C_{SO2} = inlet concentration of SO2, %v

22 400 = molar volume, ml/mol

The PM production rate was simply calculated using the equation II.6

$$PM_{rate} = \frac{m_{pm}}{t_{sp}} \qquad \text{(II.6)}$$

Where,

m_{pm} = mass of PM recovered, mg

t_{sp} = total sampling time, min

The equivalent direct secondary $PM_{2.5}$ formed from NH_3 can be estimated from the equation II.7. This requires the PSD of the recovered PM and the percentage cut of all the particles with diameters ≤ 2.5 µm (% $PM_{2.5}$). A unit PM emission is defined as $\frac{m_{pm}}{m_{NH3}}$.

$$2^0\text{PM2.5 Emission} = \frac{m_{pm}}{m_{NH3}} \text{ x \% PM2.5 from PSD} \qquad \text{(II.7)}$$

Where,

m_{pm} = mass of PM recovered, mg

m_{NH3} = mass of NH_3 used, kg

Two cases were considered in order to account for the mass of PM recovered, m_{pm}, from the experiment. The *first case* was to only consider the mass collected on the filter as the m_{pm}. The PM rate was only based on the sampling time of each replicate (90 min). The *second case* was to include the mass of the PM collected on the reactor wall surface (which was initially considered as losses) with that of the mass collected on the filter. Altogether, they both comprise the m_{pm}. It should be noted that the mass of PM due to wall losses correspond to the total losses generated from the three replicates of each treatment. Since the reactors were completely sealed, there was no way of opening them up until all the replicates were completed. Hence, the second case provides an average based on the total PM recovered over the combined total sampling time of the 3 replicates (270 min).

The secondary $PM_{2.5}$ emission factor for cattle feedyard was be defined as the 2^o PM2.5 per number of cattle in thousands per day (based on ammonia emissions). This was calculated using the equation II.8.

$$2^0\mathrm{PM}_{2.5}\ \mathrm{EF} = (2^0\text{PM2.5 Emission})\mathrm{x}\ (\mathrm{NH}_3)\mathrm{EF} \qquad \text{(II.8)}$$

Where,

m_{pm} = mass of PM recovered, mg

m_{NH3} = mass of NH_3 used, kg

NH_3 EF, kg NH_3/1000 heads/day

Using a primary $PM_{2.5}$ to PM_{10} ratio of 10% and a reported PM_{10} EF of 15 lbs per 1000 heads per day (Parnel, Shaw, & Auvermann, 1998), a cattle feedyard primary $PM_{2.5}$ estimate was computed to be 0.682 kg 1^o $PM_{2.5}$/1000 head-day. The experimental ratio was estimated as,

$$\frac{2^o\ \mathrm{PM}_{2.5}}{1^o\ \mathrm{PM}_{2.5}} = \frac{2^o\ \mathrm{PM}_{2.5}\ \mathrm{EF}}{0.682} \qquad \text{(II.9)}$$

A single-factor analysis of variance (ANOVA) was conducted to evaluate any statistical difference between the resulting emission factors in relation to the varying reactant ratios, particularly between the runs with and without the presence of air (or O_2). The values $P < 0.05$ were considered statistically significant. JMP interactive statistical software by the SAS Institute Inc. was used for the statistical analysis.

II.3. Results and Discussion

The gas-to-particle (GTP) conversion is a term applied to all phase transition processes by which gases are transformed into either the liquid or the solid state. In most cases, the initial step in the GTP conversion is *nucleation* (Kaschiev, 2000). The latter can happen as "homomolecular" or "heteromolecular" nucleation, depending on whether only one gas or at least two different gases simultaneously interact to form a liquid or solid phase (Stauffer & Kiang, 1973). If there are no pre-existing solid or liquid phase within a gaseous system, then the nucleation is considered homogeneous. If the particle formation occur on existing solids or liquid phase, then the nucleation is known to be heterogeneous (Friedlander, 2000).

In the atmosphere, nucleation can either proceed through physical or chemical means. A supersaturated state should be reached then followed by a collapse through aerosol formation. The physical processes typically involves adiabatic expansion, cool air mixing or radioactive and conductive cooling. The chemical processes normally involves oxidation of gaseous species such as SO_2 to form sulfuric acid (Friedlander, 2000). The formation of condensable species in the gas phase brings the whole system into a non-equilibrium state. A nonequilibrium system will always try to achieve equilibrium by either the production of new particles (homogenous nucleation) or by condensation and growth on existing material (heterogeneous nucleation).

Homogeneous nucleation between SO_2 and water vapor (heteromolecular), can transform high vapor pressure SO_2 gas into a lower vapor pressure H_2SO_4 gas which can readily condense into very small droplets. These droplets can either stick to each other

without any external influence (spontaneous nucleation) or condense on existing aerosol particles. The resulting molecules can form clusters and grow into particles. When these several clusters further stick to each other, larger particles are formed - a process called *coagulation.* Molecules can either evaporate from such particles, or can also condense on their surfaces. In the atmosphere, the initial heteromolecular nucleation process happens simultaneously with particle growth and coagulation (Stauffer & Kiang, 1973).

Nucleation measurements for spontaneous homogeneous aerosol formation from reacting gaseous species are difficult to verify. Most of the nucleation theories can only be verified through a steady-state and perfectly clean conditions which is almost impossible to achieve (Gamera & de la Mora, 2000). For this study, there was no attempt to measure the kinetics and mechanism of particle formation between ammonia and sulfur dioxide. The conditions used for the study was not considered perfectly clean. Hence, the gas-to-particle conversion was hypothesized to be more dominated by heterogeneous nucleation rather than spontaneous and homogenous nucleation.

Heterogeneous nucleation can be viewed as a surface catalyzed process, or even an assisted nucleation process. Both the NH_3 and SO_2 species can interact either on the walls of the reactor (deposition) or with any foreign particles suspended along with the reacting gases. It is known that if large aerosols are already present, the heterogeneous nucleation takes over even at much lower trace gas concentrations (Stauffer & Kiang, 1973).

In a very non-ideal environment such as the atmosphere, heterogeneous nucleation might occur much more often than homogeneous nucleation. However,

homogeneous nucleation was still accounted for this study since this involved an idealized mixing of reacting gases without air. Previous studies that focused on the formation of atmospheric aerosols reported gas-phase reactions of NH_3-SO_2 that can result in direct homogeneous formation of solid products. Gaseous adduct of NH_3-SO_2 can be generated from mixing of these two gases at different reactant ratios. It can result into a water-catalyzed nucleation process that produces a precursor solid particle for further reaction with remaining water vapor and oxygen. The complete nucleation model yields a final sulfate or sulfite product (Vance & Peters, 1976).

Further discussions of relevant GTC principles and overview of suggested particle formation mechanisms that took place within the flow system are presented in Production Rates and PSD discussions, (section II.3.5) of this chapter. However, the details of each processes are considered beyond the scope of this study.

II.3.1. Gas Flow Characteristics

The total flowrate of incoming gases, vacuum flow, and pressure changes inside the reactor were continuously monitored throughout each sampling period. Each run lasted for 90 minutes while the total flowrate entering the reactor was maintained at around 1.0 ± 0.20 L/min. The flow behavior of the whole system during sampling is shown in Figure 7.

Generally, the total incoming flow rates were slightly higher than the vacuum flow within 0.10 – 0.20 L/min range. At the start of sampling period (time = 0 min), the flow rates were observed to be higher than the set-point but later achieve stability after 5 to 10 minutes. The total gas flowrates were consistently stable after the 10 minute mark for all the observations, particularly for runs at low NH_3 levels (low reactant ratio).

The total flowrates during the reaction period were relatively stable for single component gas (1C) and binary mixtures (2C). However, fluctuations in the flow were observed to be more frequent upon mixing of more than 3 gases (Figure 7c & 7d). Generally, instability of flow is an indicator of mixing especially for single-phase flow patterns. Simpler flows often depend on inherent fluid properties, volume fractions and initial volume flux (Brennen, 2005). However, difference in the molecular weights of multi-component compressible gases becomes a significant factor on the stability characteristics of mixing (Kozusko & Lasseigne, 1996) together with disturbance brought about by spontaneous phase change (gas to solid) and pressure drop change due to particle-saturated particles.

Significant fluctuations in the incoming flowrates can be observed starting at 70 min mark. As the NH_3 levels increase, the fluctuations are further delayed until 75 min to 80 min during sampling. These fluctuations were accompanied by a steady drop of vacuum flow and an erratic increase in the pressure readings.

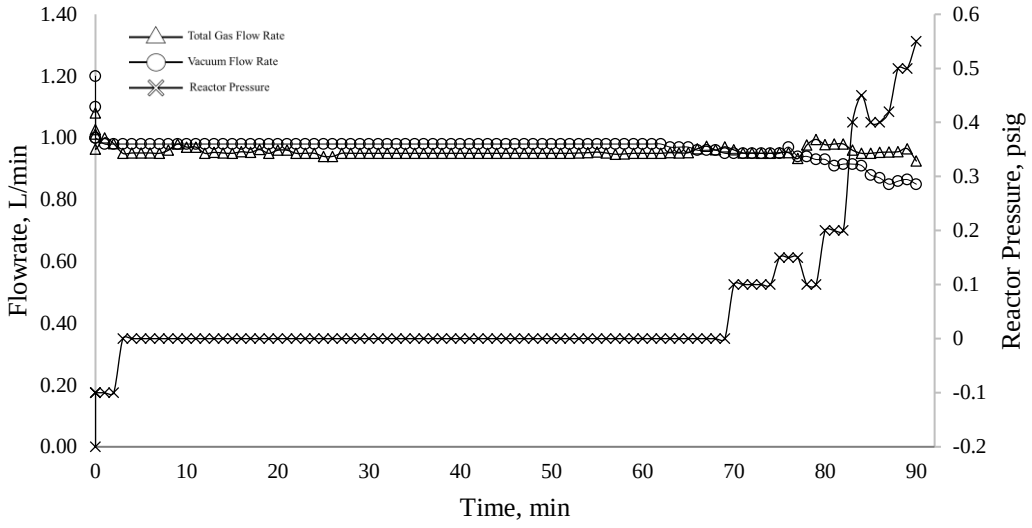

(a)

Figure 7. Flow behavior showing the total gas flow rates, vacuum flow and pressure reactor at different NH_3/SO_2 reactant ratios (a) 5:1; (b) 10:1; (c) 30:1; (d) 60:1:10% O_2 and (e) 60:1:20% O_2

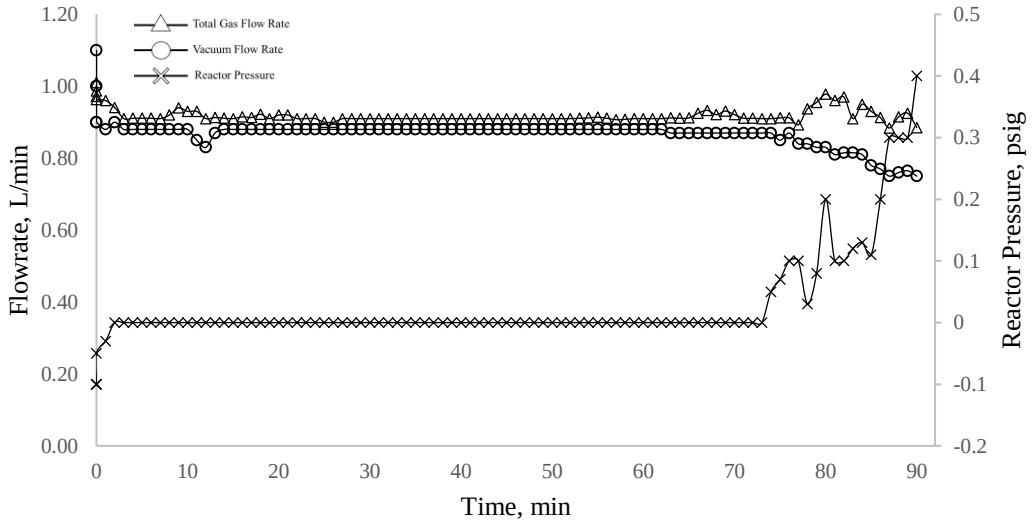

(b)

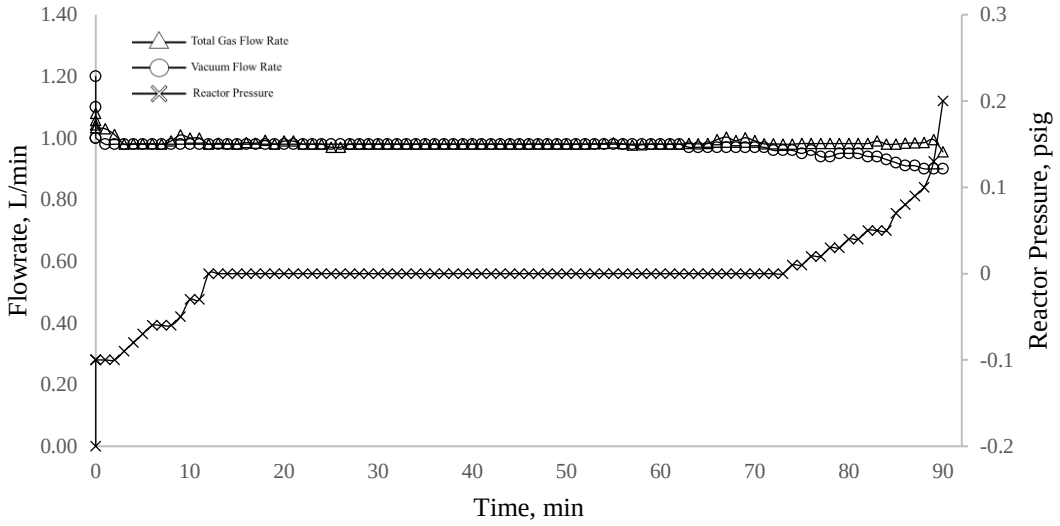

(c)

Figure 7 Continued

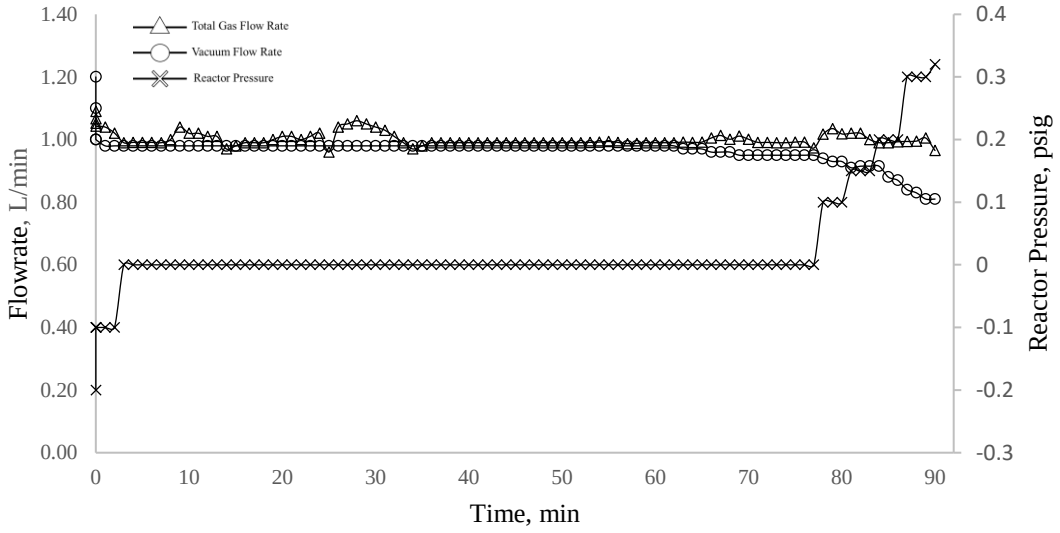

(d)

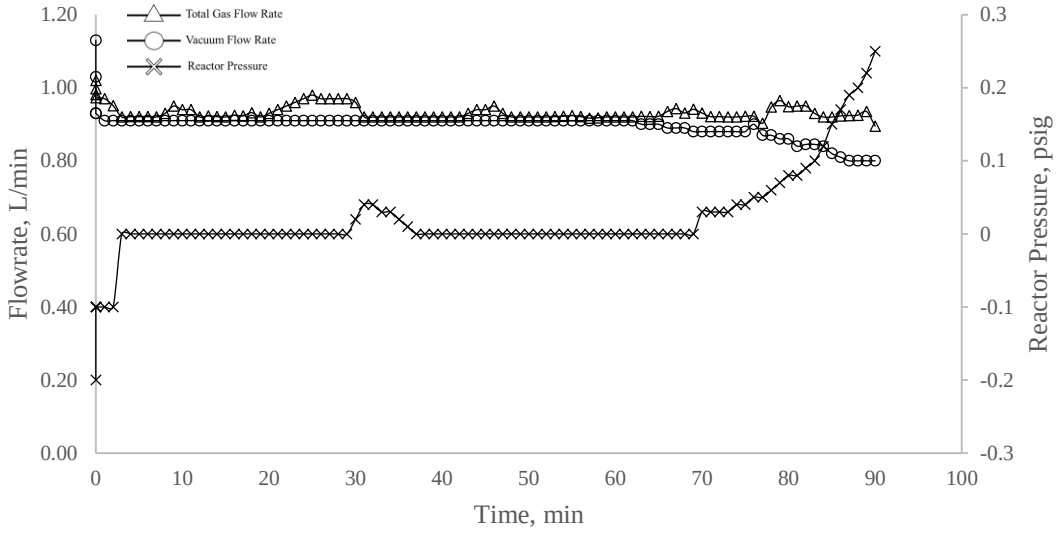

(e)

Figure 7 Continued

These flow rate fluctuations could signal the accumulation of PM on the filter surface. By looking into the flow behavior for all treatments, the flow disturbance on the incoming gases has a corresponding decrease on the vacuum flow. As more particles start to accumulate on the filter, it becomes harder for the vacuum pump to equalize the incoming and outgoing flows across the filter. As a result, the flow regulator for the vacuum records a decreasing flow through time as the filter becomes more saturated with PM. Meanwhile, erratic flow readings were recorded for the incoming gases because of the instability due to PM accumulation on the downstream end of the system.

Initially, an increase of internal pressure was expected during the saturation phase as the mixing gases fully occupy the whole reactor volume. Upon application of vacuum, the pressure inside the reactor was observed to spike below 0 psig during the sampling time of 1 – 3 min. However, the pressure reading immediately stabilizes around 0 psig when the flow of the incoming gases equalize with that of the vacuum flow. Without the vacuum, the gases will just accumulate within the system until it reaches the required pressure to permit the flow across the filter. The 0 psig reading inside the reactor only indicates that the vacuum induced to the system was able to overcome the pressure drop across the filter sampler. Thereby, ensuring a steady flow within the system during the sampling period.

However, during PM accumulation on the filter, the total flow in the system experiences an unsteady-state. It means that more gases remain in the reactor compared to the ones that exit towards the vacuum end. As a result, the pressure in the reactor

starts to build up within a range of 0.10 to 0.5 psig until the sampling is terminated at 90 min mark.

The flow through porous media is typically governed by the Darcy's Law which describes the influence of pressure drop across a filter thickness and filter permeability on the required flow rate within a flow system (Figure 8). Fluids will not flow across the filter until pressure gradient is higher than the value of threshold pressure gradient (TPG) dictated by the filter (Ren-yi, et al., 2016). The flow velocity is directly proportional to the flowrate and inversely proportional to the available flow area across the filter. The available area is dictated by the void spaces within the filter.

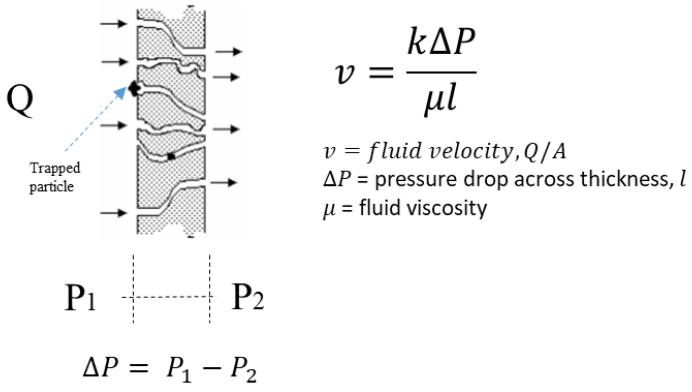

Figure 8. Fluid flow across a permeable filter under Darcy's Law.

The existence of particles trapped within these void spaces significantly reduces the available area for fluid flow. To preserve the continuity of flow, the entering gas stream will have to squeeze through the available smaller area. As a consequence, higher velocity (hence higher flowrate) is required to maintain a continuous flow across a restricted flow area due to particle clogging. By Darcy's law, higher velocity

requirement can be a consequence of increased pressure drop across the filter thickness which explains the increase of reactor pressure, P_1 during the latter part of the PM sampling period.

The evident flow disturbances within the system should be an indicator of PM formation. It is also possible that the presence of particles may have no direct effect on the bulk flow of the gases. However, the phase changes that happen within the gas system is undesirable for various flow metering technologies (NEL Technologies, 2012). The increasing concentration of particles (and additionally condensed droplets) in the gas stream can disrupt flow rate readings. However, in an ideal mixing flow condition, the gas-to-particle conversion was found out to cause sustained oscillations of particle density and affect the behavior of flow systems (Friedlander, 2000).

These resulting particles involved in a flow system are often characterized with the shape, size and chemical contents (Lushnikov, Zaganov, & Lyubovtseva, 2010). These characteristics are all presented on the following sections.

II.3.2. Chemical Composition

II.3.2.1. PTFE Reactor wall and reactant gases

The possible interaction between the internal reactor wall with the reactant gases was investigated by comparing the compounds present in the PM product with that of the reactor. A PTFE material is typically comprised of synthetic flouropolymer, consisting of a carbon and two flourine (F) atom links (CF_2) in a polymer unit called tetrafluoroethylene (Figure 9).

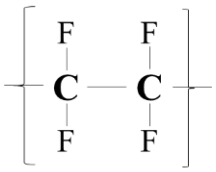

Figure 9. Tetrafluoroethylene polymer unit of PTFE materials.

Figure 10 shows the spectral bands generated from FTIR analysis of a sample taken from the inside of reactor wall. For PTFE materials, the C-F_2 asymetric stretching and C-C stretching corresponds to a spectral band around 1299/cm. A very sharp peak at 1199/cm indicate another C-F_2 symmetric stretching. On the lower end of the spectrum, medium and sharp peaks should be observed which indicate both CF_2 bending and CF_2 twisting, respectively. These peaks usually happen at around 553/cm and 507/cm (Mihaly, et al., 2006). All of these peaks were observed in the PTFE sample (see Figure 10). Additional peaks were observed between the range of 620-640/cm which should indicate C-F deformation.

The results of the FTIR confirm the presence of C-F bonds based on the previous spectral bands of PTFE generated from a comprehensive study of polymers using FTIR and FT-Raman spectroscopy (Mihaly, et al., 2006). The FTIR results of both the PTFE reactor and the PM sample were layered together to see whether the PM sample contains any presence of C-F functionality.

Figure 10 shows no overlap of spectral bands between the PM and reactor samples. The spectral bands generated from the PM sample indicate no presence of any C-F bonds. Therefore, the possible chemical interaction between the reactor and the

reacting gases was ruled out in this study. The elemental analysis of the PM provides further confirmation about this result (Section II.3.3.)

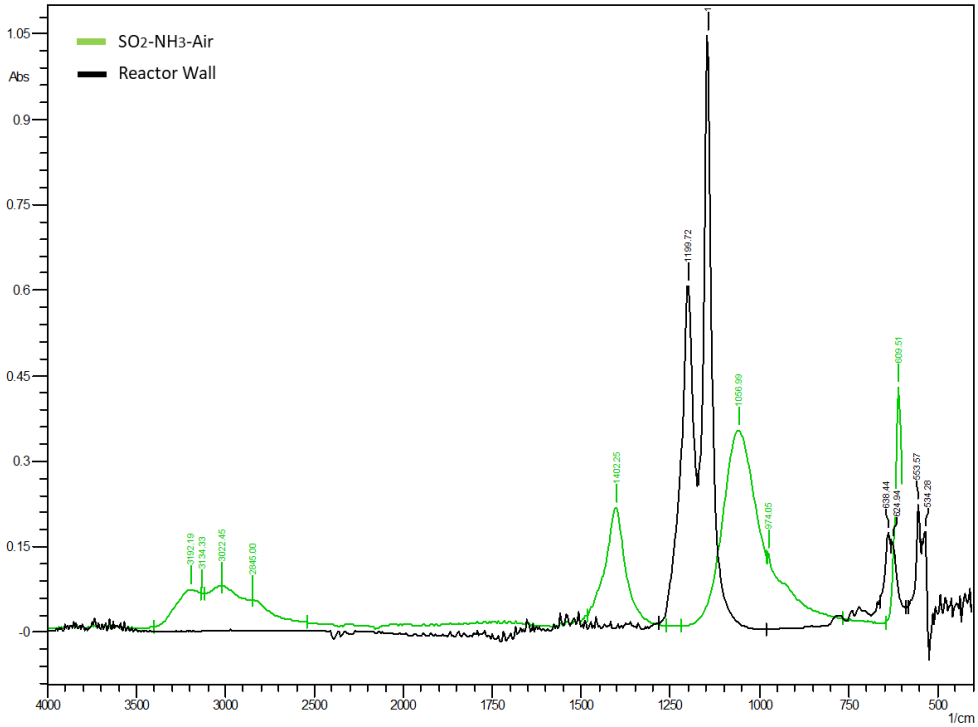

Figure 10. Spectral bands of both PTFE reactor wall material and PM product from SO_2-NH_3-Air.

II.3.2.2. FTIR Spectral Analysis

For reactions without air (or O_2), only the SO_2, NH_3 and N_2 were assumed to be involved in the flow system. Figures 11 to 13 present the FTIR spectra of the reaction products obtained at different NH_3:SO_2 ratios. Three strong absorption peaks (1-A, 1-B, 1C) accompanied by weak broad peaks between wavenumbers 2700 to 3500/cm indicate the presence of ammonium sulfate ($(NH_4)_2SO_4$). Sharp absorption peaks for ammonium sulfate can be normally observed within the ranges of 1000 – 1250/cm and 1300-1500/cm and a weak broader peak in the range of 2750 to 3400/cm (NIST, NIST

Chemistry WebBook, SRD 69, 2017). At the lower wavenumbers, the two strong peaks represent sulfates (SO_4^{2-}) while the weaker IR band that usually peaks at around 3050/cm represent ammonium ($NH4^+$) species (McClenny, Childers, Rohl, & Palmer, 1985).

Another noticeable peak (2-A) is not a characteristic of ammonium sulfate. But instead, sharp peaks between 750 to 1000/cm indicate intermediates products, which are within the S-O bond stretch (Hisatsune & Heicklen, 1975). The products display random peaks at the lower infrared region which can be assigned to a 1:1 adduct, amidosulfurous acid NH_3SO_2 and another 2:1 adduct, ammonium amido sulfite $(NH_3)_2SO_2$. However, the multiplicites of absorption bands observed in the lower spectrum suggests the latter adduct is more dominating. The medium peaks from 285-576/cm are characteristics of SO_2 deformations at lower energy, which makes these intermediate products relatively unstable.

The IR bands of these two adducts have also similarities with that of sulfite and bisulfite ions. It was reported that the spectra of these intermediate products were difficult to interpret. Extensive experimental data were gathered but unfortunately the solid sample was found out to be always contaminated with sulfite and bisulfite ions, and possibly with other species (Hisatsune & Heicklen, 1975).

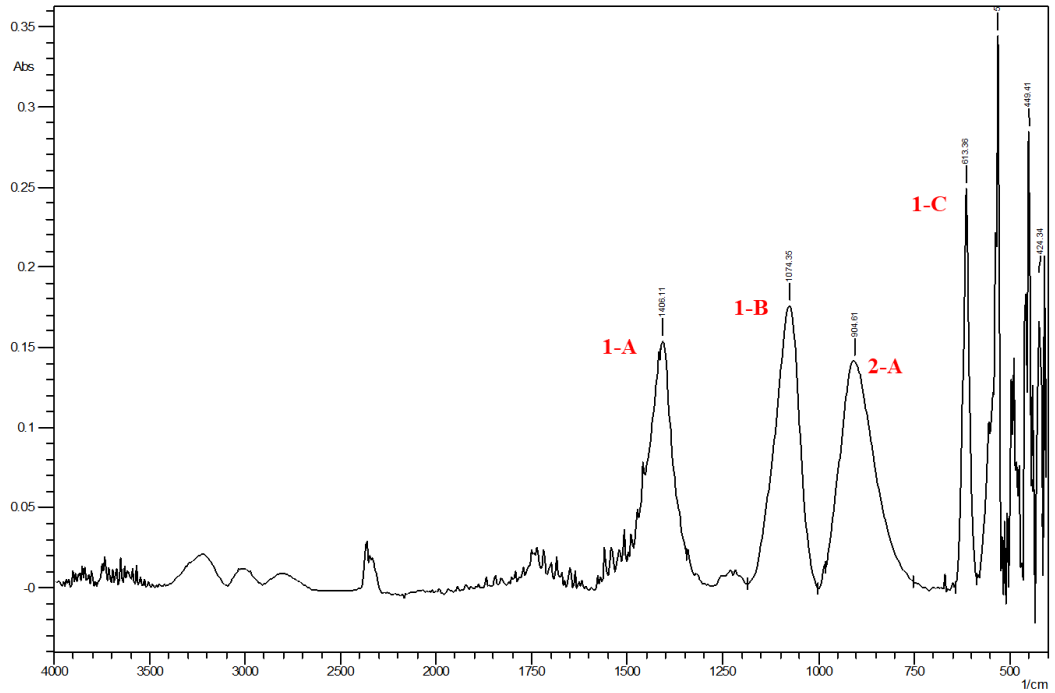

Figure 11. FTIR spectrum of PM collected at 5:1 ratio of NH_3/SO_2 reactants.

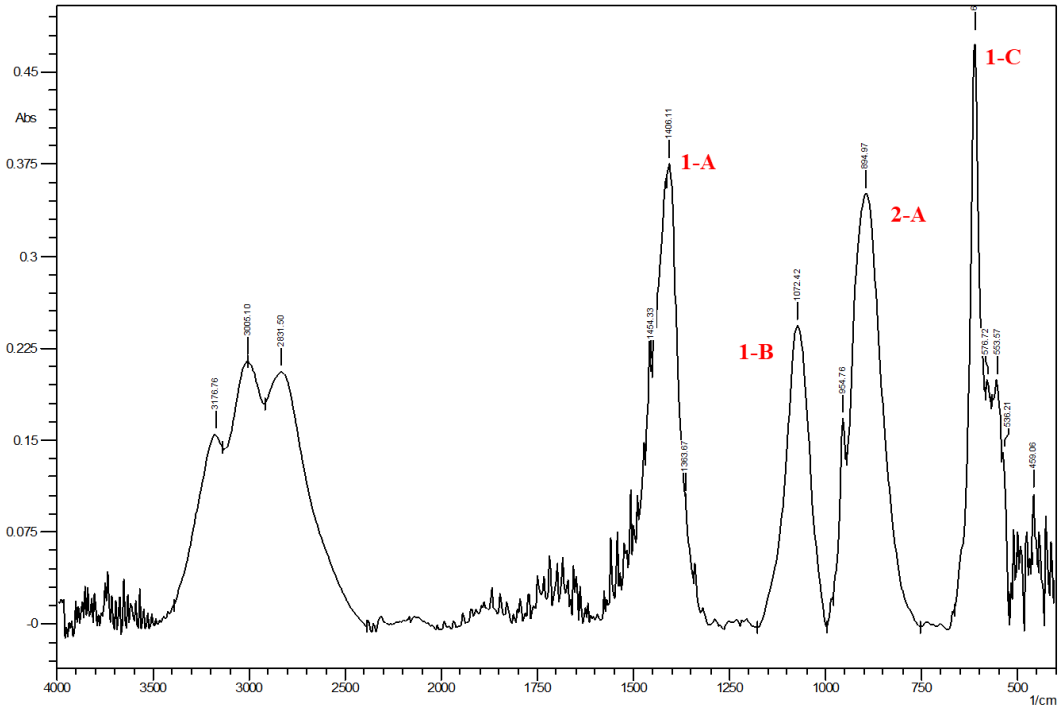

Figure 12. FTIR spectrum of PM collected at 10:1 ratio of NH_3/SO_2 reactants.

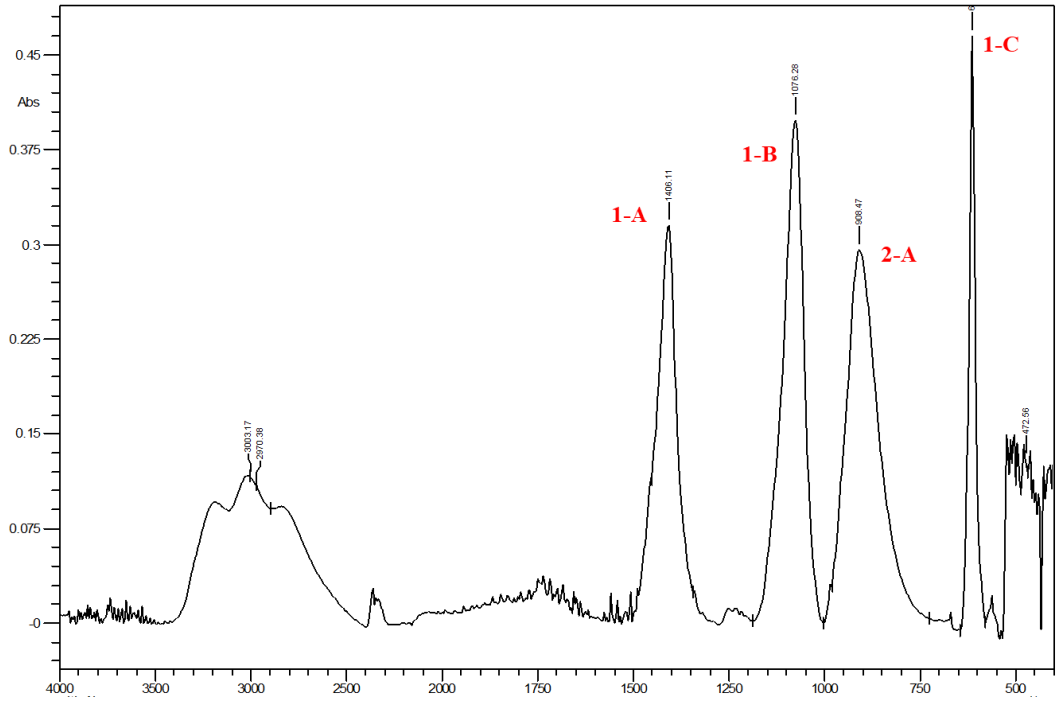

Figure 13. FTIR spectrum of PM collected at 30:1 ratio of NH_3/SO_2 reactants.

Aside from the identification of possible compounds present in the PM reaction product, the FTIR spectra can also provide an estimate of their relative abundance (Hirota, Makela, & Tokunaga, 1996). The depth of an absorption peak is assumed to be proportional to the amount of each component. Two characteristic absorption peaks can be used, 1-B and 2-A, which represent ammonium sulfate and the intermediate products, respectively. The depth ratio between these two peaks estimates the relative abundance of NH_4SO_4 to the intermediate products of the ammonia and sulfur dioxide reaction. At a 5:1 NH_3/SO_2, the relative abundance ratio was calculated to be 1.25 which suggests a slightly abundant presence of ammonium sulfate. The abundance ratio decreased to 0.78 for 10:1 NH_3/SO_2 but went back up to 1.34 at higher NH_3 concentration at 30:1 reactant ratio. There was no definite trend observed based solely on the relative abundance of

products in terms of reactant ratio. Increasing the ammonia concentration in the reaction might seem to have no effect on the relative amount of ammonium sulfate formed in the PM product. However, this result should be properly verified by conducting a more rigorous quantification analysis which would require huge amount of time to develop. A method proposed by (Coury & Dillner, 2008) to quantify functional groups in ambient aerosols can be used for verification. It involves a multivariate calibration of the IR spectra by generating multiple standard spectra of relevant functional classes present in the ambient aerosols. The known moles and spectra for all generated calibrations serve as inputs to a Partial Least Square (PLS) algorithm to generate the final calibration to quantify each constituent compounds.

The reaction products in the presence of air (or O_2) are shown in Figures 14 & 15. For this system, ammonia concentration was further increased resulting into a reactant ratio of 60:1. The absorption peaks observed due to the addition of O_2 almost completely resembles that of the standard laboratory ammonium sulfate. The strong peak in the range of 700 to 1000/cm that represents that of the sulfite ions or adduct NH_3SO_2 compounds. However, these sulfite peaks started to disappear in the presence of O_2. For this reason, it can be implied most of the compounds present in the reaction PM product was ammonium sulfate. However, SO_2 deformation can still be observed at lower infrared region which can further indicate the presence of other intermediate species.

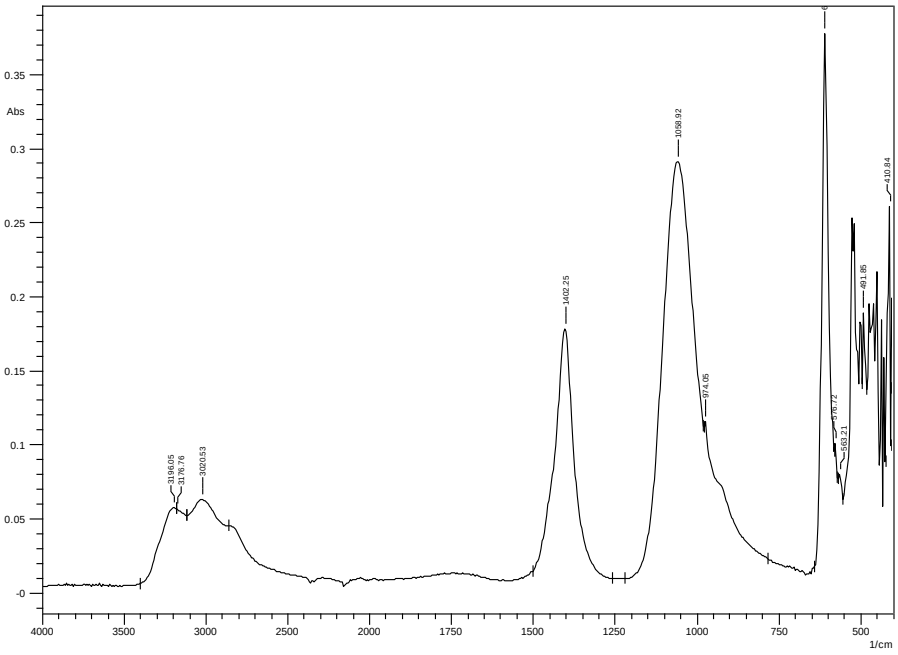

Figure 14. FTIR spectrum of PM collected at 60:1 ratio of NH_3/SO_2 reactants with 10% O_2.

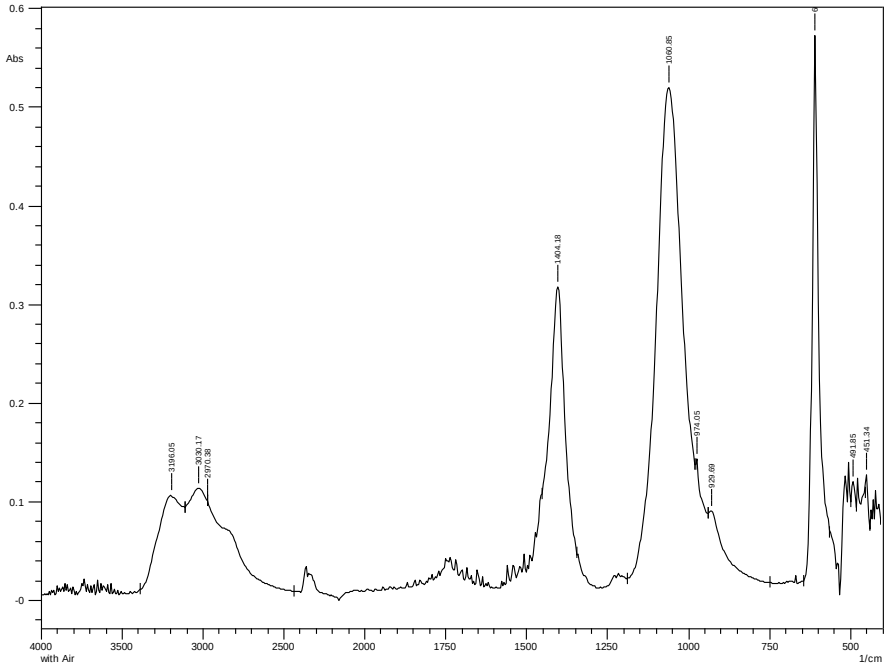

Figure 15. FTIR spectrum of PM collected at 60:1 ratio of NH_3/SO_2 reactants with 20% O_2.

The reaction products of a typical SO_2-NH_3-H_2O system are solid particles (Bai, Biswas, & Keener, 1994). The postulated reaction products are mainly dominated by ammonium sulfate, ammonium sulfite and ammonium bisulfite, particularly at low moisture conditions. At excess moisture conditions, the formation of ammonium sulfate is greatly favored (Bai, Biswas, & Keener, 1994). These crystal products were previously identified by X-ray diffraction (Stromberger, 1984). It should be noted that the diffraction patterns of both ammonia sulfate and ammonium sulfite are relatively similar. Hence, it is possible that at lower moisture conditions, it is difficult to distinguish the two compounds.

At trace water conditions, intermediates compounds dominate the particulate products. At excess ammonia concentrations, the weak peaks around the 3000/cm which is one of the characteristic bands of ammonium sulfate, start to appear. It was also observed that at lower ammonia concentration, the sulfite bands between the 400 to 750/cm dominate the low frequency range which was also observed by a previous study on excess ammonia reactions with sulfur dioxide (Meyer, Mulliken, & Weeks, 1980). Increasing the reactant ratio up to 30:1 produces FTIR spectra that resembles that of the PM products from reaction conditions with O_2. As the O_2 concentration increases, the compounds present in the PM sample were dominated mostly by ammonium sulfates (see Figure 16). This is consistent with the fact that sulfites can readily oxidize to sulfates upon addition of O_2 (Guo, Liu, Huang, Liu, & Guo, 2005)

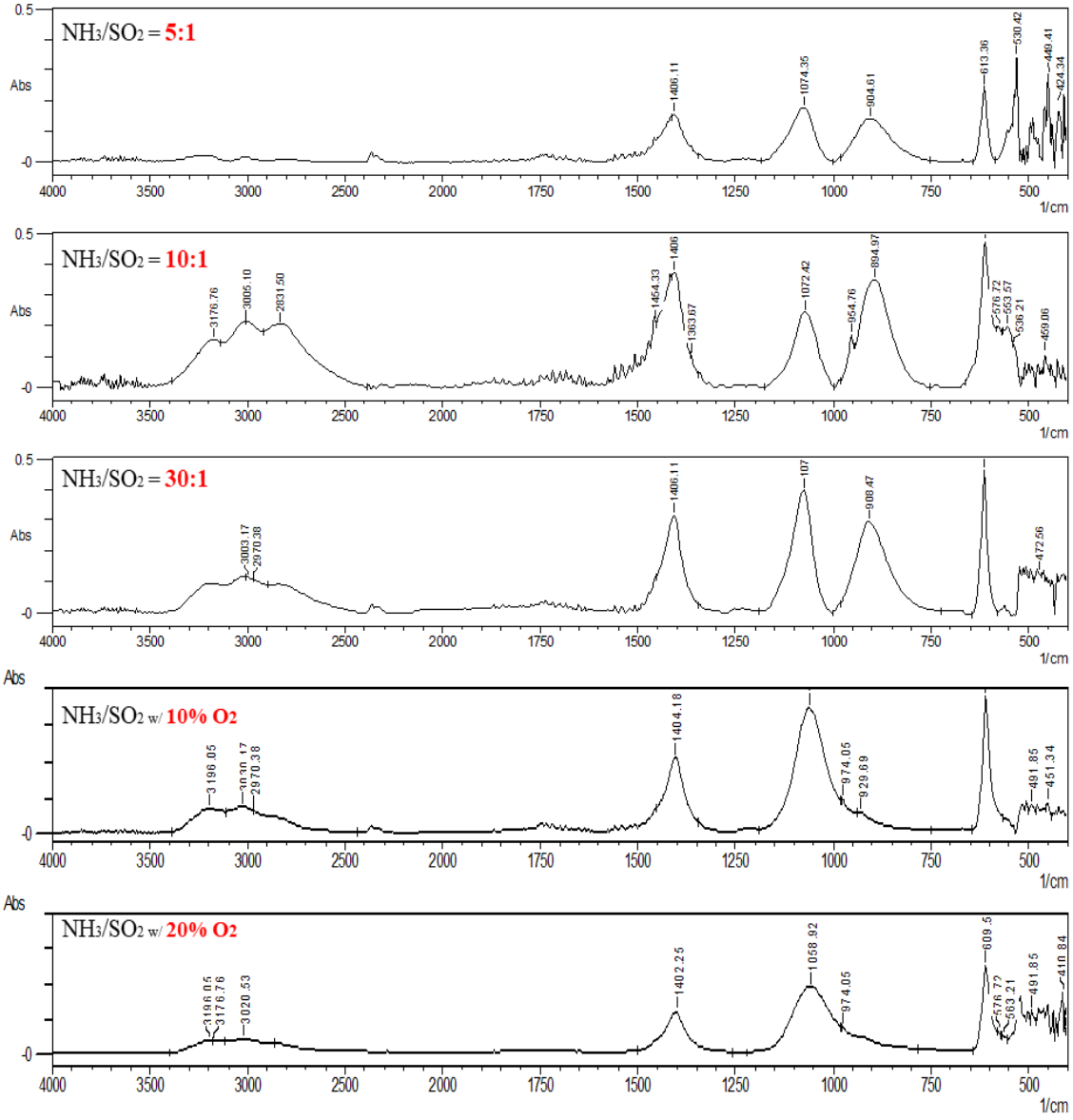

Figure 16. Comparison of FTIR spectral bands of all treatments with and without O_2.

II.3.3.3. Possible Chemical Conversion Pathways

The possible reaction products formed in the absence of oxygen and trace amount of moisture were mainly ammonium sulfate, ammonium sulfite, and intermediate products – amidosulfurous acid and ammonium amido sulfite. The presence

of O_2 further promotes the formation of ammonium sulfate by acting as an oxidizing agent for sulfur dioxide. It is believed that the addition of oxygen encourages the conversion of sulfite ions into sulfates based on the intermediate reaction shown in equation II.10.c. These sulfate ions react with ammonium ions produced from the simultaneous hydrolysis of ammonia (II.10.d). The chemical pathway for the formation of ammonium sulfate is shown in equation II.10 (Hirota, Makela, & Tokunaga, 1996).

$$SO_2 + H_2O \rightarrow HSO_4^- + H^+ \qquad \text{(II.10.a)}$$

$$HSO_3^- \rightarrow SO_3^{2-} + H^+ \qquad \text{(II.10.b)}$$

$$SO_3^{2-} + \tfrac{1}{2}\, O_2 \rightarrow SO_4^{2-} \qquad \text{(II.10.c)}$$

$$NH_3 + H_2O \rightarrow NH_4^+ + OH^- \qquad \text{(II.10.d)}$$

$$2NH_4^+ + SO_4^{2-} + \tfrac{1}{2}\, O_2 + H_2O \rightarrow (NH_4)_2SO_4 \qquad \text{(II.10.e)}$$

The combination of these intermediate steps produces the over-all reaction,

$$2NH_3 + SO_2 + \tfrac{1}{2}\, O_2 + H_2O \rightarrow (NH_4)_2SO_4 \qquad \text{(II.10.f)}$$

The relative abundance of intermediate products should also be considered especially for the experimental runs without O_2. It was previously reported that the product of gas-phase reactions at trace water levels or even anhydrous conditions can still result in the direct formation of solid products (Vance & Peters, 1976). Their study resulted into a large variety of compounds; but the primary products were amidosulfurous acid (NH_3SO_2) and ammonium amido sulfite $(NH_3)_2SO_2$. At excess ammonia conditions, the latter product was being favored, while the former was dominant when sulfur dioxide was in excess (Vance & Peters, 1976).

Gaseous adduct of NH_3SO_2 was postulated to initially form which would subsequently combined with ammonia or with itself to produce the two primary products having a 2:1 and 1:1 NH_3/SO_2 ratios. These chemical reactions would then be followed by nucleation and formation of the two species in the formation of solid particles. The production of these adducts is the initial step on the nucleation model proposed by Hartley and Matteson (1975). The proposed formation of these adducts is shown in equations II.11 (Hartley & Matteson, 1975)

$$NH_{3\,(g)} + SO_{2(g)} \overset{K_1}{\leftrightarrow} NH_3SO_{2(g)} \qquad \text{(II.11a)}$$

$$NH_3SO_{2(g)} + NH_{3\,(g)} \overset{K_2}{\leftrightarrow} (NH_3)_2SO_{2(g)} \qquad \text{(II.11b)}$$

The adduct formation is then followed by spontaneous nucleation of the particles upon reaching a sufficient level of concentration to signal supersaturation within the system. For trace moisture conditions, water vapor only acts as a catalyst for the initial particle production. The resulting solid product can subsequently to other gaseous species to form final sulfite or sulfate product (Vance & Peters, 1976).

For the experimental runs without O_2, the formation of ammonium sulfites, $(NH_4)_2SO_3$, are highly possible (Bai, Biswas, & Keener, 1994). It was previously reported that the oxidation of sulfites to sulfates should be convenient enough upon exposure to oxygen. Therefore, the oxidation of $(NH_4)_2SO_3$ particles into $(NH_4)_2SO_4$ particles may occur according to the reaction shown in Equation II.12. below,

$$(NH_4)_2SO_{3(s,aq)} + 1/2O_{2\,(g)} \leftrightarrow (NH_4)_2SO_{4(s,\,aq)} \qquad \text{(II.12)}$$

II.3.3. Elemental Composition

The reaction products were kept inside a desiccator prior to the ultimate analysis. The samples were carefully prepared at room temperature and loaded into an Vario Elemental Analyzer to determine the mass composition of the total elements in the sample. Based from the reactants, the expected elements present in the PM sample should only include N, S, O, and H. The elemental analysis was carried out to confirm the results of the FTIR analysis as well as check for any possible reaction contaminants during the experiment.

The results of the elemental analysis for all reactant ratios are shown in Table 4. There were extremely low readings for carbon (< 0.40%) during the elemental analysis. The assumption was that any detection of significant amount of C in the sample should indicate presence of dusts or any other C-based substances that can either be swept along the gas flow or participate in the chemical reaction or physical nucleation process. The total carbon present in the PM sample was almost negligible compared to the mass of the other elements. The highest C mass composition (0.37%) was recorded during the runs with air which can be possibly be attributed to the combined CO and CO_2 impurities of the zero air which was not to exceed 1 ppm. The C values were ignored and the remaining mass compositions were normalized in order to produce the percentage by mass for each element.

The data shown in Table 4 are the overall sulfur, nitrogen, hydrogen and oxygen in the products. The results indicate an increasing relative N content in the products with an increasing excess of ammonia in the reactant stream. This was also observed by a

previous study on anhydrous aerosol formation from NH_3-SO_2 reactions (Vance & Peters, 1976). The increasing ammonia levels resulted into a decrease in the total sulfur content while the hydrogen remains relatively constant except in the presence of O_2 (Figure 17). It was expected that the addition of O_2 in the gas flow system increases the oxygen content in the collected PM, which could actually be an indicator of sulfate formation (Hartley & Matteson, 1975).

Table 4. Elemental analysis of PM products obtained at different reactant ratios.

Reactant Ratio	Elements, % by mass			
	N	S	H	O
5:1	18.13	31.43	5.31	45.11
10:1	17.43	28.01	5.10	49.40
30:1	19.96	25.58	5.31	48.76
60:1:10% O2	22.30	21.73	5.28	50.60
60:1:20% O2	22.11	20.80	6.07	51.01

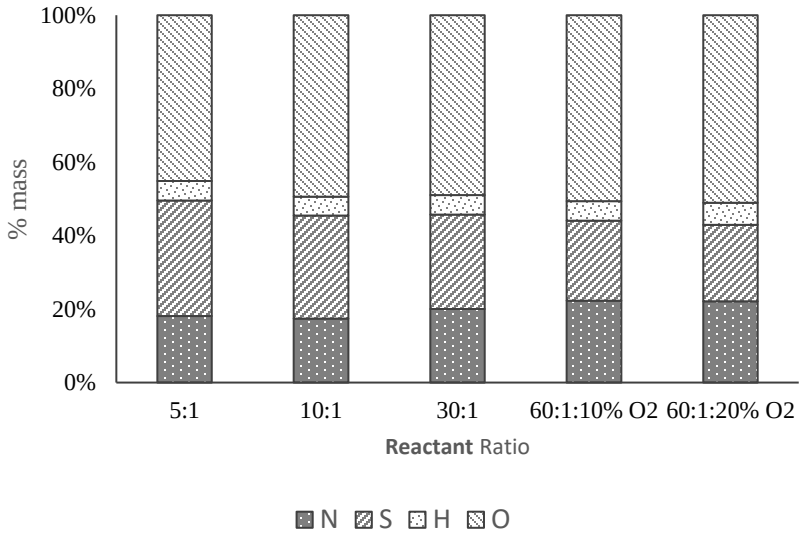

Figure 17. Elemental composition (% mass) of the PM products resulting from different NH_3/SO_2 ratios and presence of air.

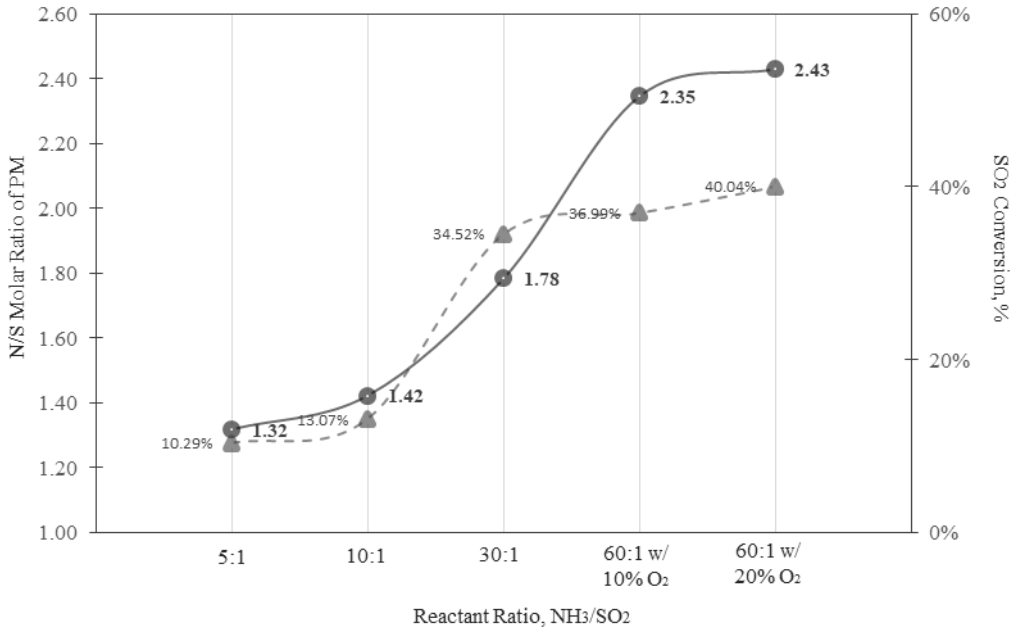

Figure 18. SO_2 conversion (%) and N/S molar ratio of collected PM samples resulting from different NH_3/SO_2 ratios and presence of air.

The conversion of SO_2 from the gas-to-particle reaction was estimated based on the total S content in the PM sample and the total SO_2 used. Figure 18 shows the relation of SO_2 conversion with the reactant ratio for both conditions of with and without O_2. The SO_2 conversion increases with the increasing excess ammonia in the reaction. A higher NH_3/SO_2 feed ratio increases the probability of the reaction to consume majority of the SO_2 present in the gas system and favors the forward reaction to produce PM particles. The SO_2 conversion was only able to reach 40% and levelled off at 20% oxygen concentration.

The effects of NH_3/SO_2 molar ratio was previously studied as a function of residence time and temperature (Guo, Liu, Huang, Liu, & Guo, 2005). It was found out that the SO_2 conversion also increases within excess NH3 conditions. However,

increasing temperature resulted into a decrease in the percent conversion. At trace moisture conditions, it was concluded that lower temperature and higher molar feed ratio favors the ammonia and sulfur dioxide reactions. The gas reaction system developed by Guo et al. (2005) was able to achieve a maximum of 80% SO_2 conversion at room temperature but with the addition of 10% water vapor.

The molar ratio of the total N and S in the PM sample was also computed for each treatment based on the elemental analysis. The resulting N/S ratio were plotted against reactant ratio in Figure 18. The relation between the molar N/S ratio with the increasing NH_3/SO_2 feed ratio was consistent with that of the SO_2 conversion. This means that more NH_3 is required in order to achieve a better SO_2 conversion. For a lower reactant ratio without O_2, the total N/S in the PM product was around 1.

The reaction products under trace moisture conditions were previously discussed and conjectured by several independent researchers (Vance & Peters, 1976; Bai, Biswas, & Keener, 1994; Hirota, Makela, & Tokunaga, 1996) to be either the chemical adducts NH_3SO_2, $(NH3)_2SO_2$, the intermediate products of $(NH_3)_2SO_3$, $(NH_3)_2HSO_3$ or the main product which is $(NH_4)_2SO_4$. These products can be classified as either 1:1 or 2:1 product based on the molar ratio of their N and S.

It is seen from the plot of N/S molar ratio (Figure 18) that a mixture of 1:1 and 2:1 products tends to form between the reactant ratio range of 5:1 and 30:1. The 2:1 products are generally favored as the the system contains increasing excess ammonia. At lower reactant ratio, the 1:1 products were observed to be dominant. These are the chemical adducts and possibly ammonium pyrosulfite, $(NH_4)_2S_2O_5$). However the later

normally forms at humid conditions (Bai, Biswas, & Keener, 1994). This observation confirms the FTIR results where the peaks were generally observed at the intermediate products band range.

The 2:1 products become more dominant upon further increasing the reactant ratio, particularly for the system with oxygen. This could probably mean that sulfite and sulfate particles are the dominant products of the reaction at higher reactant ratio and oxygen concentration. This result is also consistent with the identifying spectral bands observed from the FTIR analysis. However, the diffraction pattern of the ammonium sulfite and ammonium sulfate can be similar in most cases (Bai, Biswas, & Keener, 1994).

The most probable compounds that could be present in the PM sample for conditions of high excess ammonia would be the $(NH_4)_2SO_3$ and $(NH_4)_2SO_4$. The latter is expected to be more abundant with higher O_2 concentration. No further analysis was conducted to distinguish these 2:1 products. Since the focus of this study is mainly on the amount of PM produced and the particle size distribution, distinction of these products was considered to be not of a major concern.

II.3.4. Morphology and Surface Characteristics

When gaseous NH_3, SO_2 and enough amount of water vapor are mixed, white crystallite materials are formed (Bai, Biswas, & Keener, 1994). Even in trace moisture conditions, aerosol products form ammonia and sulfur dioxide reactions appeared to be white in color (Vance & Peters, 1976). Recent studies on chemical formation and

kinetics of NH_3-SO_2 system agree on white powder to crystalline appearance of resulting aerosols (Guo, et al., 2005; Vaden, et al., 2010).

Figure 19 present the actual PM collected from the reaction without O_2 (20a) and with O_2 (19b). By visual inspection, all the collected PM were consistent with the physical observations from previous studies. The white PM formed from the reactions without O_2 seems to be lighter and more powdery compared to that of the products with O_2 (Figure 19b), which are more crystal-like (Figure 20a).

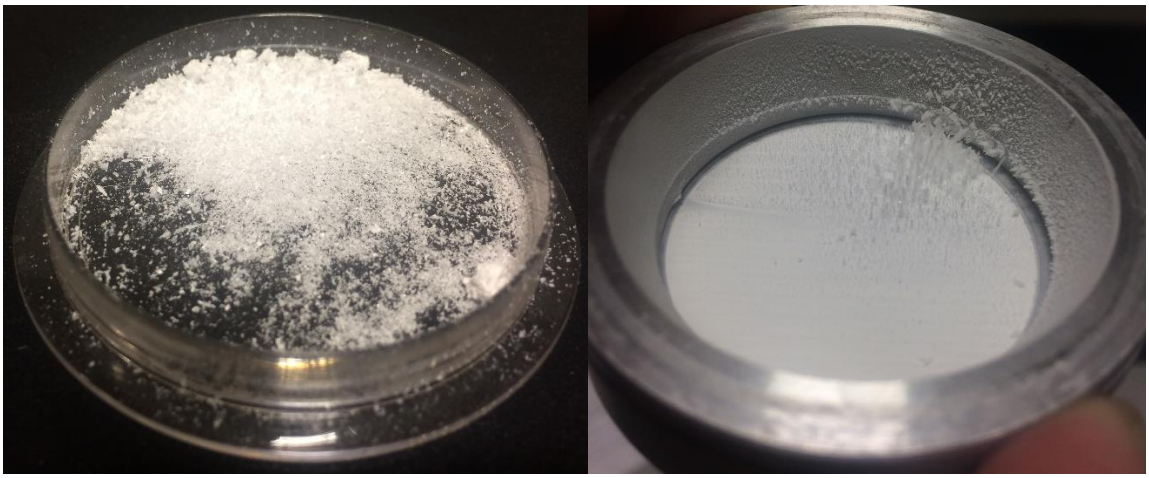

(a) (b)

Figure 19. Collected PM products from (a) O_2-rich reaction, (b) O_2-less reaction

A closer examination of the morphology of the PM products was facilitated by using a scanning electron microscope (Figure 20). The SEM image generated for the PM from O_2-less reaction were observed to be dominated with spherical particles, while there were aggregates of two or more rectangular or irregularly-shaped particles. Most of the spherical particles have noticeable porous structure which might explain why they

appear lighter compared to PM formed from O_2-rich reaction. The latter appearance was also observed using SEM.

There was no general distinct shape for the collected PM particles. Instead, the PM formed from the presence of O_2 were more clustered like crystals. In a previous attempt to characterize ambient $PM_{2.5}$, a similar observation was reported via quantitative SEM (Martello, et al. 2001). Using FRM samplers to collect ambient PM2.5, the SEM image generated has the same morphology and shape for particles with sulfur deposits. Under strong electron beam, complex secondary particles containing N, O, S and K have no distinct shapes. Particles containing ammonium sulfates and ammonium bisulfates have unique morphology and microstructures (Geng, et al., 2010). On the other hand, spherical particles are more distinct for primary PM such as fly ash and organic particulates (Li & Shao, 2009).

The analysis for the elements present on the PM surface is shown in Figure 21. An energy-dispersive x-ray spectroscopy (EDS) was used as another alternative for elemental analysis. This is a non-destructive method of chemical analysis that makes use of X-ray spectrum emitted by a solid sample upon subjecting under a focused beam of electrons. A quantitative EDS enables the determination of the relative concentrations of the surface elements present by measuring the intensities corresponding to every identified element. Since EDS is already a proven technique for surface elemental analysis, a comprehensive database for calibration and standards is already in place (Hodoroaba, et al. 2016).

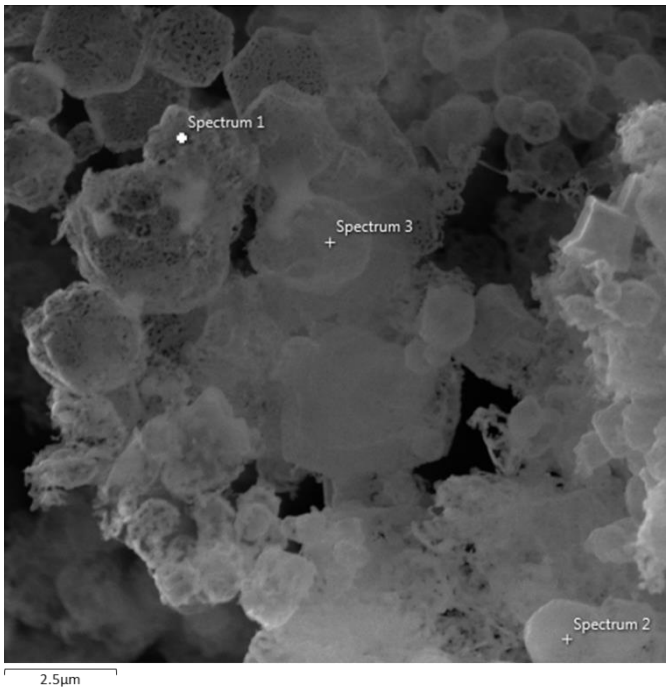

(a)

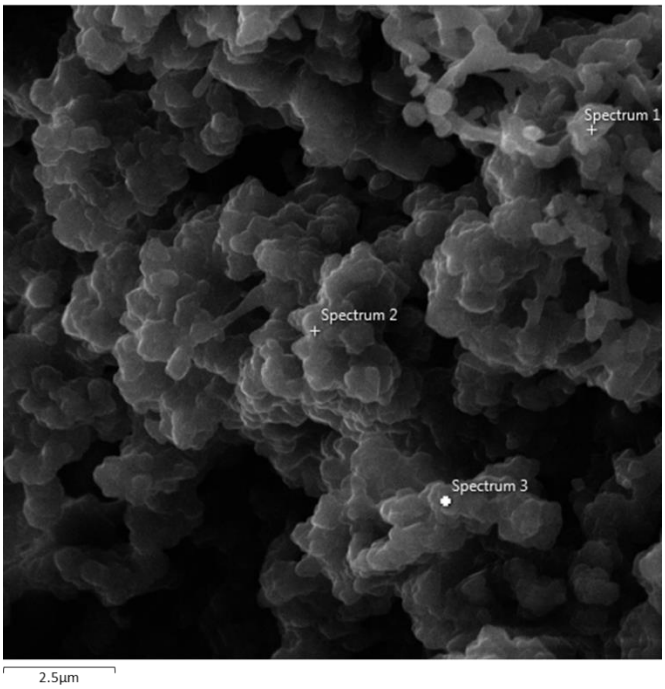

(b)

Figure 20. Electron images of collected PM products from (a) O_2-rich reaction, (b) O_2-less reaction

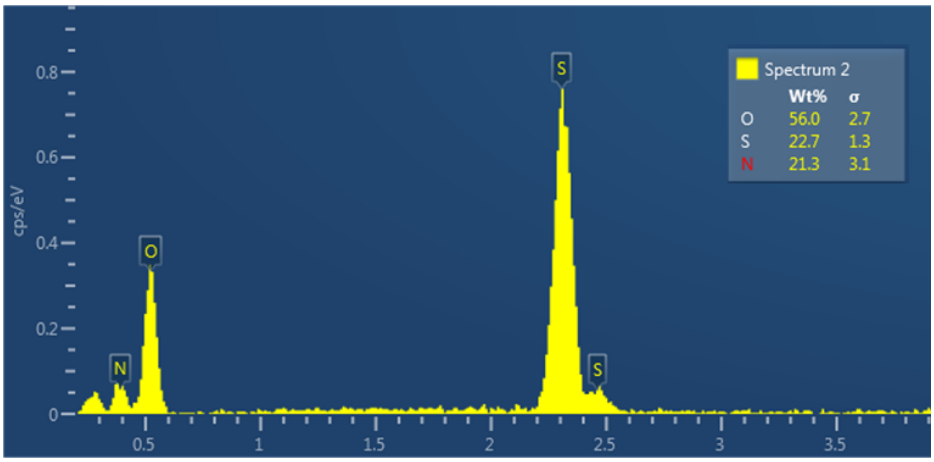

Figure 21. Surface elemental analysis using energy-dispersive x-ray (EDS) spectroscopy.

Figure 21 presents the x-ray spectrum generated for each identified element on the PM surface. The x-axis corresponds to the X-ray energy (eV) and the y-axis represents the counts of x-ray lines per channel. Specific elements generate X-ray lines within a particular range of energy, producing a Gaussian profile. The EDS analysis was able to confirm the presence of S, N and O on the surface of the PM sample. The relative distribution of the elements resembles the results of the elemental analysis (Table 4). Oxygen dominates the surface composition with relatively equal amounts of S and N. The H was not identified since this technique can only detect elements from atomic numbers 4 to 92 (Goldstein, 2003).

II.3.5. Production Rate and Particle Size Distribution

The most abundant key precursor gas in the stratosphere is the sulfuric acid (Jacob, 2004). It is commonly produced out from the oxidation of SO_2 from a wide variety of sources. The vapor pressure of H_2SO_4 is significantly lower than most of the gaseous species in the atmosphere. This favors its condensation under all atmospheric conditions to form aqueous sulfate particles.

Typical processes involved in the life cycle of aerosol particulates can be divided into three major events which is initiated by nucleation, then particle growth, and finally removal of atmospheric aerosol particles (Jacob, 2004). Gas particles are normally within the submicron range, 10^{-4} to 10^{-4} μm. Clustering of these gas particles can be driven by homogeneous or heterogeneous nucleation, producing ultrafine aerosols, normally less than 0.1 μm. This is the primary product of gas-to-particle conversion.

Beyond the nucleation mode, the growth of particles slows down. Two major reasons are that particles become large enough to promote growth by condensation and that the random movement of larger particles slows down (reducing collision rate) which lower the coagulation rate.

Particles originating from condensing gases were observed to accumulate in the 0.01 – 1.0 μm range. This is typically known as the accumulation mode, driven by simultaneous coagulation and/or condensation of vapors unto existing particles. Since these particles are still too small to sediment at a significant rate, they can stay suspended in the atmosphere (7-10 days) and can be transported a long distance from the source unless scavenged by cloud droplets and subsequent rainout (Jacob, 2004). Coarse

mode normally includes all aerosol particles more than 1.0 μm. These particles are emitted by mechanical processes, mostly by wind action. Due to their relatively large size, they can sediment at a significant rate. These particle size range has the shortest atmospheric lifetime and are similarly removed by rainout (wet deposition).

Based on the particle size distribution of the PM product at different reactant ratios (Table 5), there were no recovered particles that fall within the ultrafine range. For an ideal mixture of NH_3-SO_2 without the presence of O_2, about 43% of the particles produced were considered fine particles especially for lower reactant ratios while the rest of the particles have diameters > 1.0 μm. All particles produced in the presence of O_2 were observed to be in the coarse mode (> 1.0 μm).

Table 5. Separation of particles size range based on their PSD at different NH_3/SO_2 reactant ratios and O_2 levels.

Reactant Ratio	Ultrafine (Aitken, < 0.01 μm)	Fine (0.01 - 1 μm)	Coarse > 1 μm
5:1	-	0.58%	99.4%
10:1	-	43.40%	56.6%
60:1:10%	-	-	100.0%
60:1:20%	-	-	100.0%

II.3.5.1. Homogeneous Nucleation Model

Ideally, if the operating condition is fully clean (without any presence of initial nuclei), an assumption for particle formation is the homogeneous nucleation between the water vapor and SO_2 gas particles, via oxidation, to produce the H_2SO_4 gas. The latter has very low vapor pressure and can easily collapse into droplets at ultrafine range. The sulfuric acid droplets can ideally react with NH_3 to form NH_4SO_4 particles based on the previously mentioned equation II.10,

$$2NH_3 + SO_2 + ½\ O_2 + H_2O \rightarrow (NH_4)_2SO_4 \qquad \text{(II.10.f)}$$

However, this mechanism should be expected if moisture is in appreciable levels (Bai, Biswas, & Keener, 1994). Since the system has only trace amounts of water vapor, another way of producing aerosol nuclei is a water-catalyzed formation of gaseous adducts prior to formation of that critical size of nuclei to induce growth or condensation.

A possible explanation on how PM was formed out from the idealized NH_3-SO_2 mixing is through a simplified nucleation model for anhydrous aerosol formation from NH_3-SO_2 reactions proposed by Vance & Peters (1976). The direct addition of NH_3 to SO_2 can potentially produce gaseous adducts, primarily $NH_3.SO_2$ (amidosulfurous acid) and $(NH_3SO_2)_2SO_2$ (ammonium amido sulfite). These gaseous adducts can undergo homogeneous nucleation and act as a precursor to a final sulfate or sulfite product upon reaction with O_2 and trace water vapor. It is proposed that the two adducts are formed based on the reactions previously presented in Equation II.11.

$$NH_{3\,(g)} + SO_{2(g)} \overset{K_1}{\leftrightarrow} NH_3SO_{2(g)}$$

$$NH_3SO_{2(g)} + NH_{3\,(g)} \overset{K_2}{\leftrightarrow} (NH_3)_2SO_{2(g)}$$

For this discussion, the $NH_3SO_{2(g)}$ will be called 1:1 adduct while the $(NH_3)_2SO_{2(g)}$ will be the 2:1 adduct. At gas-phase equilibrium, the supersaturation ratio can be estimated based on the ratio of the partial pressures of the condensing species to its equilibrium vapor pressure (Vance & Peters, 1976). According to classical nucleation theory, the initial particle size (critical radius) required to initiate nucleation decreases as the supersaturation ratio increases. As supersaturation ratio increases, it is more convenient for the gas system to produce these critical sized nuclei.

It was initially assumed that the 2:1 adduct has significantly lower vapor pressure than the other. This implies that the 2:1 adduct will condense at lower concentrations compared to the 1:1 adduct. Since the supersaturation of the 2:1 adduct is higher, it will have a smaller critical radius.

At lower NH_3 levels (5:1 reactant ratio), the formation of 1:1 adduct is favored until it reaches a sufficient concentration to initiate nucleation of this species. At this point, the products formed are mainly composed of 1:1 compound (Vance & Peters, 1976). For this study, the N/S ratio of the products of 5:1 ratio was previously observed to be close to 1, which can be an indicator of 1:1 intermediate products. The results of FTIR also confirms the presence of these products which releases strong random peaks at lower wavenumber. The dominant concentration of 1:1 adduct will tend to suppress the formation of 2:1 adducts, unless more excess ammonia is added unto the system. Since 1:1 adduct becomes dominating, it could result in aerosols of relatively large

critical size (Rc_1) formed at slower rates (Figure 22). A higher sulfur dioxide level lowers the reactant ratio (NH_3/SO_2) and results into generation of larger aerosols as evidenced in the PSD of collected PM sample shown in Figure 22. The size distribution of 5:1 can be mainly observed on the coarse range while about half of the particles are within the fine range for 10:1 reactant ratio.

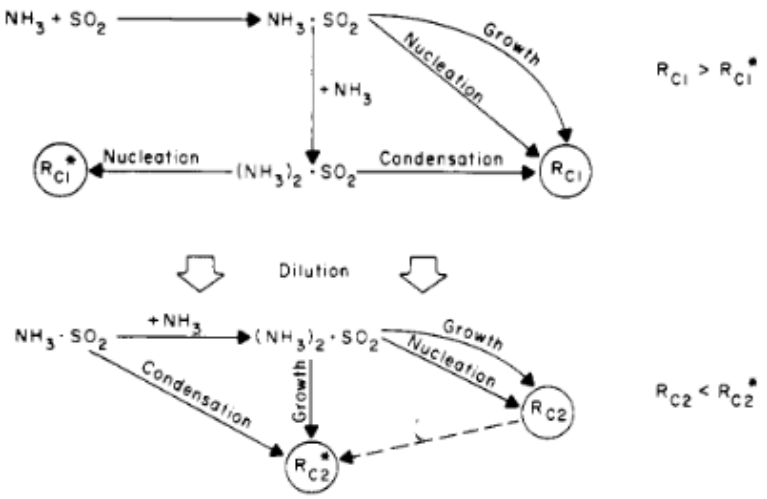

Figure 22. Schematic description of nucleation and growth model for the reactant ratios without O_2 reprinted from (Vance & Peters, 1976).

For conditions with high levels of excess NH_3 (10:1), spontaneous nucleation would result into products of 2:1 compound only. The rate of nucleation would be much faster and the resulting critical size (Rc_2) would be smaller. The 2:1 aerosol can further grow in size until it reaches the R_{C2}*, the size required for the 1:1 adduct to condense upon its surface. The particles from 10:1 were observed to be relatively smaller compared to that of 5:1 reactant ratio (Figure 23).

The aerosols based from this model are assumed to contain both species as a result of diffusional growth and condensation. However, this nucleation model was not sufficient to explain the PSD of PM resulting from conditions with 10% and 20% O_2.

The presence of O_2 should oxidize the SO_2 species into trioxides which can give way to the formation of sulfites and bisulfites. Further oxidation of the former can result into the formation of ammonium sulfates. All of these compounds should have a 2:1 N/S ratio which is consistent with both the elemental and FTIR results of this study.

The resulting size distribution of the collected PM from the oxygen-rich experiments fall within the coarse mode. About 76 to 86% of the particles made it to the PM2.5 cut while 100% of the particles from the oxygen-less runs belong to the PM2.5 cut (Figure 24). The PSD generated for the products in the absence of O_2 are fairly symmetrical, with their skewness values within the rule of thumb of -0.5 to 0.5 range. A perfectly normal distribution should have a skewness value equal to 0 (NIST, Information Technology Laboratory (ITL), 2018). The PM produced in the presence of O_2 behave differently, having a -0.68 moderate skewness value for the 10% O_2 run and a highly skewed distribution for 20% O_2 with 1.38 skewness value. The abnormal positive skewness of the 20% O_2 PSD can be attributed to less than 7% of the particles having diameter greater than 3 μm. The kurtosis values for all PSDS are relatively close to zero indicating a standard normal distribution (NIST, Information Technology Laboratory (ITL), 2018).

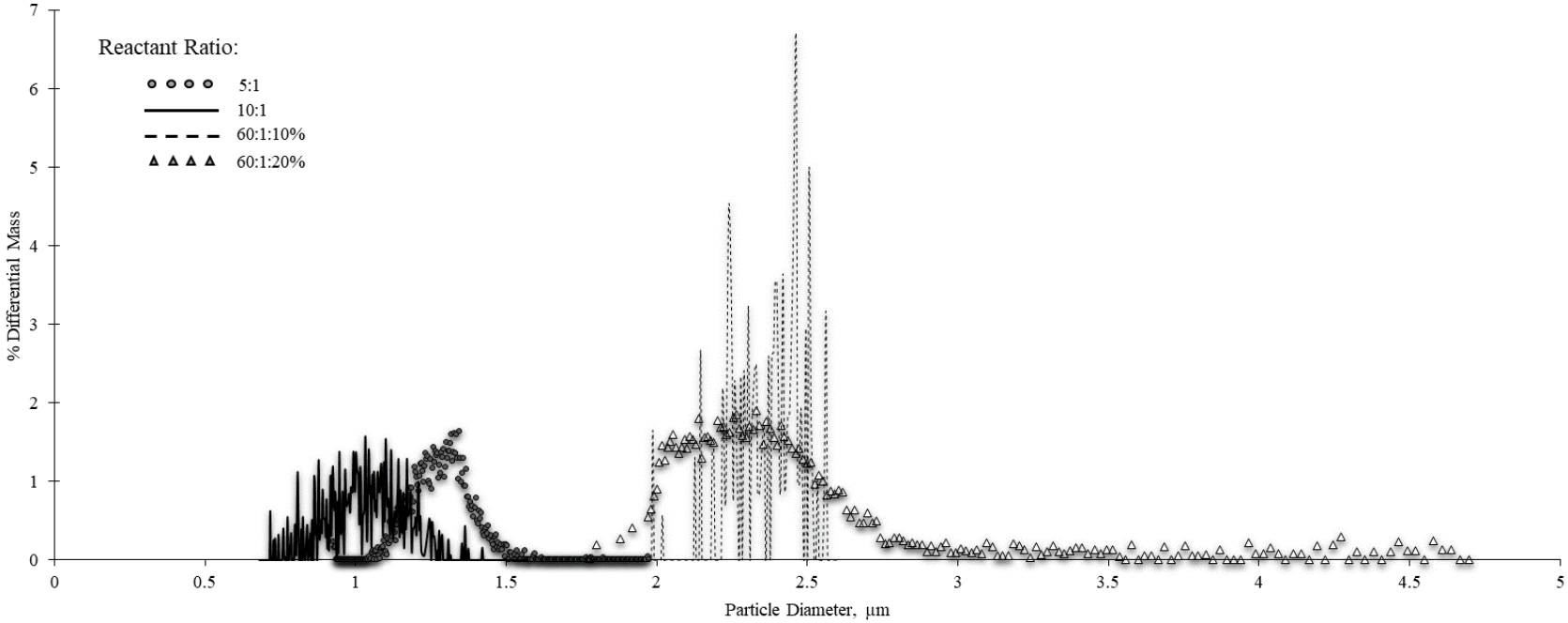

Figure 23. Over-all particle size distribution of collected PM sample resulting from varying reactant ratios of NH_3/SO_2 with or without the presence of O_2.

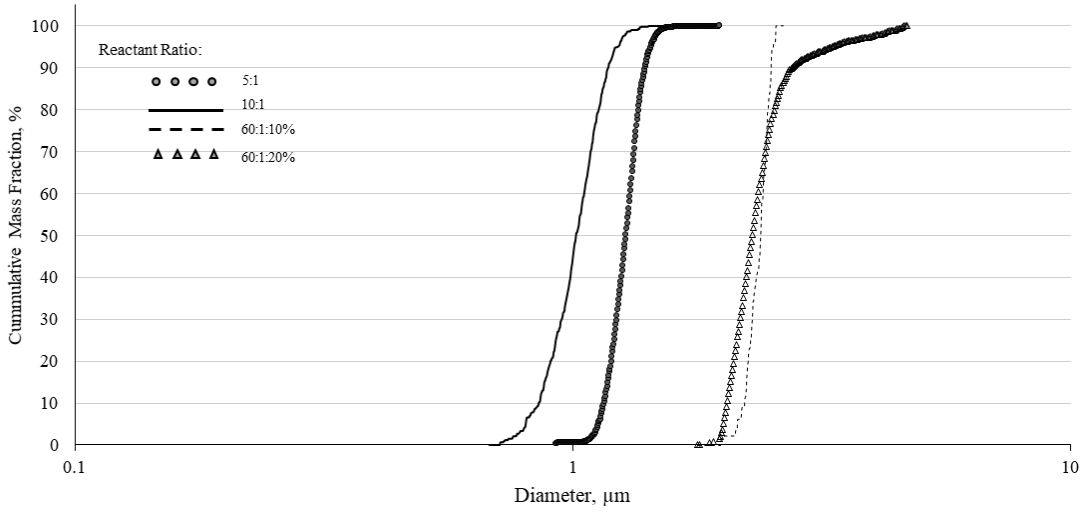

Figure 24. Cumulative mass percent distribution and particle diameter of collected PM at different NH_3/SO_2 reactant ratios and O_2 levels.

II.3.5.2. Aerosol MMD and GSD

A particle size distribution (PSD) can be presented in terms of particles by mass, volume or number. For regulatory purposes, the mass distribution is commonly preferred (Hinds, 1999). In air quality applications, the PSDS are often considered log-normal and characterized by their mass median diameter (MMD) and geometric standard deviation (GSD). The MMD is determined by plotting the log normal diameter (x-axis) against the cumulative percent mass distribution (y-axis). The MMD is taken as the intersection of the 50% cumulative mass on the curve, projected towards the x-axis. The GSD is simply the measure of how spread is the PSD of the aerosols.

Table 6 presents the different MMD and GSD computed from the cumulative mass distribution plot (Figure 24). The resulting particle MMD from the reactions in the presence of oxygen gas were twice as higher than the particle MMD resulting from reactions in the absence of oxygen gas. Despite of the MMD differences, the GSDs

appear to be consistently around 1.0. For monodispersed particles, the GSD is expected to be equal to 1 and for poly-dispersed particles, GSD is greater than 1 (Buser, Parnell, Lacey, Shaw, & Auvermann, 2001).

Table 6. Mass median diameter (MMD), geometric standard deviation (GSD) and percentage of $PM_{2.5}$ in the collected PM sample at different NH_3/SO_2 reactant ratios and O_2 levels.

Reactant Ratio	MMD, μm	GSD	PM2.5 cut (dp <= 2.5)
5:1	1.280	1.08	100.00%
10:1	1.020	1.16	100.00%
60:1:10%	2.370	1.06	86.78%
60:1:20%	2.297	1.11	76.62%

II.3.5.2. Production Rate and Surface Wall Losses

The abundance of the PM collected for each replicate (Table 7) only showed that the concentrations of NH_3 and SO_2 for all reactant ratios were sufficient enough to initiate nucleation and simultaneous particle growth. Even at significantly lower concentrations, aerosols could still possibly form, at least generate nuclei of the Aitken variety.

However, the PMs formed during the runs were not only collected on the filter. There were noticeable amount of particles formed on the inside reactor wall surface and traces of particles on the gas lines. The particles formed during sampling were initially assumed to be recovered as part of the bulk flow towards the filter. If the particles under sufficient coagulation or growth, they can fall off from the bulk flow or undergo

deposition on the wall surfaces. These will underestimate the amount of total PM produced if the PM from the filter will only be considered.

There is a possibility that the initial nuclei formed can be lost onto the wall surfaces, especially low volatility gas-phase species (La, et al., 2016). The removal of ammonium sulfate through wall loss was also studied by Griffiths & Cox (2009), in the presence of N2O5. Fine to submicron particles were reported to be recovered on the reaction chamber walls at different temperature conditions. For chamber experiments that lasts for a longer period of time, the condensation of precursor gas-phase species becomes significant (Lambe, et al., 2015). Seed particles are normally used in chamber experiments to reduce wall losses but they were not utilized for this study.

The participation of wall surface in the aerosol formation was believed to encourage heterogeneous nucleation and became a more dominant mechanism over homogenous nucleation. The trapped particles on the surface wall can serve as ideal sites for condensation and coagulation to promote particle growth.

It is also possible that the latter replicates tend to have particles with higher diameter compared to the first replicates. Again, the influence of the particle deposits on the internal wall surface can provide surfaces to induce heterogeneous nucleation of the reacting species. However, it is also possible that the particles deposited on the surface of the wall cannot be swept anymore by the gas flow. This might diminish the effects of wall deposition on the PSD. The PSD generated from this experiment were categorized in the fine and coarse particle range. This might be a consequence of the dominating heterogeneous growth of particles which makes the particle diameters larger than that of

the ideal particle formation. Nonetheless, the ideal particle diameters should still belong to the PM2.5 cut.

The PM production rates at different reactant ratios are shown in both Tables 7 and 8 (accounting for the wall losses). A one-way ANOVA was conducted to compare the mean production rates based on the PM filter collected among different reactant ratio. At 95% level of significance, it was revealed that all the means for the treatment levels without O_2 do not have any significant difference. A non-significant result also was computed for treatments with O_2. However, the means of the PM production rates from O_2-less treatments were significantly different from the PM rates of O_2-rich treatments. It was further observed that a higher uncertainty was computed for higher reactant ratio based on the 95% confidence interval.

The PM rates based on the total PM collected from the filter and the surface wall are shown in Table 8. The resulting PM rates were generally 10 – 20% higher than the values reported in Table 7. It should be noted that an outlier wall loss data was recorded for reactant ratio of 30:1. At this reactant ratio, the recovered filter were visually observed to be ‘wet’ after each run. There was an appreciable increase in the mass of the final filter but the recoverable solid particle on the surface were significantly lesser than the other treatment levels. It was speculated that most of the particles were trapped within the filter matrix and the final phase of the PM formed was a mixture of solid and liquid.

In a previous chamber study conducted by Lambe, et al. (2015), the aerosol yields were corrected for ammonium sulfate particle wall losses. The magnitude of the particle wall loss used for corrections was typically ranged from 10 to 30 %. For this study, the over-all average percent loss was around 12.40%.

Table 7. Mean production rates based on the filter PM collected at different NH_3/SO_2 reactant ratio within 95% confidence interval.

	Production rates - without PMwall				
	without Air (O_2-less)			with Air (O_2-rich)	
	5:1	10:1	30:1	60:1:10%	60:1:20%
PM_{filter} = $PM_{collected}$, mg	7.12 *± 1.48*	6.00 *± 1.47*	5.79 *± 3.16*	3.54 *± 2.48*	4.00 *± 2.75*
PM rate, mg/min*	0.078 *± 0.014[a]*	0.066 *± 0.013[a]*	0.064 *± 0.013[a]*	0.039 *± 0.014[b]*	0.044 *± 0.014[b]*

[*] Levels having similar letters are considered not significant: ANOVA F ratio = 6.9038 with Prob > F of 0.0062 (tested at α = 0.05)
**Uncertainty values were generated based on 95% confidence interval*

Table 8. Average PM production rates based on the filter PM and wall PM collected after each treatment at different NH_3/SO_2 reactant ratio.

	Production rates - with PMwall				
	without Air (O2-less)			with Air (O2-rich)	
	5:1	10:1	30:1	60:1:10%	60:1:20%
PM_{filter} + PM_{wall}, mg					
Total PM_{filter}	21.06	17.02	17.39	10.63	12.01
Total PM_{wall}	2.53	3.02	0.90	2.02	1.97
Total $PM_{collected}$, mg	23.59	21.04	18.29	12.65	13.98
PM rate, mg/min	0.087	0.074	0.068	0.047	0.052
% losses due to wall	*10.74%*	*14.38%*	*4.92%*	*15.98%*	*14.11%*

II.3.6. Emission Factor Estimation

The amount of PM formed for every amount of ammonia gas used during the total sampling period was considered as the unit emission factor, $\frac{m_{pm}}{m_{NH3}}$. These mean unit emissions are presented in Table 9. Statistical results showed (Table 10) at 95% confidence, that all means were significantly different between treatments with and without O_2 in all reactant ratio levels. This is based from a null hypothesis that there was no significant difference from the means of treatments with or without addition of O_2. Therefore, the presence of O_2 might have a significant effect on the PM formation with that of only NH_3-SO_2 systems.

Comparison of mean differences at each level was conducted using Student's t-test. The mean differences between all levels of reactant ratios without O_2 were found to be non-significant. A non-significant result were also determined for the mean differences between reactant ratios with O_2.

At these given range of NH_3 and SO_2 concentrations (5:1 up to 30:1), it can be implied that there was no significant difference in the resulting PM emission factor whether at lower reactant ratio or at higher ratio for the system without O_2. The same can also be implied for the system with O_2. There was no significant difference between the unit emission factor computed for 10% and 20% O_2 levels. For these reasons, the unit emission factors were arithmetically averaged for each system, between reactant ratio either with or without O_2.

Table 9. Unit PM emission factors at different NH_3/SO_2 reactant ratios and O_2 levels.

Reactant Ratio	Mean, mgPM/mgNH_3 (based on PM_{filter})	Total average, mgPM/mgNH_3 (based on PM_{filter} + PM_{wall})
5:1[a]	0.0109 ± 0.0019	0.0122
10:1[a]	0.0088 ± 0.0014	0.0104
30:1[a]	0.0090 ± 0.0019	0.0095
60:1:10%O2[b]	0.0055 ± 0.0019	0.0066
60:1:20%O2[b]	0.0062 ± 0.0019	0.0073

** Levels having similar letters are considered not significant: ANOVA F ratio = 6.84with Prob > F of 0.0064 (tested at α = 0.05)*
**Uncertainty values were generated based on 95% confidence interval*

Table 10. Mean emission unit factor ordered differences for each pair using Student's t-test at different NH_3/SO_2 reactant ratios and O_2 levels.

Level	- Level	p-Value	
5:1	60:1:10%O2	0.0013*	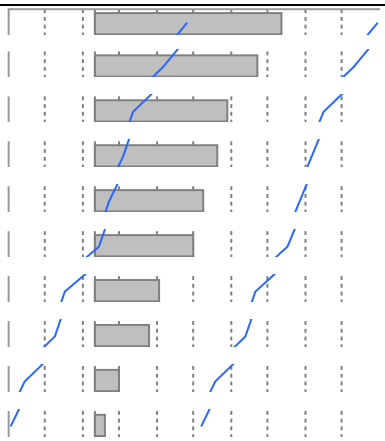
5:1	60:1:20%O2	0.0033*	
10;1	60:1:10%O2	0.0108*	
30:1	60:1:10%O2	0.0163*	
10:1	60:1:20%O2	0.0286*	
30:1	60:1:20%O2	0.0435*	
5:1	30:1	0.1589	
5:1	10:1	0.2302	
1:60:20%O2	1:60:10%O2	0.5807	
1:10	1:30	0.8117	

**p-value < 0.05 are considered significant*

The resulting average unit EFs are shown in Table 11. For the PM formed from the gaseous system without O_2, two values were determined based on PM_{filter} only and another with the addition of PM_{wall}. By inspection, the average unit EF from the PM_{filter} has a 95% confidence interval range which include the value for the average unit EF

with the addition of PM_{wall}. For a conservative estimate, the unit EF based from PM_{filter} + PM_{wall} was used in calculating the emission factor.

Table 11. Average unit emission factors from gaseous system with and without O_2.

	Average unit EF, mgPM/mgNH_3	
	(based on PM_{filter})	(based on PM_{filter} + PM_{wall})
Reaction without O_2	0.0096 ± 0.0017	0.0107
Reaction with O_2	0.0059 ± 0.0019	0.0069

The selected unit emission factors were multiplied by the literature value of NH_3 EF and the $PM_{2.5}$ cut to estimate the direct secondary PM2.5 equivalent from the total ammonia used following the previous equations II.6 and II.7. The resulting emission factors, kg 2^o $PM_{2.5}$ from the mass (kg) of ammonia used per 1000 head-day, are shown in Table 12.

Table 12. Summary of secondary PM2.5 emission factors from both NH_3-SO_2 gaseous systems.

	Gaseous System	
	without O_2	with O_2
Unit EF, mg total PM/mg NH3 used	0.0107	0.00690
$PM_{2.5}$ cut (% of particles with dp ≤ 2.5μm) [a]	*100.00%*	*81.70%*
2^o $PM_{2.5}$ unit EF, mg 2^o PM2.5/mg NH3 used	**0.0107**	**0.00564**
2^o $PM_{2.5}$ EMISSION FACTOR[b], kg 2^o $PM_{2.5\ eq}$/1000 head/day	1.610	0.850

[a] based from PSD results (Table 6)

[b] based from annual 0.15 kg $_{NH3/head/day}$ emission factor from dairy and cattle feed yards (Flesch, Harper, Powell, & Wilson, 2009) (Bonifacio, Rotz, Leytem, Waldrip, & Todd, 2015)

The 2^o $PM_{2.5}$ emission factor from ammonia in cattle feed yards were estimated to be 1.61 kg/1000 head/day and/or a smaller emission factor of 0.85 kg/1000 head/day using a flow reactor environment. At this point, the 2^o $PM_{2.5}$ EF calculated can be

presented as a range of 0.85 – 1.61 kg/1000 head/day, based from an idealized condition for aerosol formation.

The comparison with the EPA ratio was based on a PM_{10} emission factor for cattle feed yards of 15 lbs/1000 hd/day (Parnel, Shaw, & Auvermann, 1998) and an assumed value of primary $PM_{2.5}/PM_{10}$ ratio of 10%. It was previously reported that the typical primary $PM_{2.5}/PM_{10}$ ratio in agriculture should be around 10 – 15% (Parnel, Shaw, & Auvermann, 1998). Using a higher primary $PM_{2.5}/PM_{10}$ ratio in the calculation can actually further decrease the 2^o PM2.5 EF from this study. However, the 10% ratio was selected to produce a more conservative estimate.

It can be assumed that the exposure of interacting gaseous species inside a flow reactor can be equivalent to multiple days of exposure time in the atmospheric conditions (Lambe, et al., 2015). This can lead to a significantly higher aerosol formation rate than what is expected in the ambient atmosphere.

The flow reactor may not be an appropriate environment to simulate atmospheric interactions of gaseous system during gas-to-particle formations. The calculated 2^o PM2.5 EF was 1.24 to 2.35 times higher than the primary PM2.5 EF, which should not be the expected reality in an actual cattle feed facility. The higher rate of formation and measured yields than what was expected in the atmosphere was also previously observed in a number of laboratory experiments for secondary organic aerosols. The primary factors that affect the secondary aerosols yields are precursor concentration/volatility (Presto & Donahue, 2006) and oxidation exposure (Lambe, et al., 2015). The precursor concentrations involved in the reaction were expected to be higher by several magnitude

than in the ambient atmosphere. The high levels of reactant concentrations used were sufficient to produce PM at a higher production rate. However, it was previously reported that nucleation and particle growth can still proceed even at low ammonia concentrations of the order of a few parts per trillion (ppt) and a slightly higher order of a few ppb of SO_2 for the ambient environment (Kerminen, Pirjola, & Kulmala, 2001).

Nonetheless, the results of this flow reactor study revealed essential information about the chemical and physical characteristics of secondary $PM_{2.5}$ from NH_3. The knowledge about its relative yield, size distribution and chemical components serves as a valuable preliminary starting point for future field studies in estimating 2^o PM2.5 emission factors from ammonia emission of cattle feed yards. However, caution should be exercised on using the estimated EF since these were generated on an ideal and controlled environment which could result a gross overestimation of secondary PM2.5 emissions in a CAFO.

In order to better approximate the ambient atmosphere conditions, the use of wind tunnel for estimating the secondary PM2.5 emission factor from ammonia is presented in Chapter III.

II.4. Summary and Conclusion

The EPA has recently mandated the inclusion of secondary $PM_{2.5}$ on air pollution regulations and impact analysis for permitting purposes. At present, there is still no available secondary $PM_{2.5}$ emission factor that the agricultural sector can use for compliance. Under the hybrid secondary $PM_{2.5}$ assessment of EPA, a secondary PM2.5

emission factor can be estimated in terms of the direct particle formation from precursor gases, specifically ammonia.

By using an idealized aerosol flow reactor, the formation of secondary aerosols from ammonia and sulfur dioxide was empirically studied. The resulting PM was characterized based only on general appearance and particle morphology, elemental composition, final products formed, and particle size distribution (PSD). There was no attempt to distinguish the identified compounds based on their compositional distribution in the PM sample. Only the presence of the possible compounds was considered from the results of the characterization analysis. Fundamentals of aerosol nucleation and particle growth were used to elucidate the PM formation process. However, in-depth analyses of particle formation were considered beyond the scope of this study.

The chemical composition of the PM products were characterized by using FTIR, elemental analysis and EDS surface analysis. The addition of O_2 served as an oxidizing agent to promote sulfate formation. The whole reaction system recorded a maximum SO_2 conversion of 40% at 20% oxygen concentration. The primary compounds that could be present in the PM sample for conditions of high excess ammonia would be the $(NH_4)_2SO_3$ and $(NH_4)_2SO_4$. The latter is expected to be more abundant with higher O_2 concentration. No further analysis was conducted to distinguish these 2:1 products. Since the focus of this study is mainly on the amount of PM produced and the particle size distribution, distinction of these products was considered to be not of a major concern.

The white PM formed from the reactions without O_2 seems to be lighter and more powdery compared to that of the products with O_2 which are more crystal-like based from the electron images. The EDS analysis was able to confirm the presence of S, N and O on the surface of the PM sample.

The particle size distribution revealed that majority of the particles are within the fine and coarse range on a typical gas-to-particle event (86% to 100% belongs to PM2.5 cut). For the reactions without air and trace moisture content, homogeneous nucleation by forming gaseous adducts was proposed to be the primary mechanism followed by simultaneous surface condensation/coagulation and growth. However, the reactor wall effects was considered to significantly affect particle formation and size distribution. Heterogeneous nucleation may be considered as the dominating mechanism for particle formation due to pre-existing particles trapped inside the reactor.

The flow reactor was considered to be an inappropriate environment to simulate atmospheric interactions due to higher precursor concentration levels, oxidation exposure and wall effects. The calculated 2^o $PM_{2.5}$ EF was 1.24 to 2.35 times higher than the 1^o $PM_{2.5}$ EF, which should not be the expected reality in an actual cattle feed facility. Nonetheless, the knowledge gathered about the aerosol relative yield, size distribution and chemical components should serve as a vital starting point for future field studies in estimating 2^o $PM_{2.5}$ emission factors from ammonia emission of cattle feed yards.

CHAPTER III

PM2.5 FORMATION FROM THE INTERACTION OF AGRICULTURAL DUST AND PRECURSOR GASES AT WIND TUNNEL CONDITIONS

III.1. Introduction

Most experiments conducted for gas-to-particle conversions were conducted in idealized set-ups which may not properly simulate the dynamics in the atmosphere. One of the most commonly used techniques to study aerosol formations is by the use of aerosol flow reactors. This type of system is especially useful for scavenging studies of sulfuric acid aerosols by ammonia. However, the possible interference of the inside wall can result into several issues with the particle size distribution, composition and formation rates (Barker, 1995). Recent studies involving flow reactors were reported to have a higher formation rate of aerosols by an order of magnitude of several days greater than the normal exposure of reacting gaseous species in the atmosphere (Lambe, et al., 2015) (Ahlberg, et al., 2017).

Since most laboratory flow reactors are considered imperfect simulations of the atmosphere (Ezzell, et al., 2010), an appropriate set-up that would better simulate field studies would be the use of a wind tunnel. The latter is typically used to investigate air sampling in ambient environment (Chen, et al., 2004) (Lee, Yu, & Kim, 2013) and is recommended to be used by EPA for testing and performance evaluation of PM_{10} samplers under the Title 40 of the Code of Federal Regulations (EPA, United States Environmental Protection Agenc, 2017).

The fine particles collected during air quality sampling (AQS) from both urban or rural sources, are usually a combination of primary and secondary aerosols. The primary particles are generated directly by mechanical actions (e.g. milling and grinding) or by chemical processes (e.g. combustion emissions of power plants). On a cattle or dairy facility, the main sources of primary particles are animal movements on loose feedlot grounds, feeding operations, and vehicular transport on unpaved roads. Secondary particles are formed through a multi-step complex reactions, mainly dominated by acid/base and light-catalyzed redox reactions. In CAFOs, secondary particles are formed principally from gas-phase ammonia as the main precursor gas (Sakirkin, Maghirang, Ammoson, & Auvermann, 2012). Ammonia is known to react with sulfates, nitrates and other acid-based species to form particles ranging from sub-micron to micron range.

The formation of secondary fine particles ($PM_{2.5}$) from interactions of ammonia and other reacting species in the atmosphere can be either through homogeneous nucleation (generation of new particles) or heterogeneous nucleation (condensation and/or growth on existing particles). The nuclei formed from ammonia with other precursor gases are mainly dominated by homogeneous nucleation. These nuclei will ultimately be scavenged by coagulation on the surface of preexisting aerosols or larger particles (such as fine dusts) and/or undergo a slow self-growth to detectable particle sizes (Kerminen, Pirjola, & Kulmala, 2001).

The fact that newly formed particles can be entrained significantly or even totally together with existing particles in the ambient air has important consequences on air

sampling measurements. The tendency of ammonium aerosols to form new particles or coagulate/condense on existing particles can influence the mass of the total particles, especially within the fine range (0.1 to 1 μm). As a consequence, there is a possibility that any measured $PM_{2.5}$ mass using EPA's $PM_{2.5}$ Federal Reference Method (FRM) samplers can increase due to the contribution of secondary $PM_{2.5}$ formation.

To investigate this possibility, polydispersed fine dusts as representative for agricultural dusts (having an MMD of 18 μm). The dusts were dispersed inside a wind tunnel together with precursor gases, NH_3 and SO_2. A FRM $PM_{2.5}$ sampler was used to collect particles that have diameters of ≤ 2.5 μm. The result of the study provides an empirical investigation of the possible contribution of secondary PM2.5 on the mass of $PM_{2.5}$ collected during typical field air sampling activities.

This study ultimately yields a direct secondary PM2.5 unit emission factor based on the differences of $PM_{2.5}$ masses collected between that of dispersed dusts only (control tests) and that of which precursor gases were involved (aerosol tests). The final 2^o $PM_{2.5}$ emission factor was compared with the results of the reactor flow study and of EPA's.

III.2. Objectives

This study was conducted primarily to determine the contribution of secondary $PM_{2.5}$ particle formation to the mass of $PM_{2.5}$ dusts collected using an FRM PM2.5 in an ambient wind tunnel.

Specifically, the objectives of this study were:

1. To empirically estimate the contribution by mass of secondary PM2.5 particles during the dispersion of test dusts (assumed to be primary PM2.5) together with NH_3 and SO_2 gases.
2. To determine the physical and chemical characteristics of the PM2.5 samples collected from the aerosol tests.

III.3. Methodology

III.3.1. Test Dust Feeder

For agricultural aerosols, the mass median diameter (MMD) is usually around 15 µm or larger (Faulkner, Shaw, & Lacey, 2007). This study utilized an ISO 12103-1, poly-dispersed fine test dust with an MMD around 18 µm in order to represent a typical agricultural dust from CAFOs. The test dust was heated at 105 ^{o}C for an hour and kept in a desiccator prior to use in order to lessen the moisture content and avoid any caking problems during dust feeding.

A Wright Dust Feeder II by BGI Inc, MA, USA was used to introduce the test dust into the wind tunnel. It is equipped with a carbide blade that continuously scrapes the surface of the dust in a packed cylindrical container. The dust feeder requires a compacted dust input which was facilitated by using an MTS compaction system. The dust were exposed to a compaction pressure of 1.5 kilo-pounds for 2 minutes. The scraping mechanism of the feeder is achieved by means of a rotating platform attached to a small motor. A certain velocity of air is introduced to blow away the scraped dust

through of the outlet nozzle. The emission rate of the dust particles is dependent on the speed of rotation, which is dictated by a digital controller. The feeder has a broad range of emission rate output from 0.0026 to 60 g/h (Guha, 2009). For this study, a dust feed rate was fixed at 500 mg/min.

III.3.2. Experimental Set-up

The wind tunnel located at the PM Building, West Campus of Texas A&M University was used for this aerosol study. It was designed and fabricated by the Center for Agricultural Air Quality Engineering and Science (CAAQES) at Texas A&M University based on the EPA performance standards for sampler evaluations specified in 40 CFR Part 53, Subpart D (Code of Federal Regulations, 2006).

Figure 25 presents the overhead view of the wind tunnel lay-out. A backward inclined, PLR-206 class 4 centrifugal fan with a capacity of up to 170,000 cubic-feet per minute (cfm) was used to draw in air into the wind tunnel. It was equipped with a variable frequency drive to regulate its speed. The fan blows up through a vertical premixing duct (B) towards the transition box (C). The whole body of the wind tunnel was installed on an elevated platform to minimize vibration effects. The transition box (C) serve as an elbow to encourage turbulence from the incoming air flow. It was strategically designed before inflow duct (D) which is the entry point of the precursor gases. The transition box was meant to provide a turbulent flow prior to the source of precursor gases to promote mixing and improve the collision rate of the gaseous species (Hinds, 1999). The dust was introduced into the mixing chamber (E). This is the portion of the wind tunnel where the dust and the pre-mixed precursor gases were assumed to

had undergone an initial interaction. The air, together with the particles and precursor gases, passes through a 1 x 1 m flow-stabilizing tunnel (F). A Sterman disc was installed immediately after the initial point of the stabilizing tunnel to ensure mixing of all components, and followed by flow straightener. At the end of the tunnel is the test chamber (G). The test chamber was designed to have an expanded cross-sectional area to minimize wall effects and for ease of installation of multiple PM samplers. The air exits out of the test chamber through the a 90^{o} exhaust duct.

III.3.3. FRM PM2.5 Sampler and Operation

In contrast with the reactor flow study (Chapter II) wherein PSD was used to determine the $PM_{2.5}$ cut, the FRM sampler should be able to achieve this role. The cut-point of the FRM $PM_{2.5}$ sampler is known to be within the 2.5 ± 0.20 μm. The collected particles should fall within this range which was further confirmed by a random PSD check test during establishing the dust control experiments. The PSD was generated using a coulter counter analysis, a method which was detailed in Chapter II.

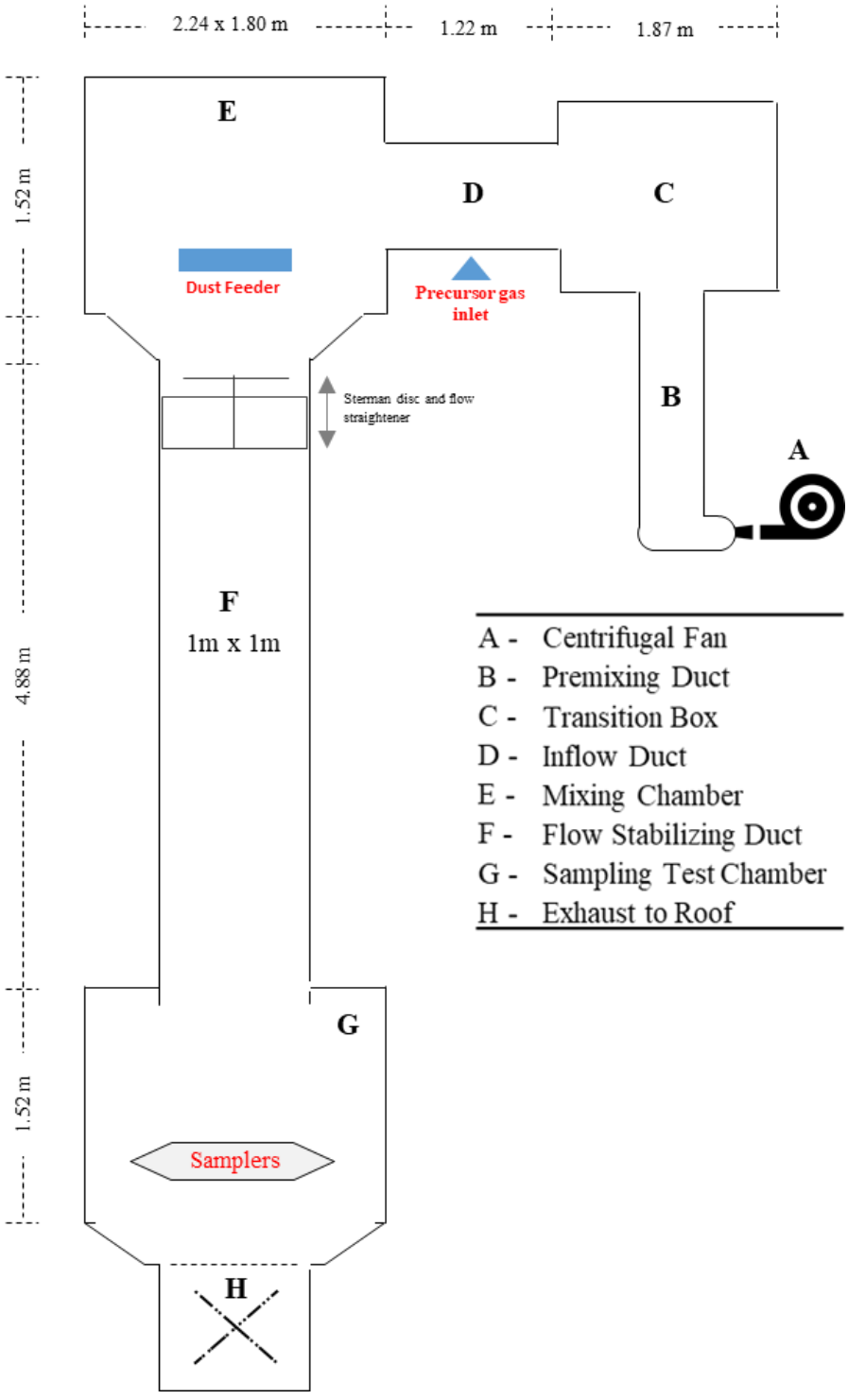

Figure 25. Wind tunnel dimensions and lay-out.

A BGI PQ200 Sampler was used and equipped with a $PM_{2.5}$ very sharp cut cyclone (VSCC). The whole sampling system is designated as EPA FRM (RFPS-0498-116). The operating principle for the sampling system generally followed the EPA sampling methodology detailed on the $PM_{2.5}$ Speciation Guide document (EPA, 1999). Basically the air was drawn into the sample PTFE 47mm filter at a controlled rate of 16.7 L/min. It was designed to sustain a 5-minute averaged flow rate with a flow variation within ± 5% tolerance limit.

III.3.4. Monitoring of Operating Parameters

The velocities at the entrance and exit of the flow stabilizing duct were checked for uniformity before the start of the aerosol wind tunnel experiment. The velocities were obtained by using WindMate 350 multi-purpose sensors with a precision of 0.01 m/s and accuracy of ± 3%. The ambient temperature (T) and relative humidity (RH) were also measured every minute, and reported as an average of five minutes for the whole 1-hour aerosol wind tunnel test.

Since the wind tunnel cannot regulate the T and RH during the wind tunnel tests, all the runs were conducted within 9 am – 3 pm from January 20 to January 28, 2018 in the attempt to set a working range of T and RH. All recorded ambient T and RH data were reported as 30-minute averages.

III.3.5. Wind Tunnel Testing Protocol

For each test, the wind tunnel was carefully cleaned starting from the inflow duct up to the test chamber to minimize any effects from any pre-existing particles on the

surface. Any visible dusts on the PM sampler's pre-collector were also removed prior to each test. The whole testing protocol consist of three stages – pre-experiment, wind tunnel testing, and post-experiment.

The *pre-experimental stage* consist of filter preparation, installation of the PM sampler and tunnel conditioning. All PTFE filters (Whatman) and their corresponding cassettes (Pall Laboratories) were passed through an anti-static system (Mettler Toledo) prior usage. All filters used for each day were pre-weighed using ultra-microbalance (Sartorius) with 0.1 µg readability and conditioned inside a desiccator under room temperature. The clean PM sampler was then installed and the pre-weighed filter was loaded into the sample holder. The tunnel was then tightly closed in preparation for conditioning. The latter lasts for about 15 minutes prior the actual test. The centrifugal fan was turned on at a frequency of 7.8 Hz which is equivalent to about 2 km/h (0.5 m/s) of wind speed. Conditioning was initially done to equilibrate the tightly sealed tunnel and further remove any suspended pre-existing particles. It should be noted that at this point the sampler pumps were still closed so it was assumed that no particles were collected.

The *wind tunnel testing* consist of two treatments: A – dust only and B – dust + precursor gases. A 40:1 NH3/SO2 ratio (by volume) was used in this study. This corresponds to an effective NH3 concentrations of 7 200 ppm of NH_3 and 180 ppm of SO_2 upon mixing with air. The dust feeder and the sampler pumps were turned at the same time. Both the NH_3 and SO_2 gas tanks were simultaneously introduced during the

aerosol tests (Treatment B). The total wind tunnel test lasted for an hour. After the test, whole system was turned off.

The *post-experiment stage* involves the careful removal of the filter from the PM sampler. The test chamber remained closed while removing the filter to avoid any influence from the external environment. The removed filter together with the collected $PM_{2.5}$ was placed back into its labelled cassette and transferred inside a desiccator for conditioning. After removal of filter, the centrifugal pump was turned on at 4 kph to remove any left-over particles and precursor gases inside the wind tunnel system. The sampler head was cleaned and the internal tunnel surfaces were wiped off of any dust residues in preparation for the next run.

III.3.6. PM Characterization

The preparation of filters (Whatman) used, $PM_{2.5}$ recovery and post-weighing were all based on the Standard Operating Procedure for PM Gravimetric Analysis (EPA, 2008). All filter cassettes (Pall Laboratory) were sterilized by gamma irradiation and are tight sealed to lock in humidity. Each cassette was passed through an anti-static system (Mettler Toledo) prior usage.

Filters were pre-weighed and conditioned inside a desiccator under room temperature. After each run, the filters together with the recovered PM2.5 passed through an anti-static system in order to neutralize disruptive electrostatic charged samples that may distort precise weighing. The pre- and post-weighing of the PM2.5 samples continue until the change in the mass read-outs was within ± 5%. An ultra-microbalance (Sartorius) with 0.1 µg readability was used. The difference between the

initial and final weights corresponds to the weight of the $PM_{2.5}$ particles, reported in milligrams (mg).

The FTIR analysis was used for chemical characterization. A representative test dust FTIR spectrum collected from Treatment A was generated and then compared with the FTIR spectrum of the samples collected from Treatment B (dust + secondary aerosols).

The over-all particle morphology and surface elemental characterization was also determined using a Tescan Vega Scanning Electron Microscope (SEM) of the Microscopy and Imaging Center of Texas A&M University. It is equipped with an Oxford EDS detector that allows elemental analysis, particularly on the surface of the particle. The SEM images were used to identify visible changes on the surface characteristics of the test dust upon interaction with the secondary aerosols.

The test dust chemical composition is presented in Table 13. More than 70% of the dust are made up of silica while the rest are all powdered mineral oxides. Using these composition as the baseline chemical characteristic for test dust, any presence of sulfur elements on the surface of the dust, as determined by the EDS analysis, should indicate an effective interaction with the precursor gases. This interaction may be through heterogeneous nucleation or simply coagulation on the particle dust surface.

Table 13. Chemical composition of the poly-dispersed fine test dust (PTI, 2016).

Components	Quantity
Silica	69-77%
Aluminum Oxide	8-14%
Calcium Oxide	2.5-5.5%
Potassium Oxide	2-5%
Sodium Oxide	1-4%
Iron (III) Oxide	4-7%
Magnesium oxide	1-2%
Titanium oxide	0-1%

III.3.7. Data Analysis

To check if the particles collected by the $PM_{2.5}$ FRM sampler were indeed $PM_{2.5}$, a sample was analyzed for particle size distribution using coulter counter (Figure 26). It was revealed that 98.13% of the particles were able to make into the $PM_{2.5}$ cut. This percentage goes higher up to 99.37%, considering the upper size threshold of FRM sampler (± 0.20 µm) which is 2.7 µm.

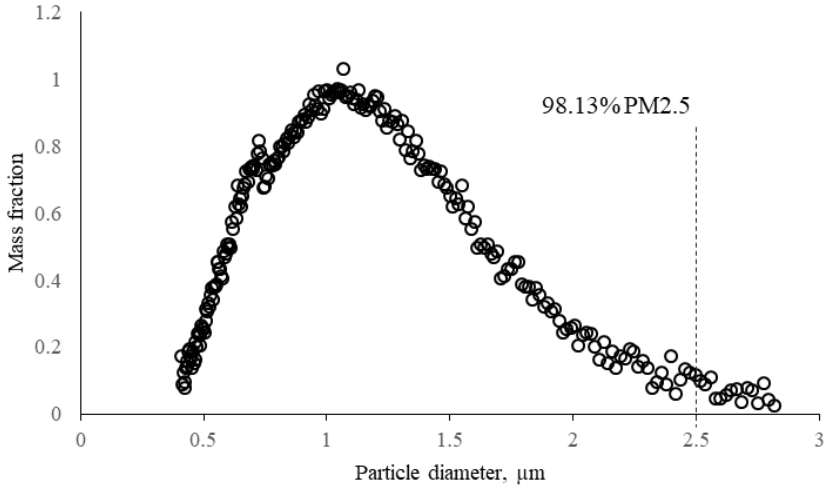

Figure 26. PSD of test dusts collected from $PM_{2.5}$ FRM Sampler.

The difference between the initial and final filter weights corresponds to the weight of the $PM_{2.5}$ particles, reported in milligrams (mg). The weight of the collected $PM_{2.5}$ from the filter was assumed to be the *sum* of both the fine dusts and the secondary aerosols during the aerosol tests. Multiple wind tunnel test replicates using fine dusts only (control) were made to establish uniformity of dust $PM_{2.5}$ masses, at 95% significance level using t-test comparison of means. A single mean value for the mass of dust $PM_{2.5}$ was established and used to estimate the mass of 2^o $PM_{2.5}$ based on equation III.1.

$$2^o M_{PM2.5} = (M_{PM2.5})_{\text{aerosol test replicates}} - (_{\text{mean}} M_{PM2.5})_{\text{control test, dust only}} \quad \text{(III.1)}$$

A unit PM emission was defined as mass of 2^o $PM_{2.5}$ per mass of NH_3 used, $\frac{2^o M_{PM2.5}}{M_{NH3}}$. The unit emission was used to estimate the secondary $PM_{2.5}$ emission factor for cattle feedyard, defined as the 2^o $PM_{2.5}$ per number of cattle in thousands per day. This was calculated using the equation below,

$$2^0 PM_{2.5}\ EF = (2^0 \text{ unit PM2.5 emission}) \times NH_3\ EF \quad \text{(III.2)}$$

Where,

m_{pm} = mass of PM recovered, mg

m_{NH3} = mass of NH_3 used, kg

NH_3 EF, kg NH_3/1000 heads/day

A standard t-test was conducted to evaluate any statistical difference between the means of $(M_{PM2.5})_{\text{aerosol test}}$ and $(M_{PM2.5})_{\text{control test, dust only}}$. The null hypothesis states that there is no significant difference between the masses of $PM_{2.5}$ dust only and the mass of $PM_{2.5}$ from aerosol tests *(dust + precursor gases).* The P value < 0.05 was initially considered statistically significant. If failure to reject the null hypothesis happens at 95%

confidence level, then statistical analysis for $PM_{2.5}$ masses would reconsider a 90% confidence level. A value of P less than the significance level (α) would indicate a statistically significant difference between the two masses $(M_{PM2.5})_{aerosol\ test}$ and $_{(}M_{PM2.5)control\ test}$), providing the confidence to assume that the resulting difference could be attributed to the mass of aerosols ($2^o\ M_{PM2.5}$) formed during the test. JMP interactive statistical software by the SAS Institute Inc. was used for the statistical analysis.

The resulting amount of $2^o\ M_{PM2.5}$ formed from the wind tunnel aerosol tests was then compared with that of the flow reactor study.

III.4. Results and Discussion

III.4.1. Monitoring of Operating Parameters

A number of idealized aerosol chamber, flow reactor and modelling studies were able to conclude that a combination of relatively elevated moisture and low temperature conditions would be ideal for aerosol formations involving NH_3 and SO_2 (Bai, Biswas, & Keener, 1994; Chen, et al., 2004; Guo, et al., 2005; Na, et al., 2007). At around 40 - 50% RH, a NH_3/SO_2 ratio = 3 can achieve at most 80% SO_2 conversion with NH3 (Guo, et al. 2005). Although in general, ammonium sulfate aerosols have low vapor pressure, which allows them to easily condense on particles and droplet surfaces, despite of a low relative humidity.

The wind tunnel has no capability to regulate T and RH. In order to reduce the effects due to T and RH variability, a certain operating range of T and RH was established. Only the collected $PM_{2.5}$ masses from the days that fall within 67 – 73 ^oF

and 45 to 70 % RH were considered. The T and RH profile from January 20 up to January 28 of wind tunnel tests are shown in Figure 27.

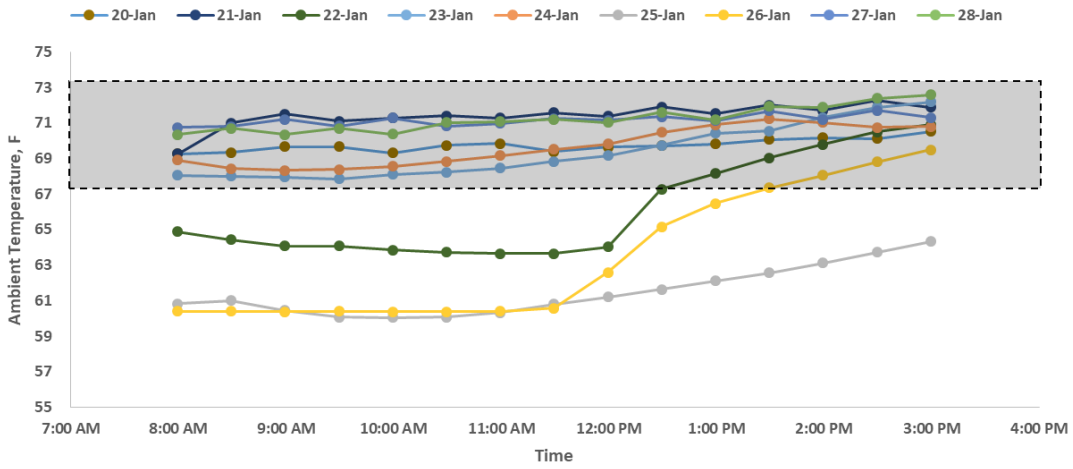

(a)

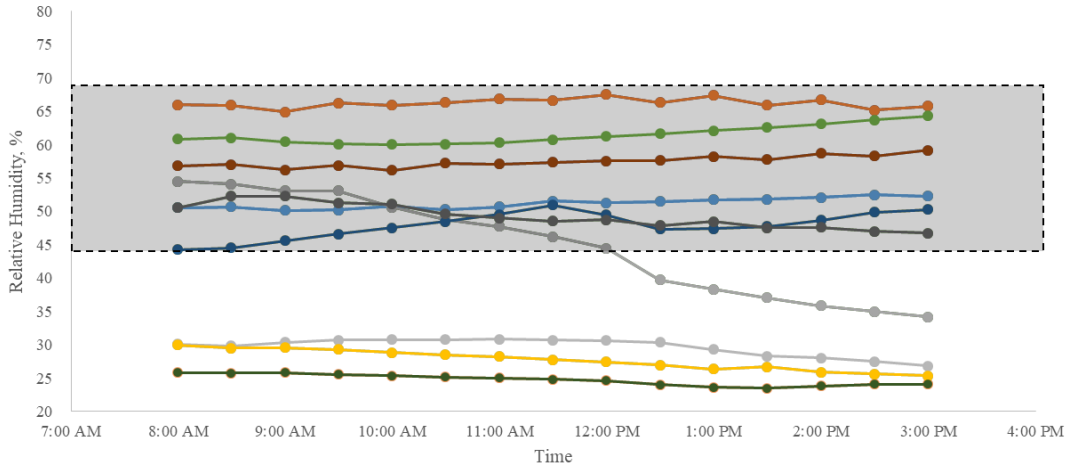

(b)

Figure 27. Relative humidity (%) profile throughout the duration of wind tunnel tests.

The uniformity of velocity was also determined throughout the stabilization tunnel in order to have an idea of the flow stability during dispersion of fine dusts and precursor gases. There was a considerable discrepancy of about 20% between the inlet wind velocity and the outlet velocity in the tunnel. However, the overall average was

still computed to be 2.03 km/h which is close to the set wind speed of 2.0 km/h from the controller.

Table 14. Velocity measurements within the stabilization tunnel, at 5-min interval.

Runtime,	Tunnel Velocity, km/h	
min	Entrance	Exit
5	1.9	1.8
10	2.4	1.9
15	2.6	1.9
20	2.1	1.8
25	2.3	1.7
30	2.2	1.7
35	2.4	1.8
40	2.3	1.8
45	2.5	1.8
50	2.3	1.8
55	2.1	1.7
60	2.2	1.8
1-hr Average	**2.275**	**1.79**

III.4.2. PM Chemical Characterization

The use of FTIR analysis is a convenient way to immediately identify and compare compounds present between two solid samples. A sample from the control runs $(PM_{2.5})_{\text{dusts only}}$ was subjected to FTIR. A clear absorbance band was detected within the spectral region of 1250 to 850 /cm, and a medium peak at 1000/cm (Figure 28a). For soil samples, most of bands generated on this region corresponds to silicon-oxygen (Si-O) functional groups wherein a weak band indicates Si-O stretching (Du, 2011). The typical peaks for Si-O-Si stretching is between 1000 -1090/cm, 945/cm for C-C, 469 – 800 for Si-H functional groups (Dafalla, Mukhtar, & Shaharun, 2010). The results of the dust

FTIR clearly identifies silicate as its primary component. This was consistent with the suppliers compositional analysis of up to 77% silicates (please refer back to Table 12).

Figure 28b shows the FTIR spectral regions for the fine dusts collected upon interaction with precursors gases. Multiple spectral regions were detected, however, the silicate peak was still preserved at 1000/cm. Sulfur-containing functional groups can be identified based on the peaks at 1400/cm and at lower wavelength of 609/cm. At excess ammonia concentrations, the weak peaks around the 3000/cm which is one of the characteristic bands of ammonium sulfate (N-H stretching) (Hisatsune & Heicklen, 1975). The FTIR spectral regions of the aerosol test results were found to be strongly similar to the $PM_{2.5}$ compounds formed from the flow reactor study (Chapter II) for the NH_3/SO_2/Air gaseous system (Figure 28c).

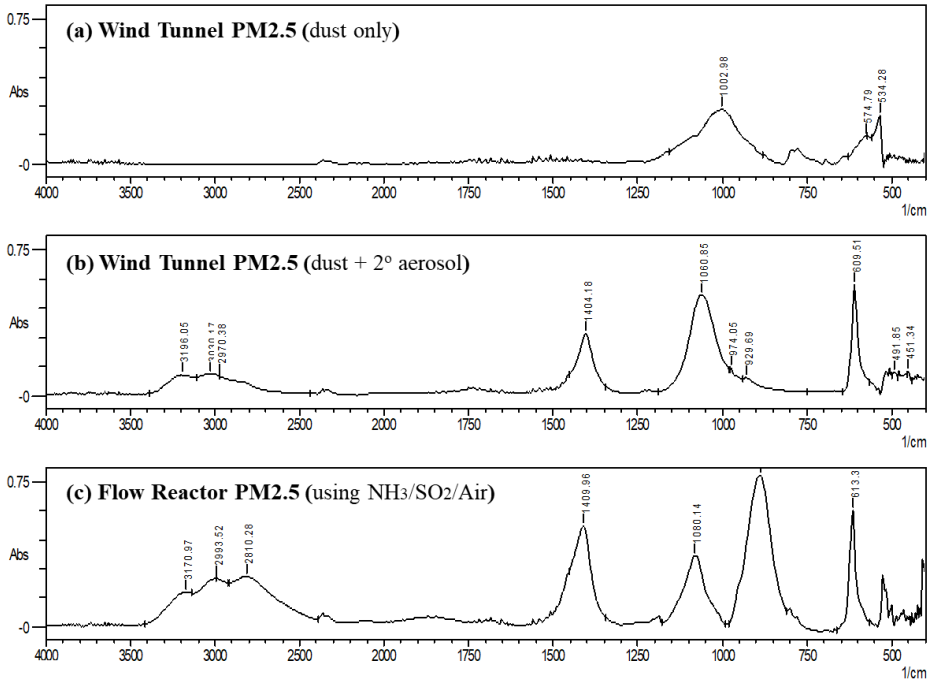

Figure 28. FTIR spectral regions with identification peak bands for samples (a) PM2.5 dust; (b) PM2.5 dusts + aerosol; and (c) PM2.5 from flow reactor study.

III.4.3. Morphology and Surface Elements

Electron images from the two treatment runs were generated using an SEM. The test dust under SEM (Figure 29a) was observed to be dark-colored, irregularly shaped, and mostly granular. Aggregated particles can also be spotted in some parts of the image. In contrast with the image from the aerosol test $PM_{2.5}$ sample, there is a noticeable layer of white powdery particle deposits. These white particles should be the same particles that were generated from the flow reactor study, which were observed to be dominated by 2:1 products of NH_3/SO_2 reaction such as ammonium sulfate.

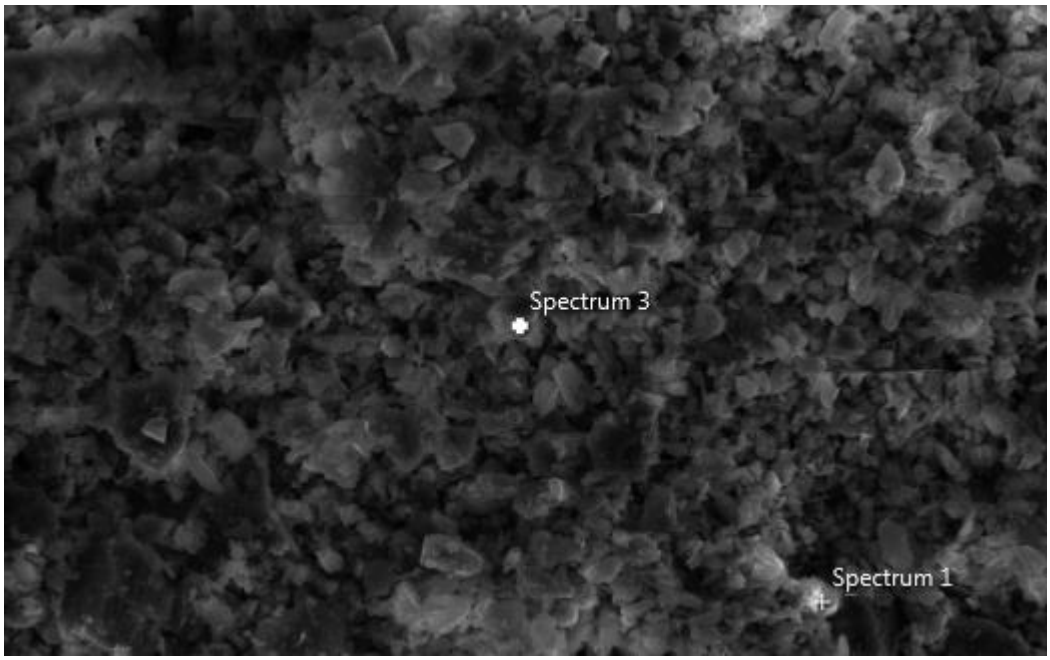

(a)

Figure 29. Electron images of collected $PM_{2.5}$ (a) dust only; (b) dust with precursor gas interaction showing white particle deposits.

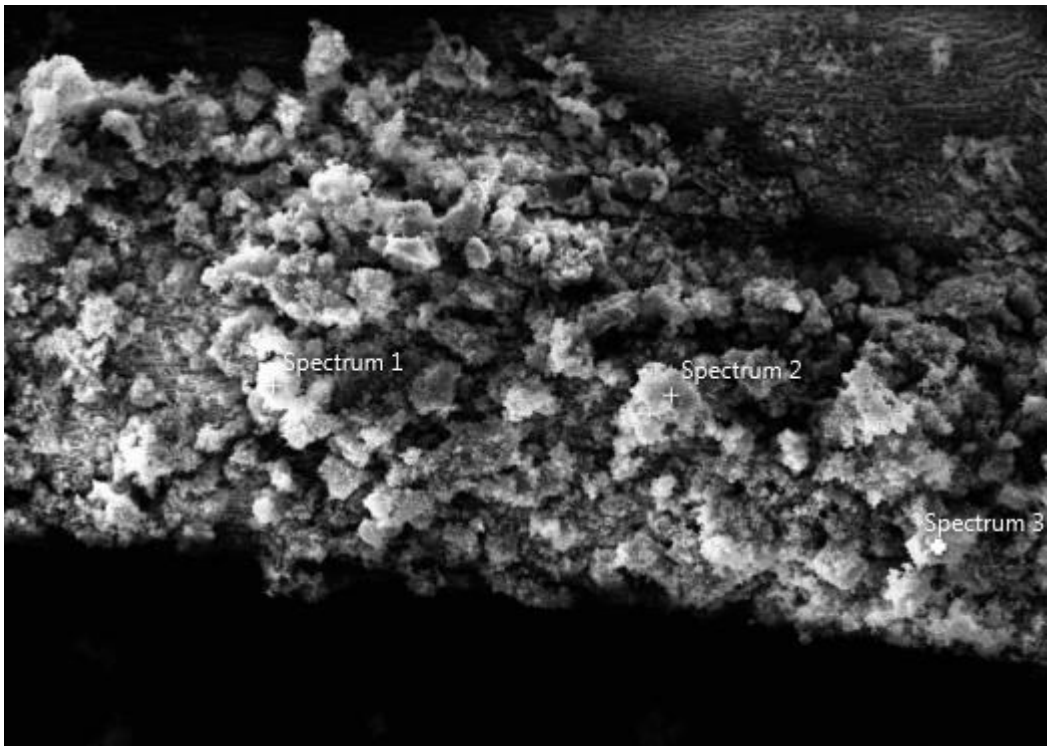

(b)

Figure 29 Continued

The observed white deposits in Figure 29b were found out to be composed of Si, O, Al and S elements. Based on the supplier's compositional analysis, sulfur should not be present on the test dust (Table 12), or at least very minimal in quantity. However, the results of the aerosol test revealed the presence of sulfur from both surface spectral sites (see Figure 30) which appeared to be considerably significant in quantity.

The presence of sulfur-based compounds could provide evidence that the dust particles can serve as a strong sink for nuclei formed from homogeneous nucleation within NH_3/SO_2 and ambient air. It means that the newly formed aerosol particles might have been scavenged by the dust particles during their interaction. The occurrence of heterogeneous nucleation for particle formation might also be possible. Very small dust

particles may induce surface-catalyzed nucleation, particularly for low volatile NH_3/SO_2 product such as sulfuric acid vapor.

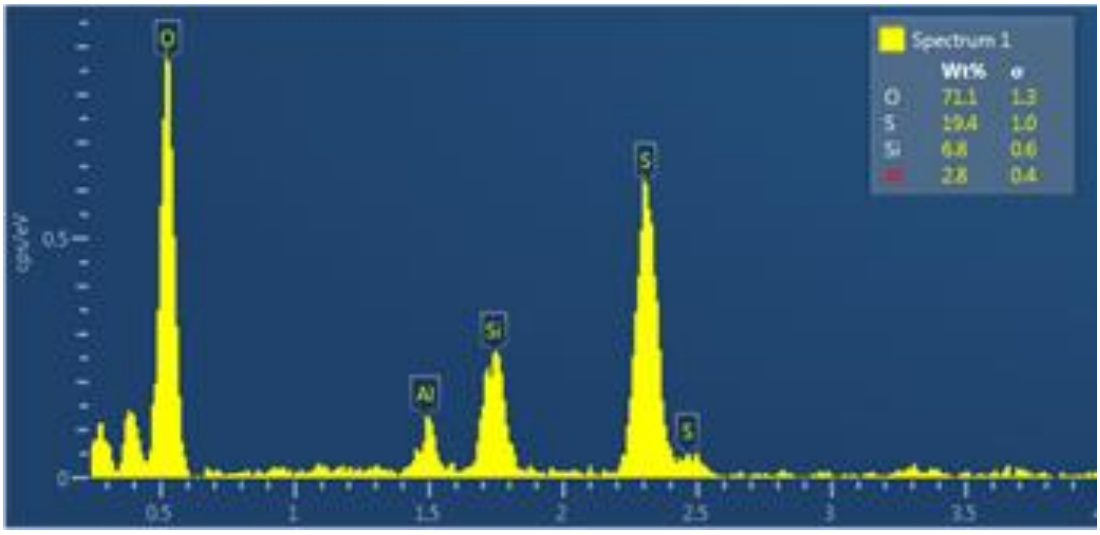

(a)

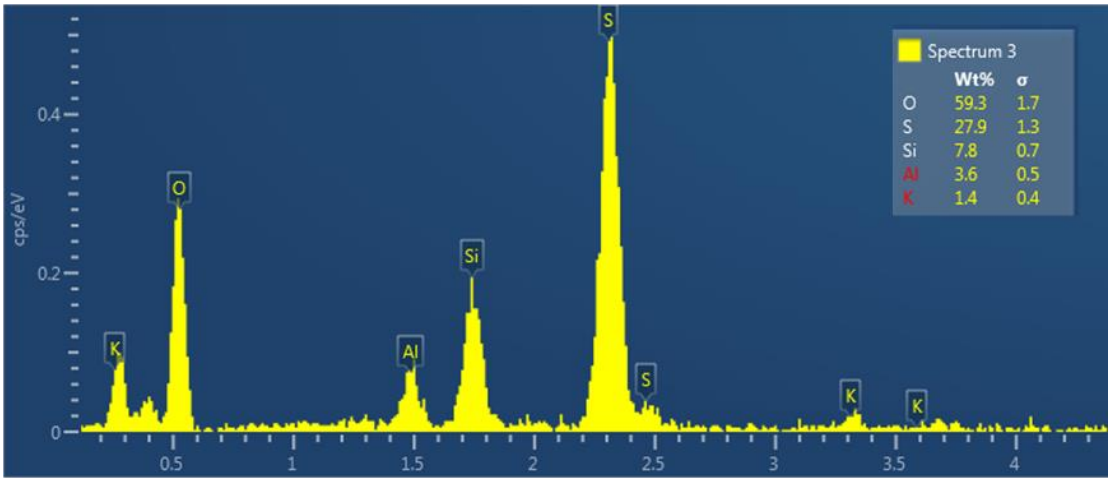

(b)

Figure 30. Surface elemental analysis using energy-dispersive x-ray (EDS) spectroscopy for $PM_{2.5}$ collected from pecursor interactions. (a) Spectrum site 1; (b) Spectrum site 2 (*refer to Figure 31 for spectrum sites*)

The characterization of the $PM_{2.5}$ samples provides a strong evidence of the presence of secondary aerosols together with the dusts. Altogether, they both comprise the total mass of the collected $PM_{2.5.}$ By establishing a certain mean mass of $PM_{2.5}$ for dust alone, the mass of secondary $PM_{2.5}$ (aerosol compounds) could be estimated by difference.

III.4.4. PM2.5 Emission Factor

The mass of $PM_{2.5}$ aerosols was computed based on equation III.1 shown below,

$$2^{o}\, M_{PM2.5} = (M_{PM2.5})_{\text{aerosol test}} - (_{\text{mean}}\, M_{PM2.5})_{\text{dust test, control}}$$

In order to calculate the $2^{o}\, M_{PM2.5}$ by difference, a single value for the $(_{\text{mean}}\, M_{PM2.5})_{\text{control test}}$ was initially established. The $_{\text{mean}}\, M_{PM2.5}$ for dusts was estimated based from the results of 9 consecutive wind tunnel control tests. Table 15 shows the mean (μ = 0.774 mg) of the nine dust wind tunnel tests which was used as the $(_{\text{mean}}\, M_{PM2.5})_{\text{dust only.}}$ There were no outliers among the $(PM2.5)_{\text{dust}}$ masses based on two standard deviations (2 SD) or approximately 95% confidence interval.

Table 15. Calculated mean PM2.5 masses from 'dust only' wind tunnel tests with corresponding T (^{o}F) and RH (%) conditions.

Ave Filter Weights, mg		Mass of $(PM_{2.5})_{dust\ only}$, Mg	Operating T & RH, 1-hr Ave.	
Initial (Filter)	Final (Filter + PM2.5)		T, ^{o}F	RH, %
145.28	146.03	0.741	69.30	50.59
143.20	143.90	0.696	69.53	50.57
140.17	140.91	0.745	69.61	51.09
142.76	143.78	1.021	69.94	51.77
143.03	143.78	0.749	70.13	65.94
143.24	144.23	0.987	71.34	66.10
142.84	143.55	0.707	71.64	66.93
142.13	142.78	0.651	72.01	65.95
142.02	142.69	0.672	68.03	48.71
	Mean (μ), mg	**0.774**		
	Standard Deviation (SD), mg	0.135		
	Acceptable Range, μ ± 2SD[a]	(0.50 - 1.04)		

[a]2SD would mean that 95% of the mass values will fall between the acceptable range.

The total $PM_{2.5}$ masses *(assumed to be dust + aerosol)* from the aerosol tests are shown in Table 16. There were some noticeable increase compared to the PM2.5 masses of the dust tunnel tests. However, in order to establish that the $PM_{2.5}$ masses from the aerosol tests were indeed significantly different from the masses obtained during dust only tests, a standard t-test was used (Table 17). To use the t-test, the data set should first follow a normal distribution. The data set for the aerosol tests are shown to lie around the normality line (solid red line) within the bounds of 95% confidence interval (red broken lines) as shown in Figure 31. Therefore, t-test was a valid tool to compare the means of the masses between the dust only and aerosol tests.

Table 16. Total $PM_{2.5}$ mass and 2º $PM_{2.5}$ mass from aerosol wind tunnel tests with corresponding T (ºF) and RH (%) conditions.

Total $PM_{2.5}$ mass, mg	2º $PM_{2.5}$ mass, mg	Operating T & RH, 1-hr Ave.	
(dust + aerosol)	Aerosol	T, ºF	RH, %
1.07	0.29	68.67	51.41
0.60	(0.17)	68.69	51.18
1.14	0.37	69.34	49.32
1.10	0.33	71.06	48.19
0.94	0.16	70.77	56.93
1.09	0.32	71.26	57.60
0.68	(0.09)	70.52	58.49

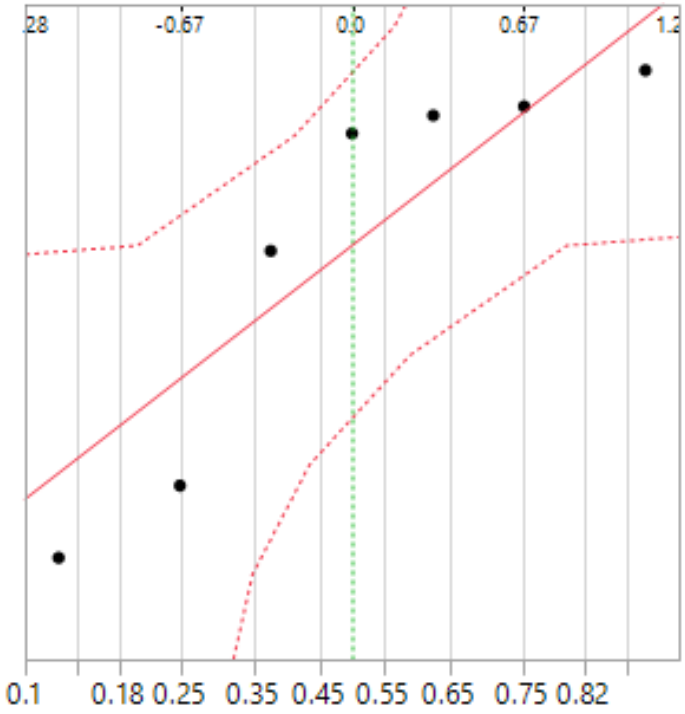

Figure 31. Normal quantile plot for the data distribution of $(PM2.5mass)_{dust + aerosol}$.

The results of T-test are shown in Table 17. The estimated mean from the aerosol test was 0.945 mg. The calculated t-statistics value was 2.07. The t-stat value serves as a measure of departure of the estimated mean of the data obtained from aerosol tests with the mean $(PM2.5)_{dust\ only}$ = 0.774 mg, and from its standard error.

The null hypothesis was that the two means from the dust test results and the aerosol test results were basically the same. If null hypothesis is accepted, subtracting the $(_{mean}M_{PM2.5})_{dust\ test}$ from the aerosol test results to estimate the mass of $(2^o\ PM_{2.5})_{aerosols}$ would become invalid.

The first test was based on a 95% confidence level ($\alpha = 0.05$). Since the Prob > /t/ is greater than 0.05, it fails to establish a significant difference between the two means. However, at a 90% confidence level ($\alpha = 0.10$), the test was able to establish a significant difference. Therefore, the mass of $(2^o\ PM_{2.5})_{aerosols}$ were estimated using equation III.1, at a 90% confidence level. The average mass of $(2^o\ PM_{2.5})_{aerosols}$ was estimated to be 0.273 mg, after removal of the negative values.

Table 17. T-*test* results for the comparison of PM2.5 masses between dust only and aerosol wind tunnel tests.

Hypothesized value = mean $(PM_{2.5})_{dust\ only}$	0.774 mg
Actual estimate = mean $(PM_{2.5})_{dust\ +\ aersol}$	0.945 mg
Degrees of freedom (DF)	6
Standard Deviation (SD), mg	0.22
t-stat	2.07
Prob > /t/	**0.0835**[a]
Prob > t	0.0417
Prob < t	0.9583

[a] not significant at $\alpha = 0.05$. However, it is significant at $\alpha = 0.10$.

The computed unit 2^o $PM_{2.5}$ emissions for aerosol was 128 mg of 2^o $PM_{2.5}$ per kilogram of NH_3 used. The wind tunnel 2^o $PM_{2.5}$ was found out to be significantly lower by several orders of magnitude than the flow reactor study. For the wind tunnel aerosol results, the ratio between the 2^o $PM_{2.5}$ EF and the 1^o $PM_{2.5}$ EF was equal to 2.81%.

III.5. Summary and Conclusion

A wind tunnel was used to simulate the interaction of fugitive fine dusts in CAFOs with precursors gases, in conditions closer to the ambient atmosphere. Aerosol tests using fine dusts (MMD=18μm) and precursors gases, NH_3 and SO_2 were conducted between January 20 to January 28 of 2018. A PM2.5 FRM sampler was used to collect only those particles having diameters $\leq 2.5 \pm 0.20$ μm.

The collective results of the physical and chemical characterization using FTIR, SEM and EDS, strongly suggest that the dust particles can serve as a strong sink for nuclei formed from homogeneous nucleation within NH_3/SO_2 and ambient air. It means that the newly formed aerosol particles might have been scavenged by the dust particles during their interaction. The occurrence of heterogeneous nucleation for particle formation might also be possible. Very small dust particles may induce surface-catalyzed nucleation, particularly for low volatile NH_3/SO_2 product such as sulfuric acid vapor.

This study was conducted primarily to determine the contribution of secondary $PM_{2.5}$ particle formation to the mass of $PM_{2.5}$ dusts collected using an FRM PM2.5 in an

ambient wind tunnel. The computed unit 2^o $PM_{2.5}$ emissions for aerosol was 128 mg of 2^o $PM_{2.5}$ per kilogram of NH_3 used.

The ratio between the 2^o $PM_{2.5}$ EF and the 1^o $PM_{2.5}$ EF in a cattle feed facility was equal to 2.81%. A significant contribution of secondary $PM_{2.5}$ to the total PM2.5 collected in a typical FRM sampler could potentially lead into exceedance of current $PM_{2.5}$ NAAQS threshold for commercial CAFOs. To further investigate the potential impact of the EFs generated, a dispersion modelling was conducted to determine the if the contribution of secondary PM2.5 would cause a cattle feed facility to violate NAAQS threshold.

CHAPTER IV

PM2.5 SOURCE IMPACT ANALYSIS ON A CATTLE FEED FACILITY USING AN ALTERNATIVE SECONDARY PM2.5 EMISSION FACTOR

IV.1. Introduction

States have historically adopted the NAAQS as an enforceable threshold for air quality permitting. The special use of NAAQS serves as a concentration limit that should not be exceeded at the property line and beyond. In order to maintain compliance within the permit conditions, any source is required to show that no PM concentration off property exceeds the NAAQS. Off-property concentrations are normally determined by direct measurements or modelling. Any exceedance to NAAQS may result to enforcement actions such as fines and mandated installation of controls. Primary source emissions are normally estimated using EPA's recommended dispersion model, AERMOD (EPA, 2016).

Instead of using CMAQ as a complicated modelling tool for estimating secondary PM2.5 contributions, an alternative direct PM2.5 EF using ammonia as a precursor gas, was estimated to be 0.019 kg $PM_{2.5}$/1000 heads-day (from aerosol wind tunnel test of Chapter III). With this preliminary EF, one only needs to measure the ammonia emission from a certain cattle feed facility and the population of animals in order to estimate the amount of secondary $PM_{2.5}$ formed. The latter can be added to the primary PM2.5 emission rate in order to perform a source impact analysis for the total PM2.5 emissions (primary and secondary) from the said cattle feed facility.

IV.2. Objectives

The primary goal of this chapter is to evaluate the applicability and impact of the developed secondary PM2.5 emission factor to the NAAQS threshold by conducting a straight-forward Gaussian dispersion modelling using AERMOD. A selected commercial cattle feed facility in Texas was used for this purpose.

IV.3. Methodology

IV.3.1. Test Site

The Wrangler cattle facility is located at the Swisher County in Texas (Figure 32). It is surrounded by a mix of semi-arid and pastureland topography. The test site was considered to be an area source. Table 18 shows further details regarding the test site.

The emission rate for area source should be in terms of flux. This was calculated based from the method proposed by CAAQES experts of Texas A&M University. The equation IV.1 is shown below:

$$\text{FLUX } (\mu g/m^2/s) * 2.65 = \text{EF } (lb/1000hd/day) @ 150\ ft^2/\text{head} \qquad \text{(IV.1)}$$

The PM10 emission factor for cattle feedyards was previously estimated to be at 10 to 20 lb/1000 hd/day. For this case, 15 lb/1000 hd/day was used. The primary PM2.5 emission flux was calculated as 3.0 $\mu g/m^2/s$ after using 10% PM2.5/PM10 ratio.

Table 18. General description of the Wrangler CAFO.

Facility	Wrangler Cattle Feed yard
Location	7231 FM 2986, Tulia, TX 79088
GIS Coordinates	34º39’7.16” N, 101º47’20.30” W
UTM Coordinates	Zone 14, Northern Region 244393.00 m E 3837990.00 m N
Effective Area	~ 2.00 square kilometers
Feed yard Area Only	~0.92 square kilometer
Topography	Semi-Arid/Pasture
Assumed PM10 emission flux **(Source: Parnell, Goodrich, Shaw, et al. ASABE LV)**	**30 µg/m^2/s** =15 lb/1000hd/day
Assumed 1º PM2.5 emission flux **(10% of PM10)**	**3.0 µg/m^2/s**
Source Designation	Area
	Terrain (flat/elevated)

Figure 32. Overview of the Wrangler Cattle facility (AERMOD, 2017)

IV.3.2. Meteorological Data Pre-Processing

There were two important pre-processing steps needed before the full dispersion modelling to occur. First is the MET data processing and the SURFACE/TERRAIN data processing. AERMET is a data preprocessor coupled with AERMOD. It can handle either on-site or met station data. Since on-site data is rarely available, MET data are usually obtained from nearby met stations through the National Weather Service (NWS). In order for AERMET to proceed, two types of weather data are needed:

1) Upper air data
2) Surface air data

Since Tulia belongs to the Swisher County where there is no met station, the TCEQ provided an alternative weather data which can be used for the Swisher County containing data from 2010 - 2015 (TCEQ Met Data 2017). Hourly surface data for the measurement sites were obtained from the NCDC Integrated Surface Database (ISD) for 2010-2015. Upper-air data were obtained from the National Oceanic and Atmospheric Administration (NOAA) Earth System Research Laboratory (ESRL) Radiosonde Database for 2010-2015. Meteorological data should always be 90% complete based from EPA standards. For minor source review air permitting needs, one year of MET data is generally sufficient. However, for existing operations such as the Wrangler facility, a five-year Met data were used. For all permitting purposes, standard year for met data should be from 2012.

Since most surface met data have high incidence of calms and missing wind conditions, AERMINUTE was used to correct this situation. AERMOD cannot simulate under these conditions. The one-minute Automated Surface Observing Stations (ASOS)

wind data for the measurement sites were obtained from the National Climatic Data Center (NCDC) website for 2010-2015. The five-minute Automated Surface Observing Stations (ASOS) wind data for the measurement sites were obtained from the National Climatic Data Center (NCDC) website for 2010-2015.

For the surface parameters, the Tables A-1 to A-3 from EPA's AERSURFACE Guide were utilized. Parameters such as Bowen Ratio, Albedo, and surface roughness were initially obtained from EPA's Guide and the remaining all throughout the year were projected using land use type option in the AERSURFACE.

About 43,806 total records were processed with only 18 missing (99.96% availability > 90% EPA standard). Most of the winds are blowing from the south as shown in the wind rose diagram in Figure 33. About 5% of the time, wind speeds exceed 8 m/s but the annual average is at 6.03 m/s. Wind rose diagram is a product of the AERMINUTE processing. It also shows corrections of calm winds. From the diagram, calm winds were only recorded as 0.07% within the 5-year Met data set.

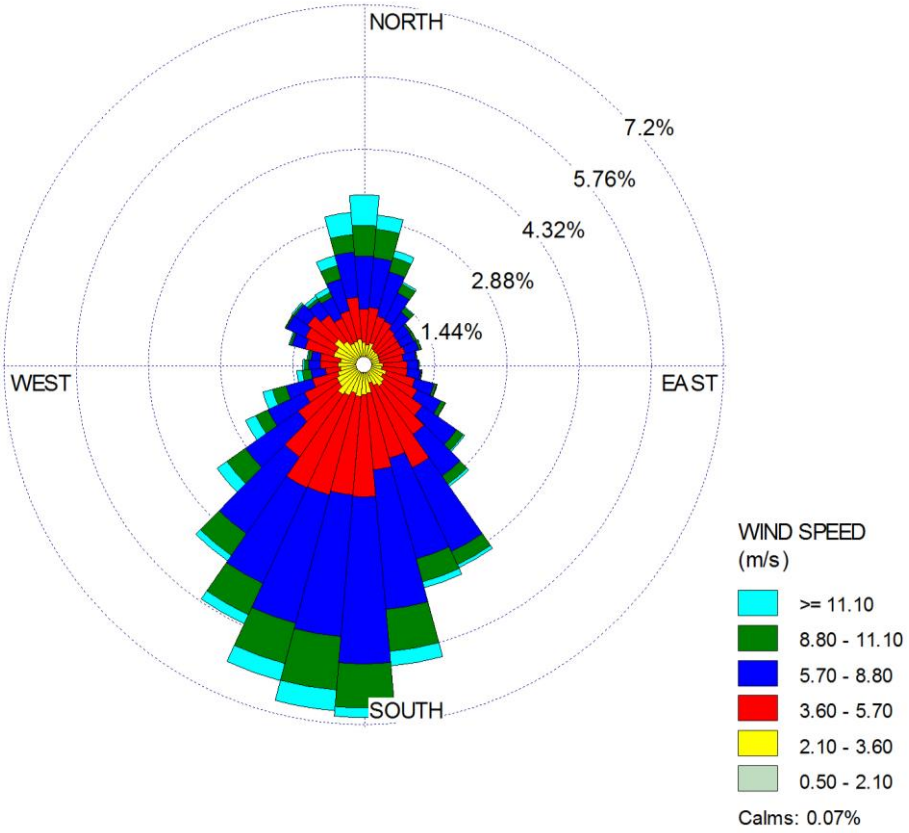

Figure 33. Wind rose profile for Swisher County, TX (AERMOD, 2017).

IV.3.3. Surface and Terrain Parameters

Google Earth map is generally not sufficient to provide an accurate representation of the target site. In order to carefully take into account the terrain and contour of the area, AERMAP processing is necessary. WEBGIS is the primary source of all the maps which are all available online. Upon combination with the recent google earth satellite image, AERMAP processed and integrated together the map downloaded from WEBGIS to reveal updated contours and terrain elevations as shown in Figures 34.

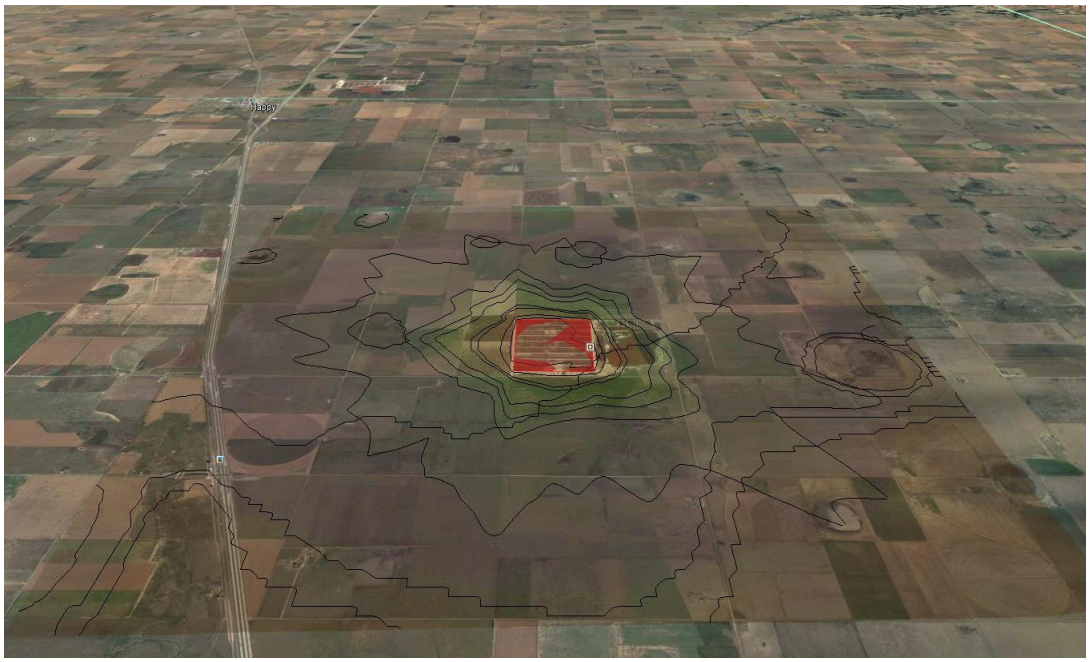

Figure 34. Terrain and Contour Map of Wrangler Facility (AERMOD, 2017)

IV.3.4. Receptors

The modelling analysis was conducted using the following fence line receptor grid design (Figure 35). The receptor grid consisted of 5 tiers beyond the facility area. The segment distance between tiers were 100m, 200m, 400m, 800m, 1000m with unit receptor spacing of 25m, 50m, 100m, 200, and 400m for each corresponding tier. The receptor grid used was based on Universal Transverse Mercator (UTM) coordinates referenced to NAD 83 datum in zone 14.

The extent of this grid was sufficient to capture the maximum modeled concentration. There were a total of 892 receptors, spread out within 3-kilometer radius. The receptor spacing were minimally set to 25m within the first 1-km radius around the

facility.. This was done to ensure the maximum impacts were resolved to a refined receptor grid spacing.

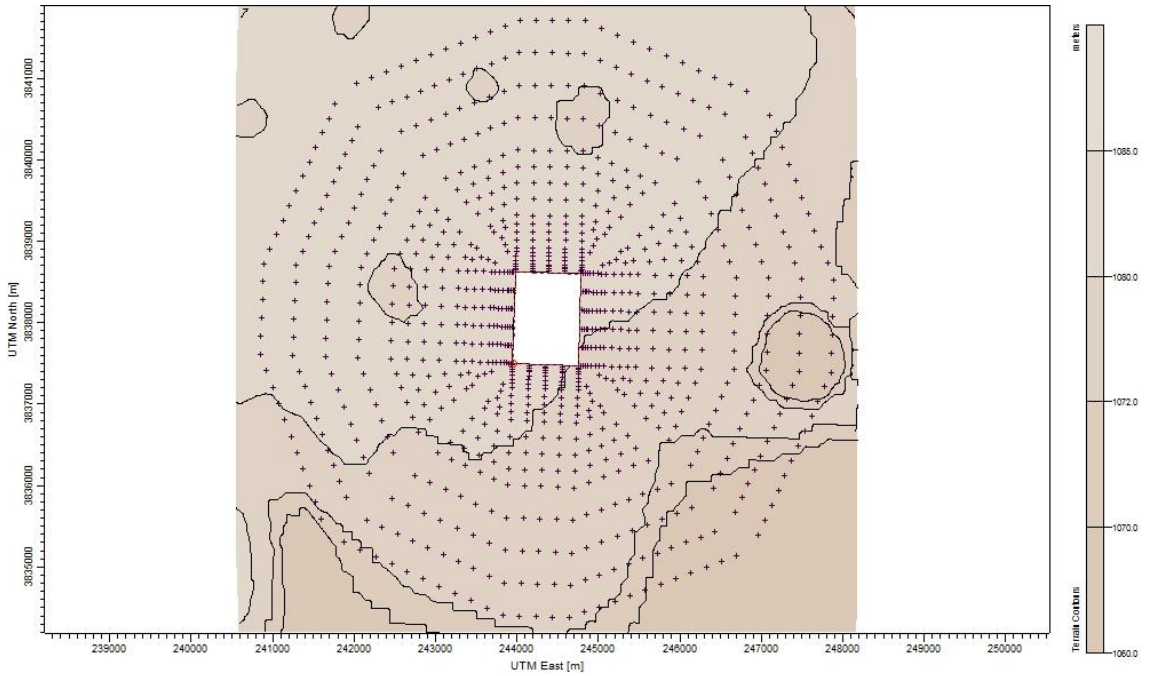

Figure 35. Fence line grid design of 892 receptors used for dispersion modelling within 3-km radius.

IV.4. Results and Discussion

The 24-hr threshold for PM2.5 is 35.0 µg/m3, taking the 98th percentile and averaged for 3-years. The PM2.5 is further assessed based on its primary and secondary form. For primary PM2.5 the design value is 12.0 µg/m3 while 15.0 µg/m3 for the secondary PM2.5. Both threshold concentrations should have annual averaging time, with annual means averaged over 3 years (EPA, NAAQS Table, 2016).

The baseline dispersion modelling was initially conducted for the primary PM2.5 emissions from the selected CAFO. The property line was designated to be 50 m away

from the facility. Hence, the maximum primary PM2.5 concentration that was considered were only those near or beyond property line so that NAAQS can be used as threshold. The maximum concentration for the primary PM2.5 on a 24-hour averaging basis was 30.52 µg/m^3, recorded south about 20m away from the property line (Figure 36). This value is less than that of the NAAQS 24-hour averaging limit.

The annual primary PM2.5 maximum concentration was 8 µg/m^3, which located at near south east of the facility, 1 meter away from the property line (Figure 37). This annual modelled value is less than the 12 µg/m^3 NAAQS.

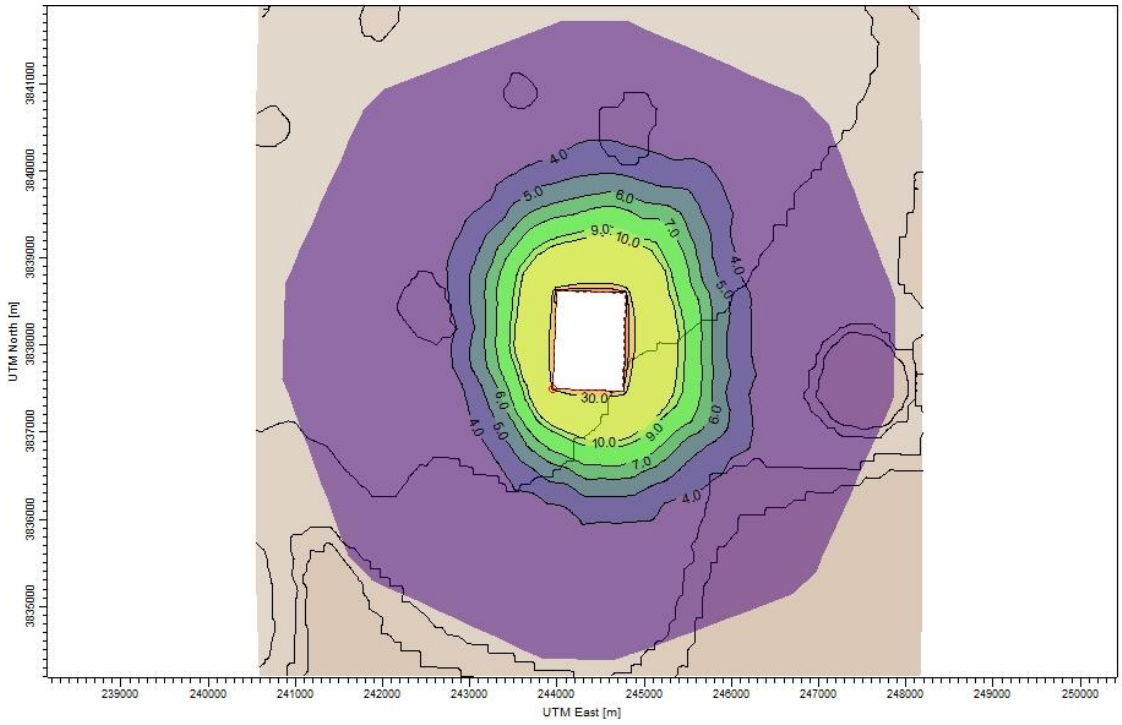

Figure 36. Wrangler CAFO 24-hour maximum primary PM2.5 concentration isopleth.

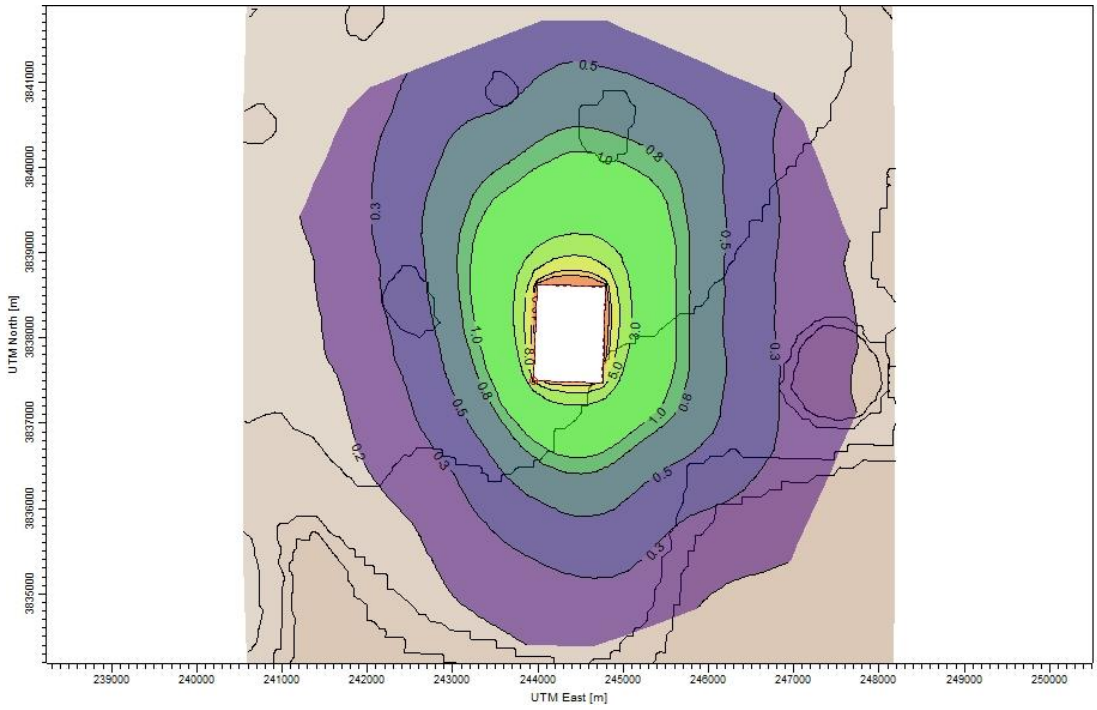

Figure 37. Wrangler CAFO annual maximum primary PM2.5 concentration isopleth.

For the secondary PM2.5 concentration, assuming the PM2.5 was mainly ammonium sulfate and formed within the facility, the dispersion of the direct PM2.5 equivalent are shown in Figure 38 & 39 for the 24-hour averaging and annual maximum concentrations, respectively.

The 24-hr maximum secondary PM2.5 concentration, 0.80 μg/m^3, was located at the southeast end of the facility, 14m away from the property line. Meanwhile, the annual secondary PM2.5 concentration. 0.01 μg/m^3, was located almost near the receptor for the 24-hr maximum secondary PM2.5 concentration.

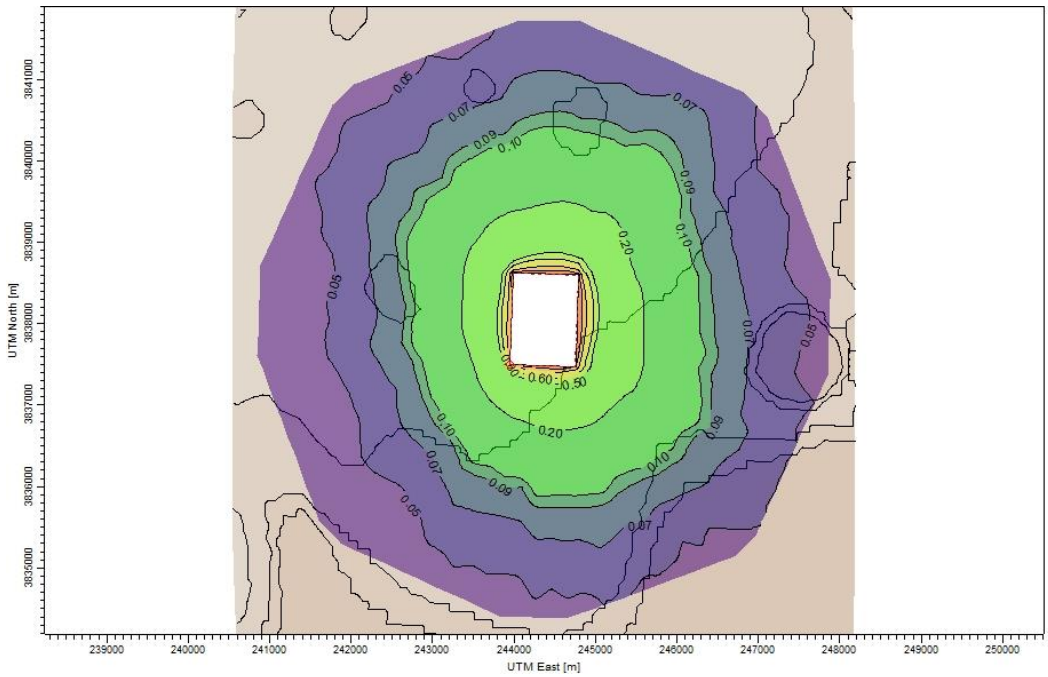

Figure 38. Wrangler CAFO 24-hour maximum secondary PM2.5 concentration isopleth.

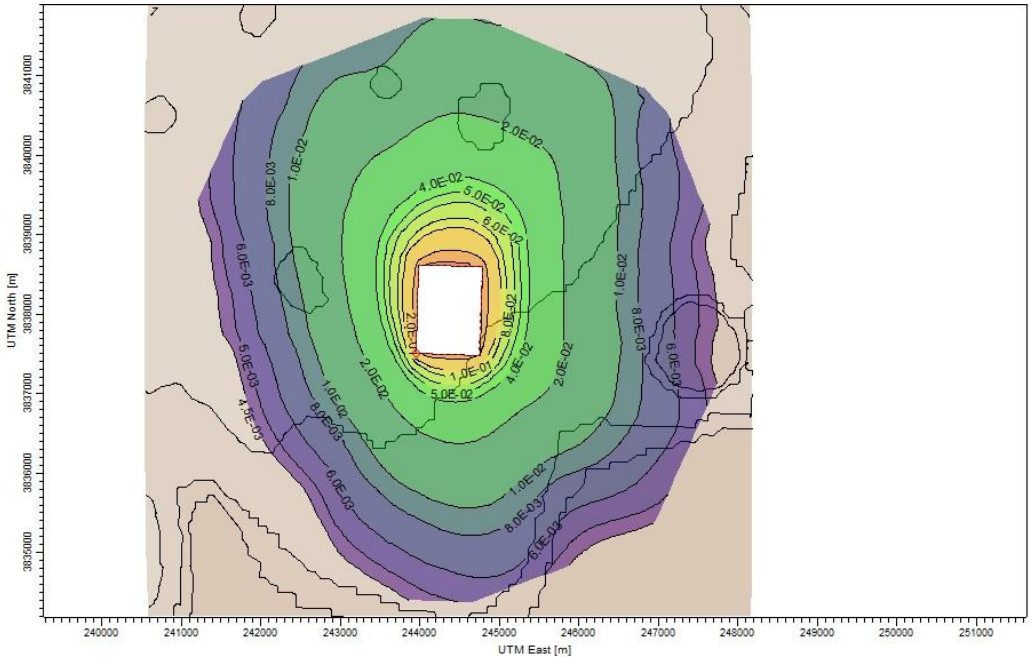

Figure 39. Wrangler CAFO 24-hour maximum secondary PM2.5 concentration isopleth.

Assuming that the maximum primary and secondary PM2.5 impacts occur on the same time and the same receptor, adding up both maximum concentrations would yield a total of 31.32 μg/m^3 for the 24-hour NAAQS while a total of 8.01 μg/m^3 for the annual NAAQS. Both of these total values were below the thresholds, implying that the facility has no PM2.5 emission violations based on NAAQS.

By general observation, the maximum concentrations modelled beyond the facility were recorded to be very close to the facility. The concentrations within the 1-kilometer radius significantly decreased by magnitudes of 3-8 than the maximum levels near the property line. Based on the receptor locations of the maximum recorded primary and secondary PM2.5 concentrations, it is very unlikely that the both types of PM2.5 would ever occur at the same receptors.

It would take a considerable conservative change to the emission factors generated from this research before the NAAQS could be threatened (Table 19).

Table 19. Total PM2.5 (Primary + Secondary) air ambient impacts with comparison to NAAQS using an alternative secondary PM2.5 emission factor.

	Modeled Primary PM2.5 (μg/m^3)	Modeled Secondary PM2.5 (μg/m^3)	Total PM2.5 (μg/m^3)	PM2.5 Standard (μg/m^3)
NAAQS 24-hr	30.52	0.80	31.32	35
NAAQS Annual	8.00	0.01	8.01	12

Another way to estimate the total PM2.5 impacts is to use the ratio of secondary PM2.5 to the primary PM2.5 emissions generated from this research, equivalent to 2.81%. By multiplying the modeled primary PM2.5 concentration with 0.0281, the

secondary PM2.5 equivalent were estimated to be 0.86 µg/m^3 for 24-hour and 0.22 µg/m^3 for annual (Table 20). The resulting total PM2.5 are still below the NAAQS.

Table 20. Total PM2.5 (Primary + Secondary) air ambient impacts with comparison to NAAQS using an alternative 2^o $PM_{2.5}$/1^o $PM_{2.5}$ for CAFO.

	Modeled Primary PM2.5 (µg/m^3)	Secondary PM2.5 Equivalent (µg/m^3)	Total PM2.5 (µg/m^3)	PM2.5 Standard (µg/m^3)
NAAQS 24-hr	30.52	0.86	31.32	35
NAAQS Annual	8.00	0.22	8.01	12

The results of both cases revealed that using the PM ratio could probably provide a quick estimate of the secondary PM2.5 equivalent for 24-hr concentrations instead of using dispersion modelling.

IV.5. Conclusion

The PM ratio ($2^oPM_{2.5}$/1^o $PM_{2.5}$ = 2.82%) generated from this research should provide an implicit conservative approach in estimating the effects of secondary PM2.5 to the total PM2.5 levels in a CAFO based on the modelling results. This conservative approach assumes that both maximum impacts of secondary and primary PM2.5 occur at the same place and same time. In reality, formation of the sulfate particles should be a fairly slow process. Therefore, the peak concentrations of secondary PM2.5 are expected to occur a significant distance downwind from the receptor location of the maximum primary PM2.5 concentration.

CHAPTER V

SUMMARY AND CONCLUSIONS

At present, there is still no available emission factor (EF) for secondary (2^o) $PM_{2.5}$, particularly for concentrated animal feeding operations which emit vast amounts of ammonia to the atmosphere. This research was focused on how much $PM_{2.5}$ can be obtained from reactions of ammonia with sulfur dioxide inside two controlled reaction environments - flow reactor and wind tunnel.

To empirically estimate the amount of 2^o PM2.5 at an idealized reaction condition, an aerosol flow reactor was fabricated. The flow reactor experiments were conducted at approximate ammonia to sulfur dioxide reactant volume ratios of 5:1, 10:1 and 30:1 for the treatments without air; and two more treatments where SO_2 is further diluted producing a 60:1 ratio in the presence of 10% and 20% O_2. Reaction concentrations were within the range of 160 – 11 000 ppm. The resulting compounds in the particles were dominated by ammonium sulfite and ammonium sulfates based on FTIR analysis, particularly at conditions of high excess ammonia and higher O_2. The whole reaction system recorded a relatively low $SO_{2\ maximum}$ conversion of 40%. All $PM_{2.5}$ formed appear to be white in color ranging from powdery to crystal-like particles based on electron images. The EDS analysis revealed abundance of sulfur (S) and Nitrogen (N) elements on the surface of the PM2.5 products. Wall loss effects and heterogeneous nucleation were both observed to be dominating factors during particle formation.

The second study involved a wind tunnel test in order to simulate the interaction of fugitive fine dusts in CAFOs with precursors gases, in conditions closer to the ambient atmosphere. A $PM_{2.5}$ FRM sampler was used to collect only those particles having diameters $\leq 2.5 \pm 0.20$ μm. The collective results of the physical and chemical characterization using FTIR, SEM and EDS, strongly suggest that the dust particles can serve as a strong sink for nuclei formed from homogeneous nucleation within NH_3/SO_2 and ambient air. The occurrence of heterogeneous nucleation utilizing very fine pre-existing particles was also of equal importance.

The idealized 2^o $PM_{2.5}$ formed per ammonia used was calculated to be within the range of 5.64 – 10.70 mg of PM2.5 per 1000 mg of NH_3 used from the flow reactor study and 0.13 mg of PM2.5 per 1000 mg of NH_3 from the wind tunnel study. The PM ratio between the 2^o $PM_{2.5}$ and the 1^o $PM_{2.5}$ based on the wind tunnel tests was estimated to be 2.81%.

The third study was a source impact analysis on a selected CAFO in Texas. The PM ratio ($2^oPM_{2.5}/1^o PM_{2.5} = 2.82\%$) generated from this research should be able to provide an implicit conservative approach in estimating the effects of secondary PM2.5 to the total PM2.5 levels in a CAFO based on the dispersion modelling. This conservative approach assumes that both maximum impacts of secondary and primary PM2.5 occur at the same place and same time. In reality, formation of the sulfate particles should be a fairly slow process, and maximum impact maybe further downwind from the maximum primary PM2.5 impact. The use of the PM ratio could possibly provide a quick estimate of the secondary PM2.5 equivalent for 24-hr concentrations.

The idealized secondary PM2.5 generated is not yet mature enough to be used for regulatory purposes. However, the results of this study should be considered as an initial step towards addressing the challenges of accounting the impacts of secondary PM2.5 formation in cattle feed yards or any facility emitting ammonia. The knowledge gained about the formation rates, yield and characteristics of secondary PM2.5 from this research should provide sufficient vital information for future field studies in order to generate an acceptable secondary PM2.5 emission factor for CAFOs based on different geographic factors and more realistic ambient atmospheric variables.

REFERENCES

AERMOD. (2017). AERMOD View: Gaussian Plume Air Dispersion Model. Ver. 9.5. Lakes Environmental.

Ahlberg, E., Falk, J., Eriksson, A., Holst, T., Brune, W., Kristensson, A., and B. Svenningsson. (2017). Secondary organic aerosol from VOC mixtures in an oxidation flow reactor. *Atmospheric Environment, 161*, 210-220.

ASTM International. (2017). ASTM E 168: Standard Practices for General Techniques of Infrared Quantitative Analysis. West Conshohocken, PA: ASTM International.

Bai, H., Biswas, P., & T. Keener. (1994). SO2 Removal by NH3 Gas Injection: Effects of Temperature and Moisture Content. *Ind. Eng. Chem. Res. 33*, 1231-1236.

Barker, J. (1995). Progress and Problems in Atmospheric Chemistry. Singapore: World Scientific Publishing Co. Pte. Ltd.

Beckman Coulter, . (2016). Fact Sheet: The Coulter Principle. Indianapolis, IN: Beckman Coulter, Inc.

Bonifacio, H., Rotz, C., Leytem, A., Waldrip, H., & R. Todd. (2015). Process-based modeling of ammonia and nitrous oxide emissions from open-lot beef and dairy facilities. *Transactions of the ASABE, 58 (3)*, 827-846.

Brennen, C. (2005). Fundamentals of Multiphase flows. California Institute of Technology, CA: Cambridge University Press.

Buser, M., Parnell, C., Lacey, R., Shaw, B., & B. Auvermann. (2001). Inherent biases of PM10 and PM2.5 samplers based on the interaction of particle size and sampler performance characteristics. *2001 ASAE Annual International Meeting* (pp. 1-24). Sacramento, CA: ASAE.

Chen, T. C., & C. Tsai. (2017). Modeling approach for emissions reduction of primary PM2.5 and secondary PM2.5 precursors to achieve the air quality target. *Atmospheric Research*, 11-18.

Chen, Y., Irshad, H., McFarland, A., Su, W., Zhou, Y., & D. Barringer. (2004). An Aerosol Wind Tunnel for Evaluation of Massive-Flow Air Samplers and Calibration of Snow White Sampler. *Aerosol Scienceand Technology, 38*, 1099-1107.

Code of Federal Regulations. (2006). Ambient air monitoring reference and equivalent methods. 40 CFR, Part 53, Subpart *D.* Washington, D.C.: US Government Printing Office.

Cohan, D., & S. Napelenok. (2011). Atmospheric Response Modeling for Decision Support. *Atmosphere*, 407-425.

Coury, C., & A. Dillner. (2008). A method to quantify organic functional groups and inorganic compounds in ambient aerosols using attenuated total reflectance FTIR spectroscopy and multivariate chemometric techniques. *Atmospheric Environment, 42*, 5923-5932.

Dafalla, S., Mukhtar, H., & M. Shaharun. (2010). Characterization of Adsorbent Developed from Rice Husk: Effect of Surface Functional Group on Phenol Adsorption. *Journal of Applied Sciences, 10*, 1060-1067.

Doyle, W. (1992). Principles and Applications of Fourier Transform Infrared (FTIR) Process Analysis. Tustin, CA: Hellma Axiom, Inc.

Du, C. (2011). Application of Infrared Photoacoustic Spectroscopy in Soil Analysis. *Applied Spectroscopy Reviews, 46 (5)*, 405-422.

EPA. (1999). PM2.5 Speciation Guidance: Final draft. Research Triangle Park, NC: U.S. Environmental Protection Agency.

EPA. (2008). *National Emissions Inventory.* Triangle Park, Raleigh: US Environmental Protection Agency.

EPA. (2008). Standard Operating Procedure for Particulate Matter (PM) Gravimetric Analysis. Research Triangle Park, NC: Environmental and Industrial Sciences Division, EPA.

EPA. (2014). Guidance for PM2.5 Permit Modelling . Research Triangle Park, NC: U.S. Environmental Protection Agency.

EPA. (2016). Final Rule: Fine Particulate Matter NAAQS for SIP Requirements. Research Triangle Park, NC: US EPA.

EPA. (2017). United States Environmental Protection Agency. Retrieved from Laws & Regulations.

EPA. (2018). CERCLA and EPCRA Reporting Requirements for Air Releases of Hazardous Substances from Animal Waste at Farms. Raleigh: United States Environmental Protection Agency: Office of Land and Emergency Management.

Ezzell, M., Johnson, S., Yu, Y., Perraud, V., Bruns, E., Alexander, L., B. Finlayson-Pitts. (2010). A New Aerosol Flow System for Photochemical and Thermal Studies of Tropospheric Aerosols. *Aerosol Science and Technology, 44*, 239-338.

Faulkner, W., Shaw, B., & R. Lacey. (2007). Coarse fraction aerosol particles: Theoretical analysis of rural versus urban environments. *Applied Engineering in Agriculture, 23 (2)*, 239-244 .

Flesch, T., Harper, L., Powell, J., & J. Wilson. (2009). Inverse-Dispersion calculation of ammonia emissions from wisconsin dairy farms. *Transactions of the ASABE, 52 (1)*, 253-265.

Friedlander, S. (2000). *Smoke, Dust, and Haze Fundamentals of Aerosol Dynamics, Second Edition.* NY, New Tork: Oxford University Press, Inc.

Gamera, M. & F. de la Mora. (2000). A condensation nucleus counter (CNC) sensitive to singly charged sub-nanometer particles. *J. Aerosol Sci, 31*, 757.

Geng, H., Kang, S., Jung, H.-J., Choel, M., Kim, H., & Ro, C.-U. (2010). Characterization of individual submicrometer aerosol particles collected in Incheon, Korea, by quantitative transmission electron microscopy energy-dispersive X-ray spectrometry. *Journal of Geophysical Research, 115*, 1-15.

Goldstein, J. (2003). *Scanning Electron Microscopy and X-ray Micronalysis, 3rd ed.* . New York: Plenum Press.

Griffiths, P. & A.Cox. (2009). Temperature dependence of heterogeneous uptake of N2O5 by ammonium sulfate aerosol. *Atmos. Sci. Let. 10*, 159–163.

Guha, A. (2009). *Evaluation of Ambient Particulate Matter Sampler Performance through Wind Tunnel Testing (Master's Thesis).* College Station, TX: Texas A&M University.

Guo, Y., Liu, Z., Huang, Z., Liu, Q., & S. Guo. (2005). Reaction Behavior of Sulfur Dioxide with Ammonia. *Ind. Eng. Chem. Res. 44*, 9989-9995.

Hartley, E. & M. Matteson. (1975). Sulfur Dioxide Reactions with Ammonia in Humid Air. *Ind. Eng. Chem. Fund. 14*, 67.

Hausinger, R. (2004). Metabolic versatility of prokaryotes for urea decomposition. *J. Bacteriology 186(9)*, 2520-2522.

Hinds, W. (1999). *Aerosol Technology - Properties, Behaviour, and Measurement of Airborne Particles, 2nd ed.* New York: John WIley & Sons, Inc.

Hirota, K., Makela, J., & O. Tokunaga. (1996). Reactions of Sulfur Dioxide with Ammonia: Dependence on Oxygen and Nitric Oxide. *Ind. Eng. Chem. Res. 35,* 3362-3368.

Hisatsune, I. & J. Heicklen. (1975). Infrared Spectroscopic Study of Ammonia - Sulfur Dioxide - Water Solid State System. *Can. J. Chem. 53.,* 2646-2656.

Hodan, W., & W. Barnard. (2005). *Evaluating the Contribution of PM2.5 Precursor Gases and Re-entrained Road Emissions to Mobile Source PM2.5 Particulate Matter Emissions.* Research Triangle Park, NC: US EPA.

Hodoroaba, V., Rades, S., Salge, T., Mielke, J. O., & R. Schmidt. (2016). Characterisation of nanoparticles by means of high-resolution SEM/EDS in transmission mode. *Materials Science and Engineering, 109,* (pp. 1-13). Germany.

Hribar, C. (2010). Understanding Concentrated Animal Feeding Operations and Their Impact on Communities. Bowling Green, Ohio: National Association of Local Boards of Health.

Hristov, A., Hanigan, M., Cole, A., Todd, R., McAllsiter, T., Ndegwa, P., & A. Rotz (2010). Review: Ammonia emissions from dairy farms and beef feedlots. *Can. J. Anim. Sci. 91,* 1-35.

Ishler, V. (2015). *Nitrogen, Ammonia Emissions and the Dairy Cow.* Building University Park, PA: PennState Extension.

Jacob, D. (2004). *Introduction to Atmospheric Chemistry.* Princeton, New Jersey: Princeton University Press.

Kaschiev, D. (2000). *Nucleation: Basic principles and application.* Butterworth, Heinemann.

Kerminen, V., Pirjola, L., & M. Kulmala. (2001). How significantly does coagulational scavenging limit atmospheric particle production? *Journal of Geophysical Researach, 106 (20),* 119-125.

Kozusko, F., & D. Lasseigne. (1996). The stability of compressible mixing layers in binary gases. *Physics of Fluids, 8,* 1954-1963.

La, Y., Camredon, M., Ziemann, P., Valorso, R., Matsunaga, A., Lannuque, V., Aumond, B. (2016). Impact of chamber wall loss of gaseous organic compounds on secondary organic aerosol formation: explicit modeling of SOA formation from alkane and alkene oxidation. *Atmos. Chem. Phys., 16,*, 1417-1431.

Lambe, A., Chhabra, P., Onasch, T., Brune, W., Hunter, J., Kroll, J., Davidovits, P. (2015). Effect of oxidant concentration, exposure time, and seed particles osecondary organic aerosol chemical composition and yield. *Atmos. Chem. Phys., 15*, 3063–3075.

Lee, S., Yu, M., & H. Kim. (2013). Development of aerosol wind tunnel and its application for evaluating the performance of ambient PM10 inlets. *Atmospheric Pollution Research, 4*, 323-328.

Li, W., & L. Shao. (2009). Transmission electron microscopy study of aerosol particles from the brown hazes in northern China. *J. Geophys. Res., 114*, 1-10.

Lushnikov, A., Zaganov, V., & Lyubovtseva, Y. (2010). *Physics of Earth and Space Environments.* USA: Springer Science + Business Media B.V.

Martello, D., Anderson, R., White, C., Cassucio, G., & S. Schlaegle. (2001). *Quantitative Scanning Electron Microscopy Methods to Characterize Ambient Air PM2.5.* Washington, D.C.: U.S. Department of Energy, NETL.

McClenny, W., Childers, J., Rohl, R., & R. Palmer. (1985). FTIR Transmission Spectrometry for the Non-destructive determination of Ammonium and Sulfate in ambiend aerosols collected in teflon filters. *Atmospheric Environment, 19 (11)*, 1891-1989.

Meyer, B., Mulliken, B., & H. Weeks. (1980). The Reactions of Sulfur Dioxide with Excess Ammonia. *Phosphorus and Sulfur, 8*, 281-290.

Mihaly, J., Sterkel, S., Ortner, H., Kocsis, L., Hajba, L., Furdyga, E., & J. Mink. (2006). FTIR and FT-Raman Spectroscopic Study on Polymer Based High Pressure Digestion Vessels. *CROATICA CHEMICA ACTA, 79 (3)*, 497-501.

Na, K., Chen, S., Switzer, C., & D. Cocker. (2007). Effect of Ammonia on Secondary Organic Aerosol Formation from r-Pinene Ozonolysis in Dry and Humid Conditions. *Environ. Sci. Technol, 41*, 6096-6102.

NEL Technologies. (2012). *Effects of Phase Change on Flow Measurement - Feasiblity Study.* Glasgow, UK: TUV SUD Ltd.

NIST. (2017). *NIST Chemistry WebBook, SRD 69.* USA: National Institute of Standards and Technology.

NIST. (2018, February 1). *Information Technology Laboratory (ITL).* Retrieved from NIST: http://www.itl.nist.gov/div898/handbook/eda/section3/eda35b.htm

Parnel, C., Shaw, B., & B. Auvermann. (1998). *Agricultural air quality fine particle project: Task 1 Livestock – feedlot particulate matter emission factors and emission inventory estimates.* Austin, TX: Texas Natural Resource Conservation Commission.

Parnell, C., & Parnell-Molloy, S. (2002). Air Pollution Regulatory Process (APRP) and Agricultural Operations. *2002 ASAE Annual International Meeting /* (pp. 1-10). Chicago, Illinois, USA: American Society of Agricultural Engineers.

Preece, S., Casey, K., & B. Auvermann. (2012). *Hydrogen Sulfide Emissions from Open/Dry-Lot Cattle-Feeding Operations.* College Station, TX: Texas A&M Agrilife Extension.

Preece, S., Cole, A., Todd, R., & B. Auvermann. (2012). *Ammonia Emissions from Cattle Feeding Operations.* College Station: Texas A&M Agrilife Extension.

Presto, A., & N. Donahue. (2006). nvestigation of a-pinene + ozone secondary organic aerosol formation at low total aerosol mass. *Environ. Sci. Technol., 40*, 3536-3543.

PTI. (2016). *Safety Data Sheet: ISO 12103-1 Fine Test Dust.* USA: Power Technology, Inc.

Ren-yi, C., Ling, C., Zee Ma, Y., Xue-ying, L., & Bai-hui, Y. (2016). Characteristics of unsteady flow in porous media while considering threshold pressure gradient with Green's function . *J. Cent. South Univ, 23*, 201−208.

Rhoades, M., Parker, D., Cole, N., Todd, R., Caraway, E., Auvermann, B., . . . Schuster, G. (2010). Continuous Ammonia Emission Measurements from a Commercial Beef Feedyard in Texas. *Transactions of the ASABE, 53 (6)*, 1823-1831.

Sakirkin, S., Maghirang, R., Ammoson, S., & Auvermann, B. (2012). *Dust Emissions from Cattle Feeding Operations. Part 1 of 2: Sources, Factors, and Characteristics.* USDA: eXtension: Air Quality in Animal Agriculture.

Sigma-Aldrich. (2012). *IR Spectra Lab Data Guide.* USA: Sigma-Aldrich.

Stauffer, D., & Kiang, C. (1973). *Heteromolecular nucleation theory for multicomponent gas mixtures.* Atlanta, GA: Tellus XXV, 295-296.

Stromberger, M. (1984). The removal of Sulfur Dioxide from Coal-Fired Boiler Flue Gas by Ammonia Injection. *M.S. Thesis, University of Cincinnati, Cincinnati*.

Todd, R., Cole, A., Rhoades, M., Parker, D., & Casey, K. (2010). Daily, Monthly, Seasonal, and Annual Ammonia Emissions from Southern High Plains Cattle Feedyards. *Journal of Environmental Quality, 40: 4*, 1090-1095.

Vaden, T., Song, C., Zaveri, R., Imre, D., & Zelenyuk, A. (2010). Morphology of mixed primary and secondary organic particles and the adsorption of spectator organic gases during aerosol formation. *PNAS, 107 (15)*, 6658-6663.

Vallis, I., Harper, L., Catchpoole, V., & K. Weier. (1982). Volatilization of ammonia from urine patches in a subtropical pastures. *Australian J. Agric. Res. 33(1)*, 97-107.

Vance, J., & L. Peters. (1976). Aerosol Formation resulting from the Reaction of Ammonia and Sulfur Dioxide. *Ind. Eng. Chem., Fundam., 15 (3)*, 202-206.

Waldrip, H., Rotz, A., Hafner, S., Todd, R., & A. Cole. (2014). Process-based Modeling of Ammonia Emission from Beef Cattle Feedyards with the Integrated Farm Systems Model. *Journal of Environmental Quality, 43 (4)*, 1159-1168.